THE INFLUENCE OF CATIONS ON DOPC ADSORBED ONTO Hg/ELECTROLYTE INTERFACE ELECTROCHEMICAL AND IMPEDANCE SPECTROSCOPY STUDY

by

JOHN ODIKO AGAK
B.Sc., Kenyatta University, 1997

A THESIS SUBMITTED IN PARTIAL FULFILMENT OF
THE REQUIREMENTS FOR THE DEGREE OF

MASTER OF SCIENCE

in

THE FACULTY OF GRADUATE STUDIES
Department of Chemistry

We accept this thesis as conforming
to the required standard

THE UNIVERSITY OF BRITISH COLUMBIA

December 2002

In presenting this thesis in partial fulfilment of the requirements for an advanced degree at the University of British Columbia, I agree that the Library shall make it freely available for reference and study. I further agree that permission for extensive copying of this thesis for scholarly purposes may be granted by the head of my department or by his or her representatives. It is understood that copying or publication of this thesis for financial gain shall not be allowed without my written permission.

Department of CHEMISTRY

The University of British Columbia
Vancouver, Canada

Date DECEMBER, 18, 2002

ABSTRACT

An electrochemical impedance spectroscopy (EIS) methodology has been developed, and combined with traditional electrochemical techniques to characterize the influence of applied potential on a dioleoyl phosphatidylcholine (DOPC) monolayer adsorbed at a Hg-0.1MKCl interface. The DOPC monolayer was initially characterized using AC voltammetry in 0.1M KCl, LiCl and TMACl. The monolayer displayed a minimum low-capacitance region, 1.85 $\mu F/cm^2$ at -0.4 V. The potential was scanned from -0.4 V to -1.2 V and two capacitance peak 1 and 2 were observed at -0.96 V and -1.04 V respectively. When the negative potential limit was made more negative, a third capacitance peak 3 was observed at -1.34 V. These peaks represent phase transformations due to changes in electrode coverage. At very negative potentials, the monolayer desorbed from Hg in KCl and TMACl but no desorption was observed in LiCl. Addition of Ca^{2+} to the KCl subphase, systematically changed the peak heights indicating a change in the kinetics of the phase transformation. In the presence of Ca^{2+}, the desorption of the lipid was incomplete. However, addition of 1.0 mM of TMA^+ enhanced the desorption of the lipid in the presence of Ca^{2+}.

In order to further characterize these layers, an EIS methodology was developed and tested on the Hg-KCl systems. The monolayer was modified by adding Ca^{2+} to the electrolyte subphase. Changes due to its interaction with the cations were characterized using the new technique. The potential was scanned from -0.4 V to the peak potentials and the impedance measured over a wide range of frequencies. The methodology allowed for the impedance measurements to be performed at a potential corresponding to the capacitance peak maximum without disrupting the monolayer organization. Impedance spectra at peak 1 indicated a phase change characterized by one time constant, peak 2 indicated a phase transformation characterized by two time constants and peak 3 showed a phase transformation characterized by three time constants. At the desorption potential value, the impedance spectra revealed the desorption of the monolayer from the Hg-KCl interface and incomplete desorption in the presence of Ca^{2+} in the subphase. The new methodology also allowed for changes in solution resistance due to the presence of adsorbed or desorbed DOPC monolayers to be observed. However, in the presence of DOPC no difference in solution resistance was observed between the adsorption and desorption potentials except when Ca^{2+} was introduced.

Table of contents

List of Figures

Dedication

To my beloved mother, Grace Aoko (*Nya Seme*). I love you so very much.

Acknowledgments

In recognizing those who have impacted the creation of this thesis, I first wish to acknowledge the invaluable contribution of my supervisor, Dr. Dan Bizzotto, whose thoughtful insights guided me in conceptualizing this research. I always recall his sound advice and critique throughout the development and processing of this thesis. From my interaction with him in many fora, I came to appreciate his immense knowledge and research skills, which enabled me to critically examine the data from which I made interesting inferences and conclusions.

Others were also instrumental in guiding and critiquing this thesis. Dr. Samson Madera Nashon posed challenging questions to the content of the thesis prompting me to search for ways of addressing them. He always read my thesis chapters and raised pertinent questions and issues that in most cases required clarification and further development. I am also thankful to all those who have been or still are members of Dr. Bizzotto's lab (Yanguo Yang, Jeff Shepherd, Robin Stoodley Edward Guerra, Emily Chung, Pavel Freundlich, Jie Gao, Anisa Aktar, Irina Manisali and Michael Lathuilliere) for the professional interest and advice in my research. My debt to them extends to a personal arena. I find it hard to express how important was all the time, attention and encouragements you offered to me. Thanks also go to the staff in the electronic and mechanical shop in the Department of Chemistry, UBC, for their help. Special thanks also to UBC for financial support, without which this study would have not been possible - I salute this institution.

My special tribute goes to John Okumu Nyawina and his family for their immeasurable contributions. I thank you most sincerely and express my unwavering gratitude for what you have been to me. I also appreciate the valuable contributions from Nyawegi Asociation-Nairobi, Onyango Association-Nairobi and Ombogo Girls' Academy for the initial support for my studies at UBC.

I would not end this acknowledgment before paying my tributes to my siblings: Boaz, Martha, Pamela and Helen. Your support and encouragements, was the source of strength and hope. Thanks to all my friends across Kenya and Canada for your help during my studies. In a special way, I salute my fiancee, Lydia Awuor for the care and support she provided. My heartfelt thanks and undying gratitude is all I can give in return. Above all, I thank God and the Lord Jesus Christ for the gift of life, sound health and protection during the entire study.

1. Introduction

Adsorption of organic compounds at electrified interfaces has been a subject of interest for many years and has been extensively investigated by many groups[1-7]. The study of adsorption of water insoluble organic molecules was first performed on a hanging mercury (Hg) drop electrode surface. The mercury electrode was the most suitable because mercury surface is liquid and provides unambiguously defined uniform liquid-liquid interface; it is hydrophobic when uncharged and almost ideally polarized [8]. Furthermore, its reproducible, atomically smooth and clean surface is ideal for investigating the fundamental features of adsorption onto the electrified interfaces.

Theories that were later developed based on the extensive studies on Hg electrodes have generated concepts that are useful to the subsequent study of adsorption at all interfaces (see Chapter 2). The recent past, however, has seen the evolution of a reproducible well characterized, single crystal solid electrodes which have since paved the way to the study of surfactant adsorption onto solid electrode materials. This is an important achievement and a huge step toward an interface more representative of the physical world.

The adsorption of surface active compounds is experienced in everyday life. For example, detergents are used as important disinfectants and cleaning agents at home or in industry to solubilize organic compounds. Therefore, insoluble surfactant molecules form an important class of compounds. Their relevance to scientific applications such as corrosion and catalysis motivated the investigation of their adsorption onto metal surfaces[9]. Phospholipid monolayers and bilayers spread onto electrodes have been used to model biological membranes[10-12].

Phospholipids are among the principal components in a biological cell membrane (see Chapter 2) and form bilayer structures, which constitute a barrier to the transport of ions. However, biological cells are not isolated systems and have chemical and electrical communication with their environments. The concentrations of ions inside and outside of the cell are different. This difference induces a potential difference (transmembrane potential) across the lipid bilayer. The lipid bilayer is a host to several membrane proteins embedded in the bilayer structure, which are active in transporting species through the membrane. These proteins function as gates and pumps that control the flow of ions in and out of the cell. Ligand-gated channels open when a chemical species (ligand)

is bound as in the acetylcholine receptor channel, which plays the role of a neurotransmitter. Voltage-gated channels open when there is a change in membrane potential. Voltage changes induced by nerve impulses at a muscle cells open protein ion channels and allow Ca^{2+} to flow, thus triggering muscle contractions. Protein ions actively pump certain solutes across the membrane against their concentration and electrochemical gradient. Changes in the conformation and the structure of the membrane proteins may be influenced by their interaction with the lipids in the bilayer structure. Therefore, understanding biomembranes involves examining the membrane-protein conformation and the dynamics of lipid-membrane protein interaction. In a recent review [13], Olivotto et. al. pointed out that the importance of transmembrane potential on the function of membrane proteins has been underestimated. In living cells, transmembrane potential occurs naturally and is used to control signaling, transport of ions across the membrane, and opening and closing voltage-gated ion channels. Malfunctioning of these proteins has consequentially been directly linked to the manifestation of several human diseases. The interaction of hydrophobic drugs with the lipid bilayers can also be indirectly influenced by membrane potential[14,15]. The treatment of secondary infections with Amphotericin B or treatment of cancerous tumors by organic drugs is most effective when delivered in liposomal forms [16].

The study of adsorption of monolayer of phospholipid supported onto a Hg electrode has been investigated. The same studies have explored incorporation of ion channels and proteins into the adsorbed monolayer. These investigations have revealed vital information regarding the influence of potential on the behavior of lipid monolayer with and without the incorporated molecules, thus making electrochemistry a fundamental tool for studying biological membrane behavior and processes. Therefore, this study aims at extending the work of adsorption of phospholipids onto Hg, thus contributing to this area of knowledge.

1.1 The Thesis

1.1.1 The rationale

A phospholipid monolayer adsorbed at a mercury-water interface has been studied by many groups [17-27] and have become an area of interest in our laboratory. Among the scientific community, there has been an increasing interest in electrochemistry to help in the interpretation of biological behavior and processes such as the transport of ions and transfer of electrons through biological membranes. Biological membranes are highly ordered structures and their functions depend on the organization of various components. The biological membrane's structure is dependent on the association of phospholipids, which form bilayer structures and constitute a barrier to the transport of ions. Therefore, a study of the interaction within phospholipid layers significantly models the interaction within the biological membranes.

To apply electrochemical methods of modeling to biological membrane processes, some electrochemical systems have been proposed [8]. Recently, a phospholipid-coated mercury electrode was developed [17,18,28], resulting in an adsorbed monolayer that can be used as a biomimetic membrane similar to the bilayer lipid membrane. In the case of a lipid-coated mercury electrode, the film consists of a half bilayer with the polar head groups directed toward the electrolyte solution. Though a monolayer, the system represents exactly half a bilayer and the interactions at the lipid-solution interface are the same as at the bilayer-solution interface. A supported monolayer system has many advantages over a free-standing bilayer system since the film is provided with inherent mechanical stability and electrical variables can be controlled and measured accurately over a wide range of potentials.

The current study (thesis) adapts and utilizes this monolayer formation technique to study the influence of potential on the behavior of lipid monolayer assumed to mimic biological membranes, especially the interaction of phospholipids in the bilayer membrane with its surroundings. A hanging Hg drop electrode was used in this study. Hg was chosen because of its important properties already stated. The molecule used in this work, dioleoyl phosphatidylcholine (DOPC) has been characterized previously [29,30] and is a molecule used in Langmuir-Blodgett applications.

1.1.2 Goals and objectives

The goal of this study was to develop an electrochemical impedance spectroscopy methodology, combined with traditional electrochemical techniques to characterize the influence of the applied potential on a DOPC monolayer supported on Hg electrode quantitatively.

Modification of the DOPC monolayer was accomplished through the addition of cations into the electrolyte subphase. Changes in the monolayer due to its interaction with the cations were characterized using the new technique.

1.2 Scope of the Thesis

The research study covers a wide area of study and knowledge, ranging from electrochemistry to surface science as well as biochemistry, physics and thermodynamics. A brief discussion of the theories relevant to this study is provided in Chapter 2. These theories are important in providing a framework for the understanding of the experiments and the discussion of the results. The chapter begins with the discussion of fundamentals of electrochemistry followed by theories of electrical double layers. The quantitative description of double layers and the thermodynamics of electrified interfaces are also discussed. Adsorption of neutral organic molecules are also described followed by a detailed discussion of biological membranes since they are important in this study. Finally, the concept of electrochemical impedance spectroscopy is explained.

A review of some literature relevant to this thesis is provided in Chapter 3. In this chapter, the adsorption and characterization of insoluble surfactant onto electrode-electrolyte interfaces are discussed followed by adsorption of phospholipids onto Hg-electrolyte interfaces. The interaction of cations with phospholipid layers and the electrochemical impedance spectroscopy are reviewed. Experimental methodology and techniques are outlined in Chapter 4. The discussion in this chapter starts with the instrumentation and methodology employed for electrochemical investigation followed by electrochemical impedance spectroscopy. Results generated from the study and the discussions of those results are given in Chapter 5. In this chapter, the electrochemical characterization of DOPC monolayer is discussed first followed by electrochemical impedance spectroscopy characterization. Chapter 6 provides key conclusions drawn from the experimental results. Lastly, some suggestions for future study in this field are provided in Chapter 7.

2 Theoretical Background

This chapter provides a theoretical background that describes the design and performance of experiments and the analysis of the results. Key concepts touching many subjects are presented since the study covers a wide area of knowledge. However, only those concepts relevant to the current study are discussed.

Some fundamentals of electrochemistry and electrochemical double layer models are discussed. These are followed by the quantitative interpretations of the electrical double layer and the thermodynamics of the electrified interfaces. Theories of adsorption of neutral organic molecules at electrified interfaces are also discussed. In addition, biological cell membranes, which are made of lipid molecules are described since the molecules studied in this thesis are constituents of cell membranes. Finally, impedance spectroscopy, which is an experimental technique for characterizing modified interfaces is briefly described.

2.1 Fundamentals of Electrochemistry

2.1.1 Introduction

Today, electrochemical processes provide humanity with materials and technologies that contribute significantly to all aspects of life. Electrochemistry involves the study of surface science under the influence of electric fields. It deals with the study of the interesting phenomenon occurring at the interface between the metal or semiconductor and the conductive media (electrolyte).

In this section, those principles of electrochemistry, which are directly applicable to the current study are presented. The general behavior of electrical capacitors is described and in turn used to illustrate the capacitances of electrified interfaces. The concept of electrical double layers, which forms the cornerstone of this study is also described.

2.1.2 Electrical capacitor

A capacitor is an electrical device (Figure 2-1) consisting of two parallel metal plates, separated by a small distance, *d*. The gap is usually filled with a dielectric (non conducting) material. A capacitor, fundamentally stores charge and electric field energy. When potential is applied across the capacitor, charges of the same magnitude but of opposite signs accumulate on the opposite metal

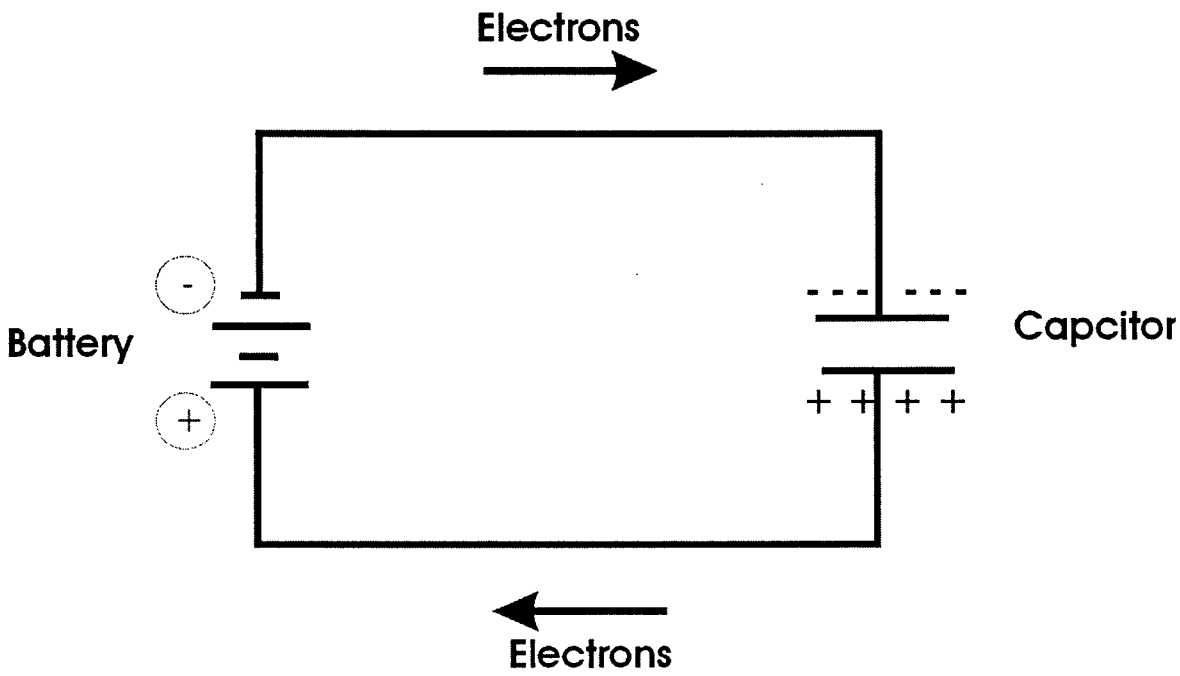

Figure 2-1 The diagram showing a capacitor and charging of a capacitor. The arrows indicate the direction of electron flow. - - - - represent electrons on one plate, + + + + represent positive charges on the other plate.

plates respectively. The magnitude of the charge q on each of the metal plates is proportional to the electric potential difference, E, between them. The proportionality constant C, is the capacitance, and its characteristics are governed by the equation

$$C = \frac{q}{E} = \frac{\varepsilon \varepsilon_o}{d} \qquad 2\text{-}1$$

Where ε is the dielectric constant of the medium between the plates, and ε_o is the permitivity of the free space. During the charging process, a current (charging) continues to flow and ceases only when the potential difference across the capacitor is equal to that of the applied potential. An array of capacitors may be combined either in series or in parallel in an electric circuit. Whichever arrangement is adopted, an effective (equivalent) capacitance will be produced. For example, two capacitors of capacitance C_1 and C_2 arranged in parallel will have the same effect as an equivalent capacitor of capacitance C_p, hence

$$C_p = C_1 + C_2 \; or \; C_p = \sum_{i=1}^{i=n} C_i \qquad 2\text{-}2$$

For two capacitors of capacitance C_1 and C_2 in series, the equivalent capacitance C_s, is derived from the fact that the potential, E_s, across the equivalent capacitor is the sum of potentials E_1 and E_2 (Since they are in series) across the capacitors respectively, hence

$$\frac{1}{C_s} = \frac{1}{C_1} + \frac{1}{C_2} \; or \; \frac{1}{C_s} = \sum_{i=1}^{i=n} \frac{1}{C_i} \qquad 2\text{-}3$$

Electrode-electrolyte interfaces have been theoretically modeled as capacitors.

2.1.3 Capacitance of the electrified interface

The description of an electrified interface is based on the concept of charge ordering at the phase boundary. Positive or negative charges accumulate at the surface of the electrode and are balanced by opposite charges of equal amounts arranged on the solution side. At equilibrium, the species in the bulk solution experience forces that are isotropic and homogeneous, hence no net electric field is generated. At the interface, the symmetry collapses and the forces acting on the

species are anisotropic. As a result, the solution side acquires a net orientation of solvent dipoles and a net ionic excess charge close to the phase boundary. As soon as the net charge is acquired by the solution side, the metal side reciprocates by developing an induced opposite charge of the same magnitude on its surface. This leads to two parallel layers of charge separation at the electrode-electrolyte interface, thus making the interface to mimic a capacitor [31].

An electrode system in which there is no charge transfer across the electrode-electrolyte interface regardless of the applied potential is referred to as ideally polarized electrode (IPE). This phenomenon cannot be achieved by any real electrode over all the potential ranges. However, under restricted conditions, some electrode-electrolyte systems may approach ideal polarization behavior. For instance, mercury in contact with deaerated potassium chloride (KCl) solution within the potential defined by mercury-potassium (Hg/K) amalgam and mercury chloride (Hg_2Cl_2) formation, can satisfy the IPE definition. This system is used in the current study.

The behavior of an electrode-electrolyte interface has been shown experimentally [32] to resemble two series capacitors. However, the only difference is that in the case of a real capacitor, the capacitance is always independent of applied potential whereas in the electrode-electrolyte system, the capacitance is generally a function of the applied potential and electrolyte concentration (Figure 2-2). Knowledge of the electrical double layer phenomenon is important in understanding the capacitive nature of the interface.

2.2 Electrified Interface and Double Layer Theories

The charge on the electrode-electrolyte interface is a contribution from the two sides of the interface. On the metal side they are made of mobile electrons, while on the aqueous solution side (electrolyte) they consist of mobile ions [33]. The charges on the electrolyte side are believed to be distributed from a plane close to the electrode surface toward the bulk solution thereby forming a diffuse layer. Similarly, charges on the solid side are distributed from the solid surface toward the solid interior forming a diffuse layer of excess electrons. Below is the discussion of the metal side of the interface followed by the aqueous solution side and double layer theories.

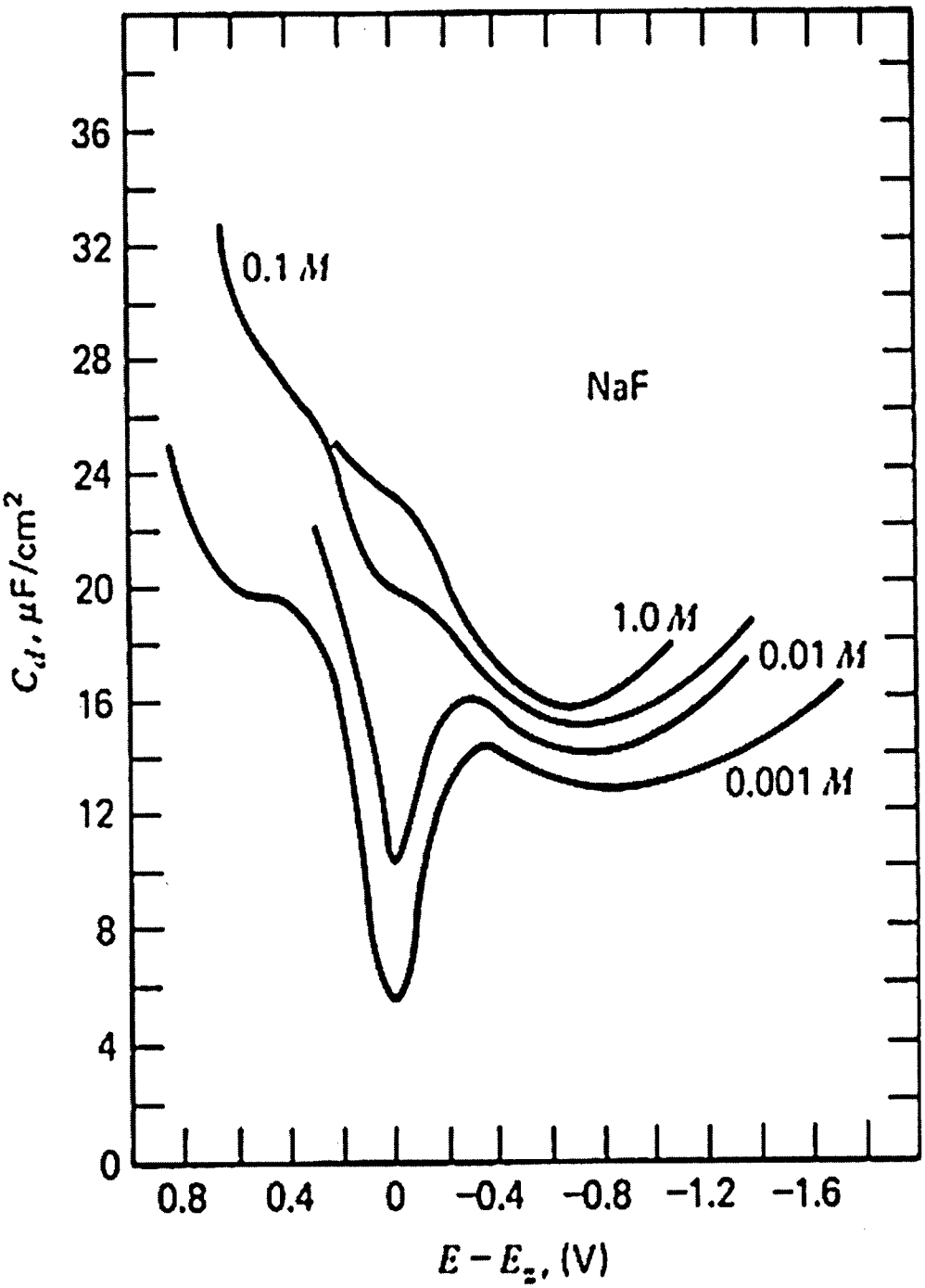

Figure 2-2 The figure showing the dependance of capacitance on electrolyte concentration using NaF as the electrolyte solution. The capacitance increases with the increasing electrolyte concentration. Taken from [32].

2.2.1 *The metal side of the interface*

Metals contain a lattice of closely packed atoms [34] with freely moving electrons due to the overlap of atomic orbitals (wave functions). The overlap of the wavefunctions effectively creates a continuum of energy states. Electrons occupy these energy states from the lowest level up to the highest filled level called the Fermi level. In general, the metal phase bears a net electrical charge on its surface due to an excess or deficit of electrons. This electronic excess or deficit may either be imposed on the metal by means of an external potential source or by action of a faradaic (charge-transfer) electrode process. As the applied electric potential on the metal is varied, the distributions of the electrons in the energy states are altered. When the applied potential is made more negative, the electrons are added to the metal, while the electrons are removed from the metal when the applied potential is made more positive. The charge accumulation is located in a very thin layer of less than 1 Å. This charge is denoted by σ_m and can be directly measured experimentally.

The metal atoms sit in a lattice and have a fixed distribution of positive charges. The electrons, however, are mobile and tend to "spill" out from the edge of the metal ion. This leads to inhomogeneous distribution of charges at the surface creating a dipole (Figure 2-3). The presence of oriented dipoles and inhomogeneous distribution of charges induce surface potential (χ), which is dependent on the atomic arrangements in the metal. When an electron is either removed or added to the metal, work must be done against the chemical interactions and against the surface potential according to the equation

$$-\Phi = \mu_e - e\chi \qquad 2\text{-}4$$

where Φ is the work function of the metal, μ_e is the chemical potential and $e\chi$ is the surface potential.

The arrangement of metal atoms on the exposed surface has an influence on the work function and is generally largest for the most densely packed surface [35]. This can be visualized based on the fact that the higher the density of the atoms at the surface, the smoother the electron density at the surface. Any roughness or less dense packing will induce additional dipole at the surface, which tends to lower the work function (Figure 2-4). The change in applied potential (or work function) is related to the change in surface potential (due to the change in the homogeneity

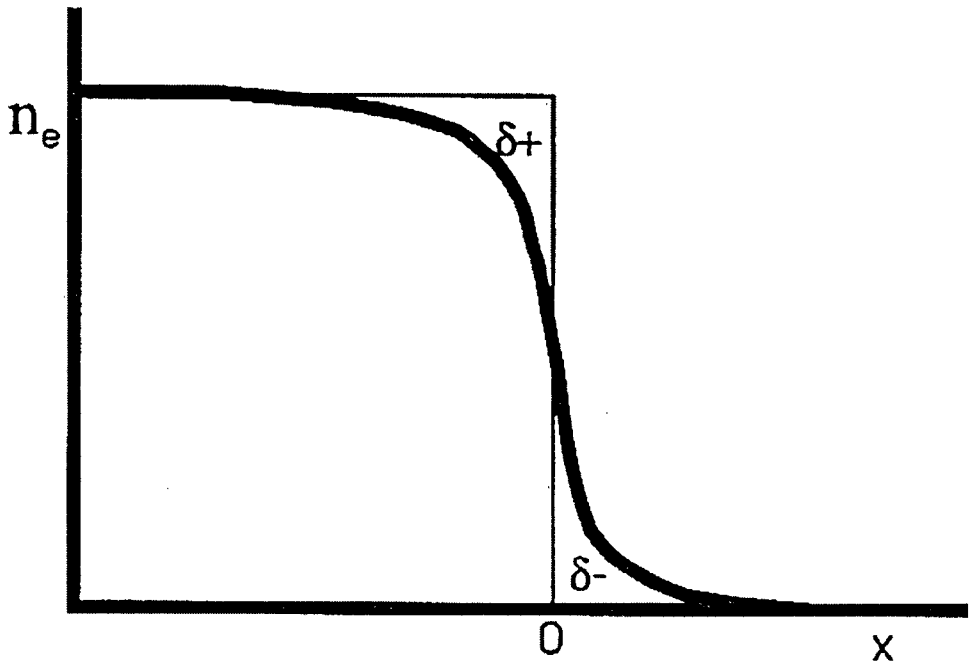

Figure 2-3 A schematic diagram showing the electron spill over from the edge of a metal ion creating a surface dipole.

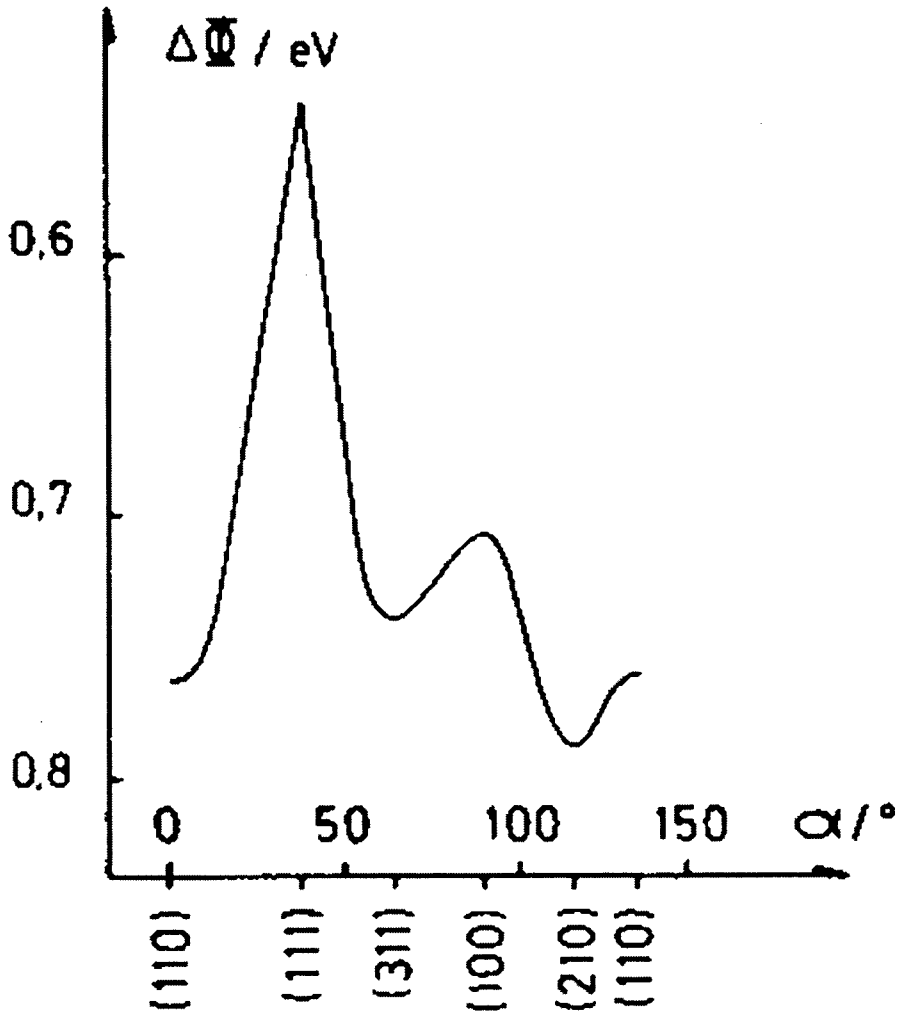

Figure 2-4 The diagram for work function of various Cu surfaces as a function of crystallographic orientation. The highest work function is measured for the most densely packed surface atoms (111).Taken from [37].

or the charge distribution, or the presence of surface dipole), hence adsorbed molecules. For example, water and ions on the surface of the metal can change the work function [36,37]. A higher work function means that the positive end of the dipole is on the surface, while a lower work function indicates that the negative end of the dipole is on the surface of the metal

2.2.2 The aqueous solution side of the interface

Electrical double layer is created by an array of charged particles existing at every electrode-electrolyte interface. Through the process of adsorption, charged particles and neutral molecules enter the interfacial region establishing an electric field. The location within the interfacial region where these charges reside is referred to as electrical double layer. Charged ions are either assembled on the solution side due to electrostatic field of the metal or adsorbed specifically (discussed later) on the electrode surface via Van der Waals, hydrophobic and chemical interactions. Typical values of the double layer region are between 10 - 40uF/cm^2.

Several theories have been put forward to explain the electrical behavior of the double layer in terms of models. All double layer models attempt to interpret the experimental results, e.g., the dependance of double layer capacity on the applied potential and electrolyte concentration. Some of these theories are discussed next. The advantages and disadvantages of each are explained. The models successively appear to reflect an ideal description of the real structure of the interface.

2.2.3 Theories of electrical double layer

According to the Helmholtz model (1879), the electrical double layer is viewed as a rigid arrangement of positive and negative charges at the two sides of the interface [31]. The double layer is pictured as resembling a parallel-plate capacitor whose plates are represented by homogeneously distributed charges in the metal, and ions of the opposite charge lying in a parallel plane in the solution at a small distance from the metal surface. The plane through the center of the ions in solution at some distance, x_2 from the electrode is known as Outer Helmholtz Plane (OHP). In ths region, the decay of electrostatic potential from the metal to the solution is linear and capacitance is constant, i.e., independent of applied potential and electrolyte concentration.

The Gouy-Chapmann model [32], postulated in the beginning of the last century (1910-

1913), is an improvement of Helmholtz model. It suggests that the electrostatic forces cannot retain ions at minimal distance from the electrode surface. The ions are subject to random thermal motion and are continually dispersed to a greater distance from the phase boundary. Therefore, the ions which neutralize the surface charge are distributed further into the solution thus forming a diffuse layer, i.e., the region between the OHP and the bulk of the solution. The highest concentrations of excess charges are found in the vicinity of the electrode because electrostatic forces overcome the thermal processes. However, further away from the electrode, bulk concentrations are realized.

According to this model, the potential decays gradually from the OHP to the bulk. The double layer capacitance, C increases with applied potential and electrolyte concentration. This behavior is accounted for by the fact that as the interface gets more polarized, the diffuse layer becomes compact. Unfortunately, the experimental results are at par with the hypothesized theoretical values only at low electrolyte concentrations. Nonetheless, the Gouy-Chapmann model is good and offers insight to the dependance of the double layer capacitance on the applied potential and ionic concentration.

The Gouy-Chapmann-Stern (GCS) model (1924), is a combination of the Helmholtz and Gouy-Chapmann models. It acknowledges the failure of Helmholtz and Gouy-Chapman models to account precisely for the characteristics of the double layers. This model (GCS) succeeds in resolving the anomalies not addressed by the other models. For instance, the GCS model explains the continuous rise in double layer capacitance (in Gouy-Chapman model) as due to the fact that the ions in solution are not restricted with respect to distance from the electrode. The ions are treated as point charges hence can approach the electrode infinitely close so that at high potential perturbations, the distance between the electrode and the solution-phase charge progressively decreases to zero. This assumption appears farfetched because ions have definite sizes and therefore must only approach the electrode to some degree. Furthermore, if the ions are solvated, the solvation sheath will increase the ionic radius and subsequently decrease the approaching distance. Therefore, a plane of closest approach for the center of the ions will always exist at some distance from the electrode.

The GCS model considers finite sizes of the ions and finite distances of closest approach. On this basis, the double layer is considered to be made up of two components; a compact layer of ions next to the electrode located at OHP and a diffuse layer extending from the OHP into the bulk

solution. This way, the double layer resembles two capacitors arranged in series, illustrated by the expression:

$$\frac{1}{C} = \frac{1}{C_i} + \frac{1}{C_d} \qquad 2\text{-}5$$

where C is the double layer capacitance, C_i is the capacitance of the compact layer and C_d is the capacitance of the diffuse layer. The potential drop across the compact layer from the electrode to the OHP is linear, but becomes nonlinear from OHP toward the bulk solution. Therefore, this model (GCS) appears to account for the behavior of real systems. However, there are still some discrepancies, in that, C_i is dependent on the potential.

Grahame's model (1947), is a refined version of the GCS model [32]. The three models discussed so far consider the long range effects, e.g., electrostatic forces, thermal energy and ionic size (radius) as the only factors that dictate the formation of excess charge on the solution side of the interface. The short range effects such as chemical interactions of ions with the electrode (specific adsorption) are ignored. Since these interactions are short range, the specifically adsorbed species are rigidly linked to the electrode. The only difference between the GCS model and Grahame's model is that Grahame's model, goes further to account for the existence of specifically adsorbed species.

Specifically adsorbed species (ions) must lose their solvation sheath in order to closely approach the electrode surface. The interaction of these species with the electrode leads to a strong binding even though in some cases, the adsorbed species may possess the same charge as the electrode. A plane drawn through the center of the specifically adsorbed ions is the inner Helmholtz plane (IHP). The OHP is the plane drawn through the center of the solvated and nonspecifically adsorbed ions while the diffuse layer extends from the OHP into the bulk solution.

Therefore, according to the Grahame model, the electrode-electrolyte interface consists of three parts (Figure 2-5): the metallic phase, the inner and the outer (diffuse) layers on the solution side of the interface [38]. In general the metallic phase bears a net electrical charge on its surface because of an excess or deficit of electrons. The excess charge density on the metal surface is σ_M.

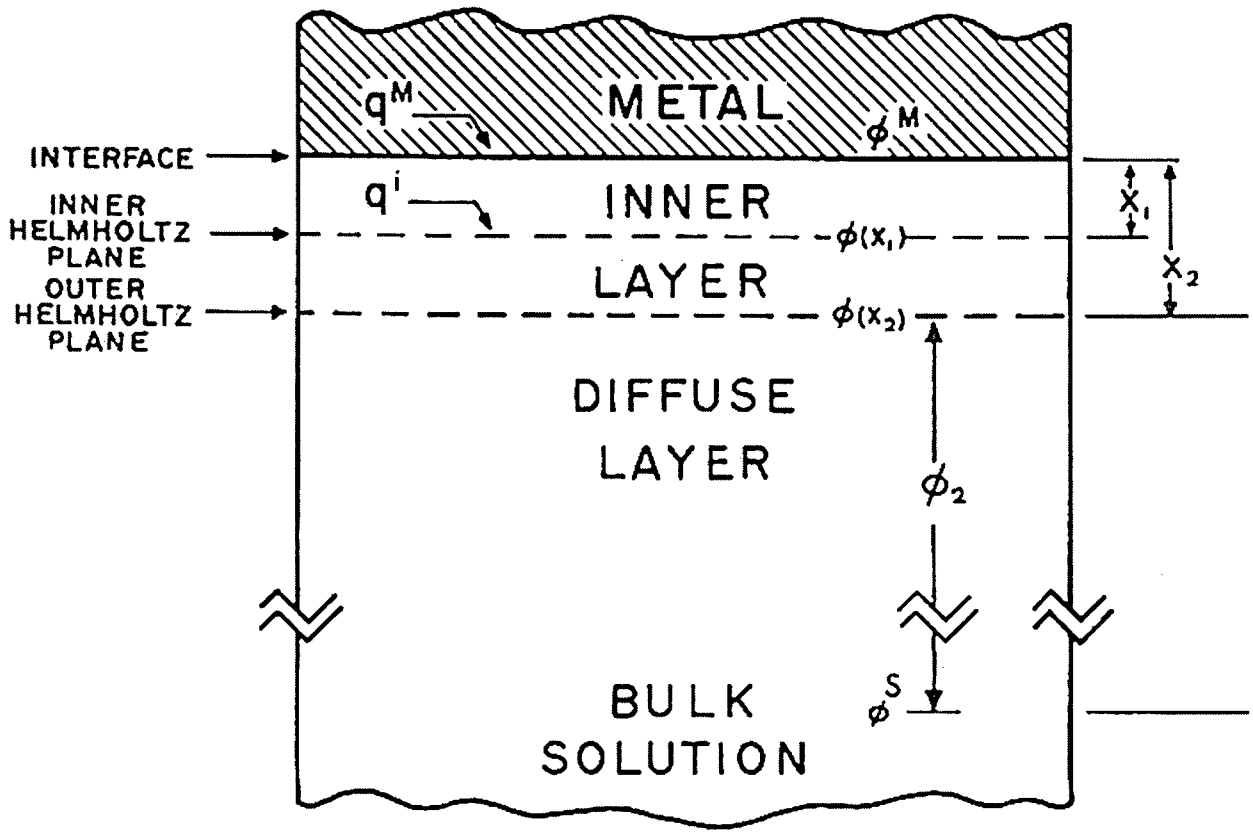

Figure 2-5 The schematic diagram showing the structure of electrical double layer for a system consisting of a metal electrode in contact with aqueous electrolyte solution. Taken from [38].

The inner layer (compact and rigid), on the solution side of the interface contains solvent molecules, adsorbed neutral molecules and a monolayer of specifically adsorbed anions (Figure 2-6). The charge density in the inner layer is σ_i and the potentials are $\phi(x_1)$ at a distance x_1 (IHP) and $\phi(x_2)$ at a distance x_2 (OHP) from the electrode surface respectively. Not all nonspecifically adsorbed ions are located at OHP but some are also contained in the diffuse layer and the excess charge density is σ_d. The total charge in the solution (inner and diffuse layers) is σ_s. At equilibrium, the electrical neutrality of the interface region must be maintained, thus

$$\sigma_M = -\sigma_s = -(\sigma_i + \sigma_d) \qquad 2\text{-}6$$

The presence of electrical charges in the interfacial region has a pronounced effect on the interfacial tension. In addition, adsorbed molecules or ions affect the interfacial tension. Measurements of interfacial tension can provide quantitative information about the double layer.

2.3 Quantitative Description of the Double Layer

2.3.1 Electrocapillary curves

Electrocapillarity, developed for mercury, involves the measurements of surface tension (γ) of a mercury-electrolyte interface with potential, E. The technique is based on counterbalancing the forces of gravity and surface tension of Hg-electrolyte interfaces. A plot of γ vs. E yields the electrocapillary curve (Figure 2-7). A modification of electrocapillarity measurements utilizes a dropping mercury electrode in which the lifetime, τ, of Hg drop is measured with respect to potential. A curve similar to the electrocapillary curve is obtained when τ is plotted vs. E. The first derivative of surface tension with respect to potential yields the interfacial charge and is the Lippman equation

$$\frac{\partial \gamma}{\partial E} = -\sigma_M = \sigma_s \qquad 2\text{-}7$$

From the Lippman equation, the charge σ_M is zero when the gradient of the electrocapillary curve is zero. The corresponding potential is the potential of zero charge (pzc), and it occurs at the maximum in the electrocapillary curve (electrocapillary maximum). The second derivative of the

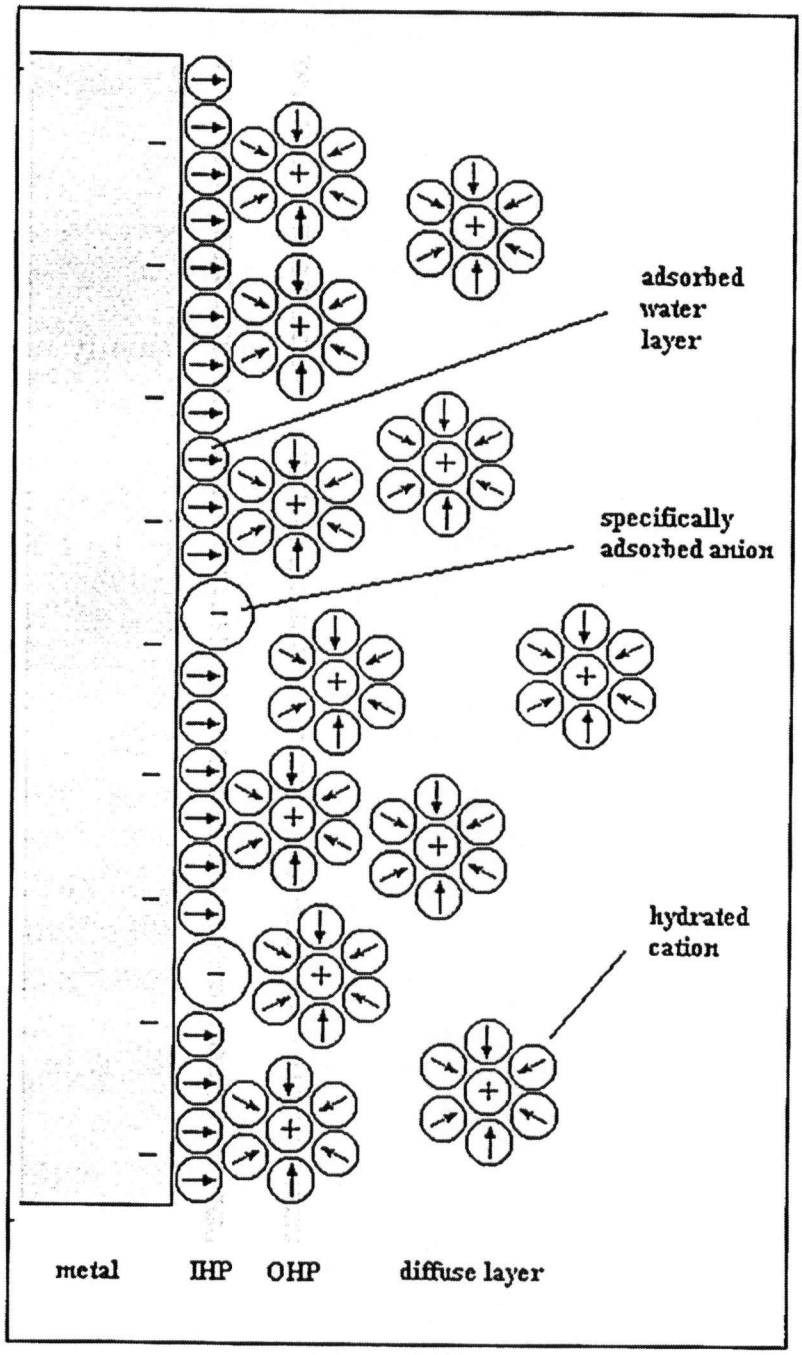

Figure 2-6 A schematic diagram showing a model of electrical double layer as proposed by Grahame. Taken from [38].

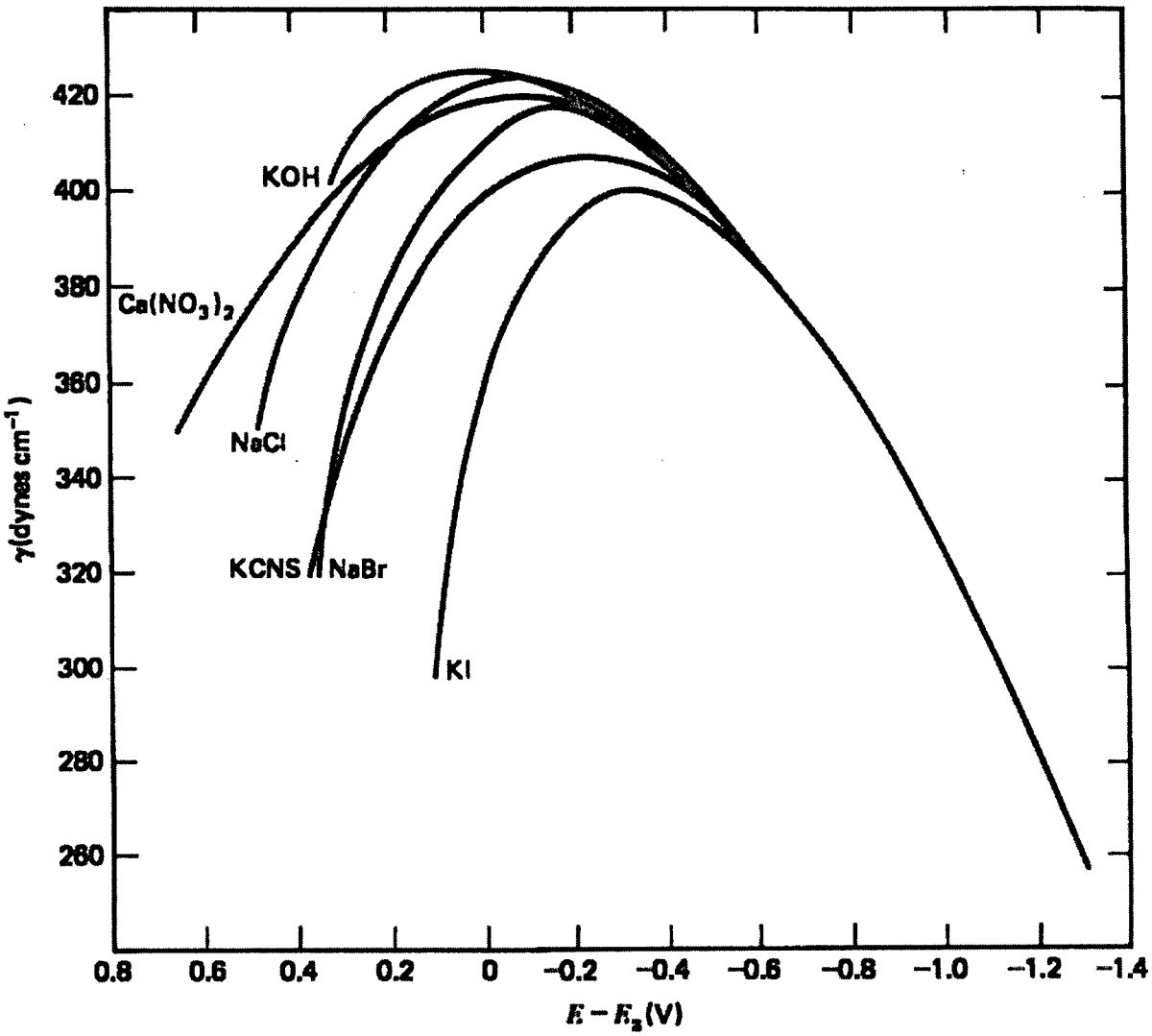

Figure 2-7 The diagram showing the electrocapillary curve of surface tension against potential for Hg electrode in contact with different electrolyte solutions as indicated in the diagram. The potential was plotted with respect to the pzc for NaF. Taken from [32].

electrocapillary curve or the first derivative of charge with respect to potential gives the interfacial capacity

$$C = \frac{\partial \sigma_M}{\partial E} = \frac{\partial^2 \gamma}{\partial E^2} \qquad 2\text{-}8$$

where C is the differential capacitance.

In the simplest double layer model (Helmholtz model) the interface is described as consisting of excess charge on the solution side in a thin slab near the metal surface. The charges in the solution counterbalances the excess charges on the metal, hence a charge separation that mimics a capacitor. This can be described by

$$\sigma_s = \frac{\varepsilon\varepsilon_o}{d} E; \frac{\partial \sigma}{\partial E} = C = \frac{\varepsilon\varepsilon_o}{d} = \frac{\varepsilon\varepsilon_o}{x_2} \qquad 2\text{-}9$$

This expression (equation 2-9) predicts that the capacitance will be constant over a large potential range, which is not true experimentally. According to this model, the potential drop across the interface is given by the equation

$$E = \frac{\sigma}{\varepsilon\varepsilon_o} x_2 \qquad 2\text{-}10$$

The potential drop has a linear behavior with distance as in the electric capacity counterpart. Differentiating equation 2-10 and substituting in Lippman equation (Equation 2-7) and rearranging gives

$$-d\gamma = \frac{x_2}{\varepsilon\varepsilon_o} \sigma d\sigma \qquad 2\text{-}11$$

Integrating equation 2-11 results into

$$\gamma + \text{const} = -\frac{x_2}{2\varepsilon\varepsilon_o} \sigma^2 \qquad 2\text{-}12$$

where the constant of integration is the maximum surface tension when $\sigma = 0$. Substituting

equation 2-12 in an expression for potential (equation 2-10) while noting that the maximum surface tension occurs at the potential of zero charge (pzc),

$$\gamma = \gamma_{\max} - \frac{\varepsilon\varepsilon_o}{2x_2}\left(E - E_{pzc}\right)^2 = \gamma_{\max} - \frac{1}{2}C\left(E - E_{pzc}\right)^2 \qquad 2\text{-}13$$

Equation 2-13 predicts that a plot of γ vs. E is a symmetric parabola. But this is not observed for all electrolyte compositions, e.g., Cl, I, and Br anions particularly at positive potentials (see Figure 2-7). The greatest advantage of the Helmholtz model is that it is simple and conforms to some experimental data. However, it fails to explain the often observed dependence of the double layer capacitance on the potential and the electrolyte concentration. It also does not account for the interactions that occur further away from the electrode.

2.3.2 Potential distribution in the interfacial region

The Gouy-Chapman model only treats the diffuse part of the double layer and this is used to describe the interface starting at OHP ($x = x_2$). The distribution of the species with distance from the electrode obeys Boltzmann's law and Poisson's equation that relates the potential with the charge distribution. Thus, the Poisson-Boltzmann equation for the system is

$$\frac{d^2\phi}{dx^2} = \frac{-e}{\varepsilon\varepsilon_o}\sum_i n_i^o z_i \exp\left(\frac{-z_i e\phi}{kT}\right) \qquad 2\text{-}14$$

where z is the signed charge on an ion i and n_i^o is the number of concentrations of ions in the bulk.

Realizing that, $\frac{d^2\phi}{dx^2} = \frac{1}{2}\frac{d}{d\phi}\left(\frac{d\phi}{dx}\right)^2$ equation 2-14 can be rewritten and integrated while noting that at a distance far away from the electrode surface, $x \to \infty$, $\phi = 0$ and $\left(d\phi/dx\right) = 0$ which allow for the determination of the integration constant, thus

$$\left(\frac{d\phi}{dx}\right)^2 = \frac{2kT}{\varepsilon\varepsilon_o}\sum_i n_i^o\left[\exp\left(\frac{-z_i e\phi}{kT}\right) - 1\right] \qquad 2\text{-}15$$

For the system containing only symmetrical electrolytes (z-z), the strength of the electric field from $x_2 \rightarrow \infty$ is given by

$$\frac{d\phi}{dx} = -\left(\frac{8RTc_{bulk}}{\varepsilon\varepsilon_o}\right)^{1/2}\sinh\left(\frac{ze\phi}{2kT}\right) \qquad 2\text{-}16$$

An expression for the potential profile in the diffuse region can be obtained by integrating equation 2-16 with the boundary condition $\phi = \phi_2$ at OHP, and defining $x = x_2$ for z-z electrolytes, thus

$$\frac{\tanh\left(ze\phi/4kT\right)}{\tanh\left(ze\phi_2/4kT\right)} = \exp\left[-\kappa\left(x - x_2\right)\right] \qquad 2\text{-}17$$

where $\kappa = \left(\frac{2z^2F^2c_{bulk}}{\varepsilon\varepsilon_o RT}\right)^{1/2}$ and is the inverse of the Debye length and characterizes the decay of potential from the OHP to the bulk solution. Equation 2-17 describes the potential profile in the diffuse layer as shown in Figure 2-8. At large ϕ_2 the drop is large because the diffuse layer is compact. As ϕ_2 becomes smaller, the potential drop is more gradual and approaches exponential form. The reciprocal of κ has a dimension of distance and characterizes the spacial decay of potential. It can be regarded as a kind of characteristic thickness of the diffuse layer.

The electric field at OHP ($x = x_2$), is calculated using Gauss's law, and the charge density at the electrode is given by

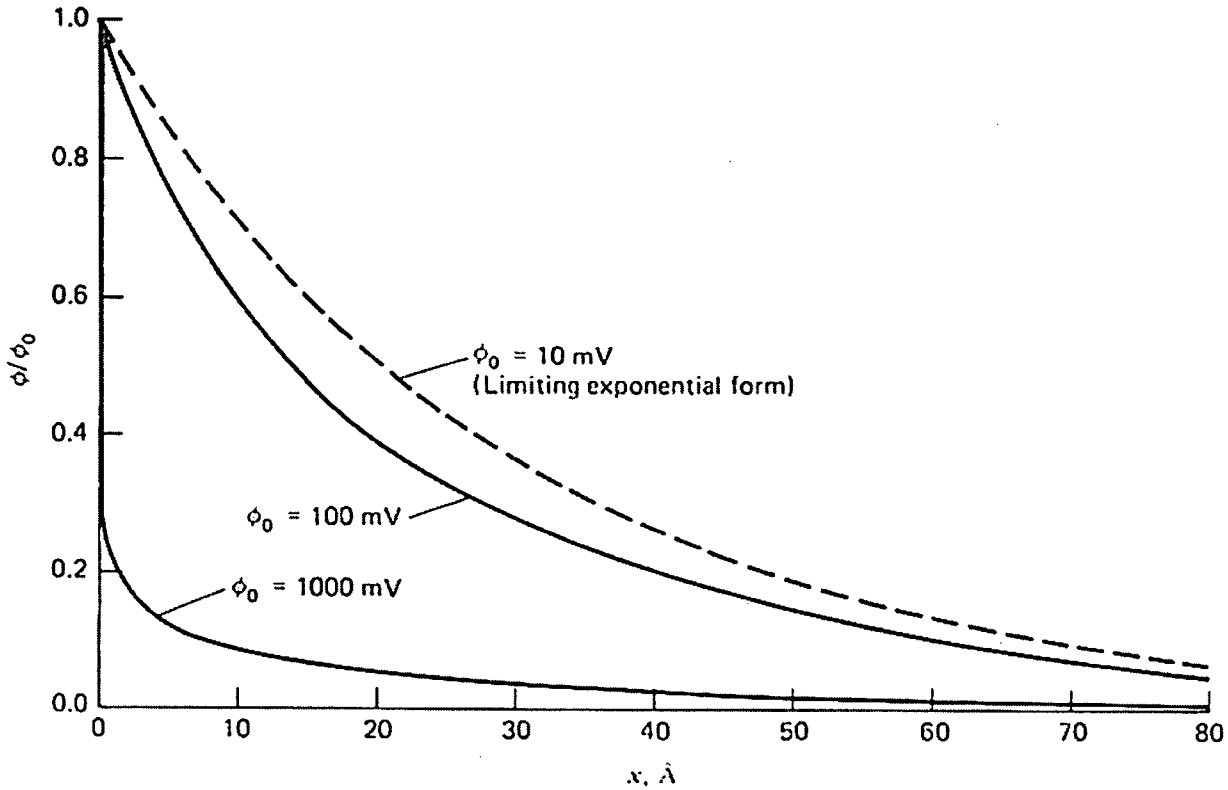

Figure 2-8 The diagram for potential profile across the diffuse region of the electrical double layer as proposed by Gouy-Chapman model. The plot was generated for a 10^{-1} M aqueous solution of a 1:1 electrolyte at 25 °C using equation 2-18. Taken from [32].

$$\sigma_M = -\sigma_s = \left(8\varepsilon\varepsilon_o RTc_{bulk}\right)^{1/2} \sinh\left(\frac{zF\phi_2}{2kT}\right) \qquad 2\text{-}18$$

The differential capacitance is predicted by differentiating equation (2-18) to give

$$C = \frac{d\sigma_M}{d\phi_2} = \left(\frac{2z^2F^2\varepsilon\varepsilon_o c_{bulk}}{kT}\right)^{1/2} \cosh\left(\frac{zF\phi_2}{2kT}\right) \qquad 2\text{-}19$$

Figure 2-9 is a graph showing the way in which C varies with the potential according to equation 2-19. There is a minimum at potential of zero charge (pzc) and a steep rise on either side. The predicted V-shaped capacitance curve does resemble the observed behavior in NaF at low concentrations not far from pzc. However, there is flattening in capacitance at more extreme potentials and the valley at pzc disappears at higher electrolyte concentrations.

According to Gouy-Chapmann-Stern model, the ions have finite sizes and are not point charges. Therefore, the ions can only approach the electrode surface at finite distances. For z-z electrolyte, the charge on the metal is given by

$$\sigma_M = (8\varepsilon\varepsilon_o RTc_{bulk})^{1/2} \sinh\left[\frac{zF}{2RT}\left(\phi_m - {}^{\sigma_m x_2}\!/_{\varepsilon\varepsilon_o}\right)\right] \qquad 2\text{-}20$$

Solving for σ_M and differentiating equation 2-20 with respect to a potential at the metal surface, the differential capacity is given by

$$\frac{1}{C} = \frac{x_2}{\varepsilon\varepsilon_o} + \frac{1}{\left(2\varepsilon\varepsilon_o z^2F^2c_{bulk}/RT\right)^{1/2}\cosh\left(zF\phi_2/2RT\right)} \qquad 2\text{-}21$$

This expression (equation 2-21) reveals that the capacitance is made up of two components that resemble exactly two capacitors in series. The double layer is separated into the inner layer ($x = 0$ at x_2) and the diffuse layer ($x \rightarrow \infty$). In the absence of specific adsorption, the electric field across the inner layer is constant and the potential drop across the inner layer is therefore linear. However,

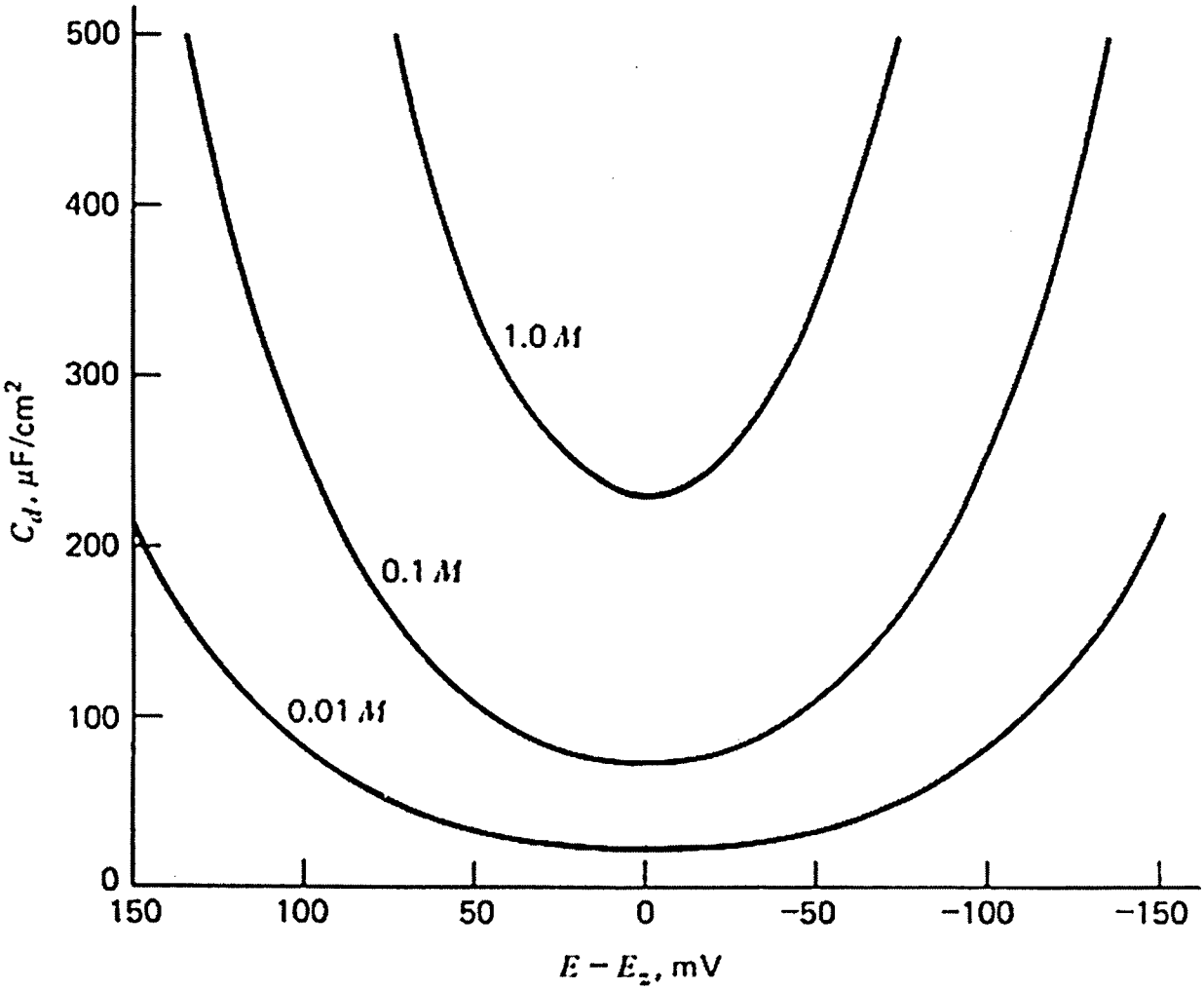

Figure 2-9 The diagram illustrating the predicted capacitance based on Gouy-Chapman theory. The graph was generated using equation 2-20 for indicated different electrolyte concentrations of a 1:1 aqueous electrolyte at 25 °C. Taken from [32].

the potential drop across the diffuse layer is nonlinear. The total potential drop ϕ_M (Figure 2-10) is then the sum of the contributions from the two regions.

Figure 2-11, shows the capacitance behavior according to the Grahame model. The capacitance of the inner layer is independent of potential whereas that of the diffuse region varies with potential. The double layer capacitance is therefore characterized by a complex behavior and is dominated by the smaller capacitance of the two. A V-shape behavior is always observed at potentials around pzc for low electrolyte concentrations, which is a typical characteristic of diffuse layers. For nonspecifically adsorbing electrolytes, a minimum occurs at pzc and provides a means of measuring the pzc. At high polarizations in low electrolyte environments or at high electrolyte concentrations, only the capacitance of the inner layer is observed because the capacitance of the diffuse layer is so large that its contribution to the double layer capacitance is negligible.

2.4 Thermodynamics of Electrified Interfaces

The Gibbs adsorption isotherm [32,34] has been applied to investigate the thermodynamics of electrified interfaces. A real interface is composed of two homogeneous phases in contact forming an interface of an undefined dimension. Therefore for two phases α and β in contact, an interfacial region of area, A, must exist. If the components in each phase are present at a uniform concentration up to the interface, a sharp boundary will divide the two phases. However, the components in the two phases are not distributed uniformly from their respective bulk concentrations up to the interface. Therefore, an excess amount of either component exists at the interface. This excess is expressed per unit interfacial area, A, and is known as surface excess (Γ) given by

$$\Gamma_i = \frac{n_i^A}{A} \qquad 2\text{-}22$$

where $n_i^A = n_i - \left(n_i^\alpha + n_i^\beta\right)$, the difference between the total amount of i in the system (n_i) and the amount in the bulk phases. This surface excess can be either negative or positive representing an excess or deficiency respectively.

Gibbs model (Figure 2-12), is an estimation of a real interface. The interfacial region is divided into two without defining the location of the dividing plane. This is crucial because the

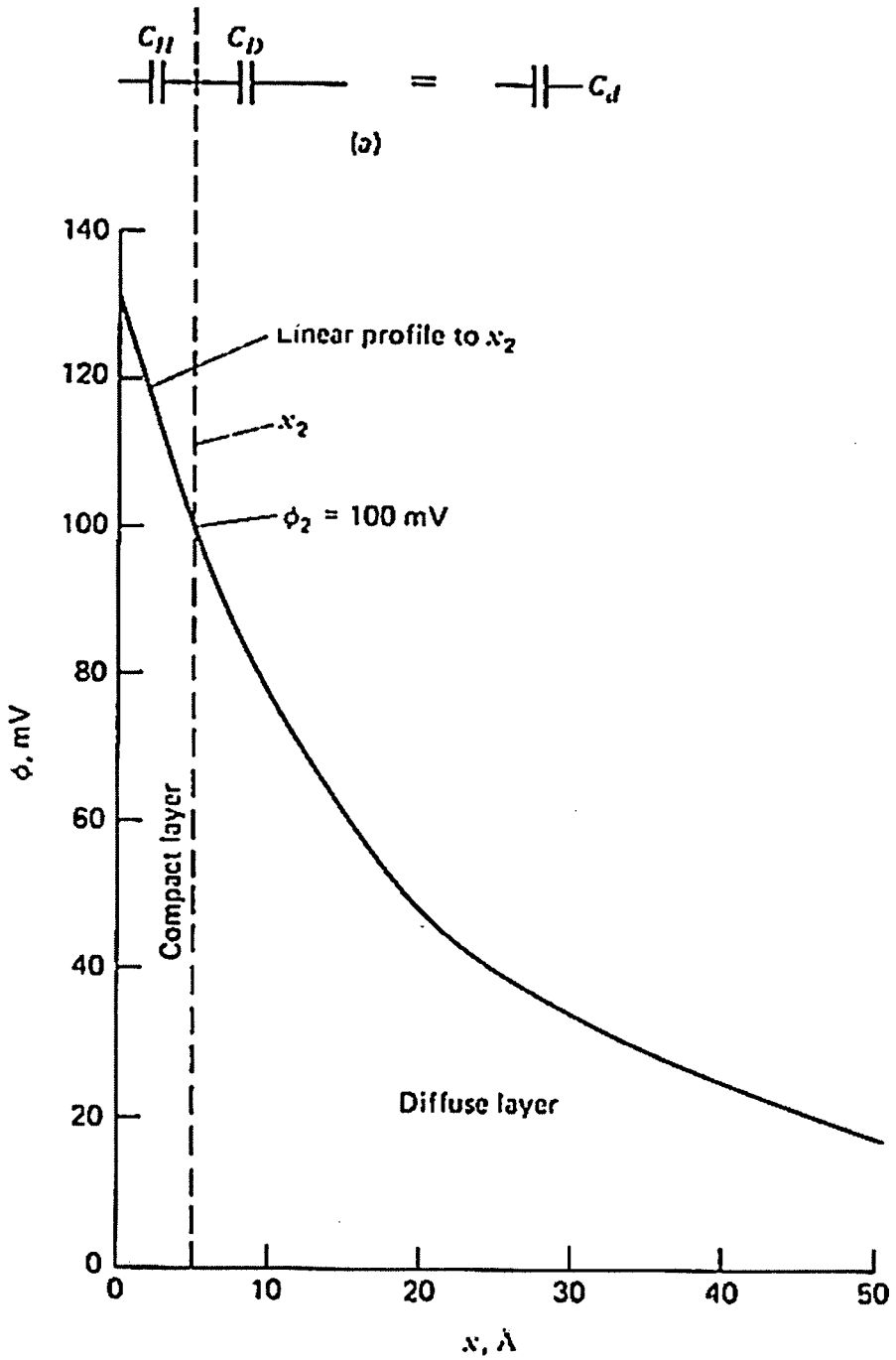

Figure 2-10 The diagram of potential profile through the electrical double layer as proposed by GCS model. (a) The equivalent circuit analog. (b) The potential profile across the double layer. Taken from [32].

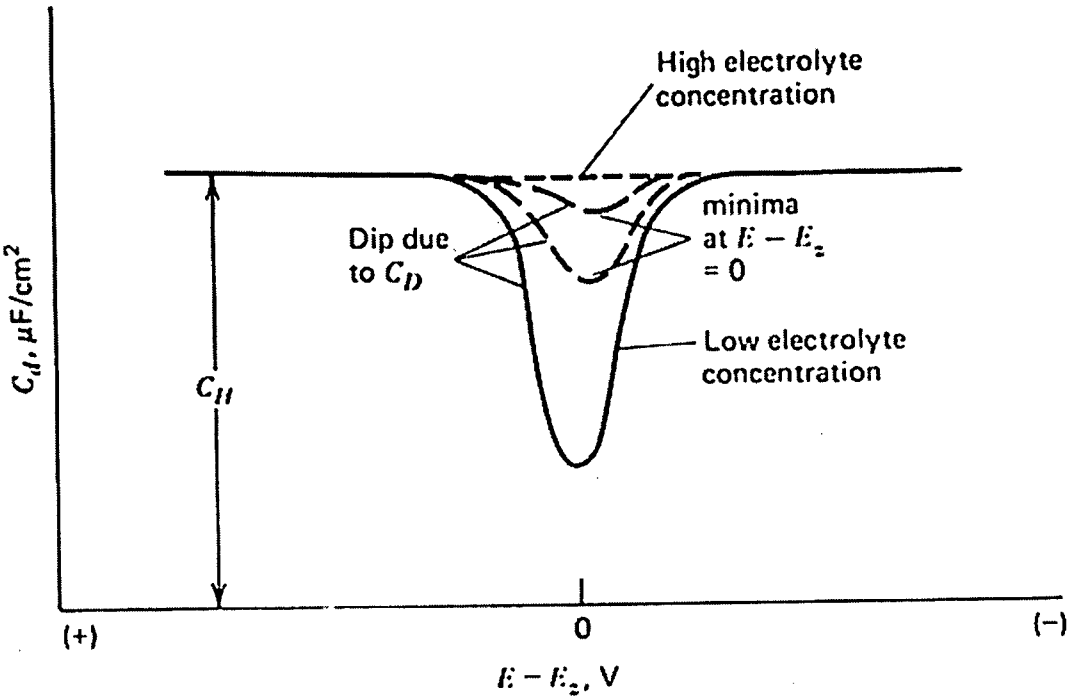

Figure 2-11 A schematic diagram of the predicted double layer capacitance behaviour as put forward by GCS theory. Taken from [32].

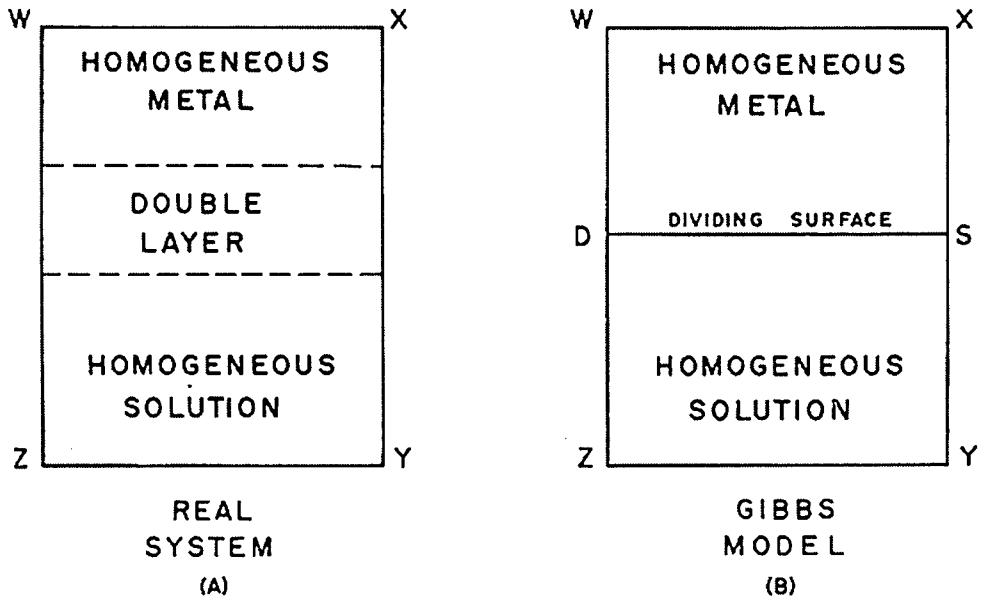

Figure 2-12 A schematic representation of (a) a real system and (b) Gibbs model. Taken from [38].

charge contained in this region cannot be placed at any particular position. An adsorption isotherm for this model is then derived relating the interfacial tension (γ) to the surface excess (Γ_i) and electrochemical potential ($\overline{\mu_i}$), thus

$$-d\gamma = \sum_i \Gamma_i d\overline{\mu_i} \qquad 2\text{-}23$$

Gibbs adsorption equation has been employed to generate the electrocapillary equation [38] for an IPE in a MX electrolyte and in the presence of a neutral molecule L. If the potential of the electrode is measured with respect to a reference electrode, which is reversible with respect to anions or water results in a general expression for the electrocapillary equation commonly known as Gibbs-Lippman equation

$$-d\gamma = \sigma_M dE_- + \sum_i \Gamma_i\left(H_2O\right)d\mu_i \qquad 2\text{-}24$$

Where $\Gamma_i\left(H_2O\right)$ is the Gibbs excess with respect to reference species (H_2O)

If the conditions are such that the solution composition remains constant, i.e., $d\mu_i = 0$, and also at constant temperature and pressure, the Gibbs-Lippman equation simplifies to become the Lippman equation

$$\left(\frac{\partial\gamma}{\partial E}\right)_{T,P,\mu_i} = -\sigma_M \qquad 2\text{-}25$$

The Lippman equation has contributed greatly to the study of adsorption onto mercury electrodes. The fundamental reason behind this success is the fact that the surface tension of mercury electrodes can be directly and easily measured from experiments.

Measurements of changes in the surface tension as a function of chemical potential yields Gibbs excess. By performing cross-differentiation on the electrocapillary equation, some useful relationships between variables are linked a shown bellow

2.5 Adsorption of Neutral Organic Molecules

In the previous section, the importance of electrocapillary equation to the investigation of adsorption of organic molecules particularly onto Hg electrodes was highlighted. The uniqueness of the equation for this type of electrode was also emphasized. The Lippman capillary electrometer technique allows for the direct determination of the interfacial tension of Hg-electrolyte interfaces as a function of rational potential ($E - E_{pzc}$). Each electrocapillary curve is parabolic with respect to potential in non specifically adsorbing electrolyte [38]. From the electrocapillary equation, Gibbs excess is given by

$$\left(\frac{\partial\gamma}{\partial\mu_i}\right)_{T,P.E_-,\mu_{j\neq i}} = -\Gamma_i\left(H_2O\right) \qquad 2\text{-}26$$

The charge density on the metal surface can be determined by differentiation, i.e., the first derivative of ($\gamma - E$) curves at constant electrolyte activity

$$\sigma_M = -\left(\frac{d\gamma}{dE}\right)_{T,P,\mu_{j\neq i}} \qquad 2\text{-}27$$

The first derivative of charge density with potential or the second derivative of surface tension with potential is the capacitance

$$C = \left(\frac{d\sigma}{dE}\right)_{T,P,\mu_{j\neq i}} = \left(\frac{d^2\gamma}{dE^2}\right)_{T,P,\mu_{j\neq i}} \qquad 2\text{-}28$$

Adsorption of surfactants (organic molecules) onto electrified interfaces has been extensively investigated and has been found to have some resemblance with ionic adsorption. In general, surfactants cause a depression in the interfacial tension at interfaces (Figure2-13). Applied potential also has an effect on the determination of the degree of interfacial tension lowering hence producing amazing electrocapillary curves. In contrast to ionic adsorption, the organic adsorption curves

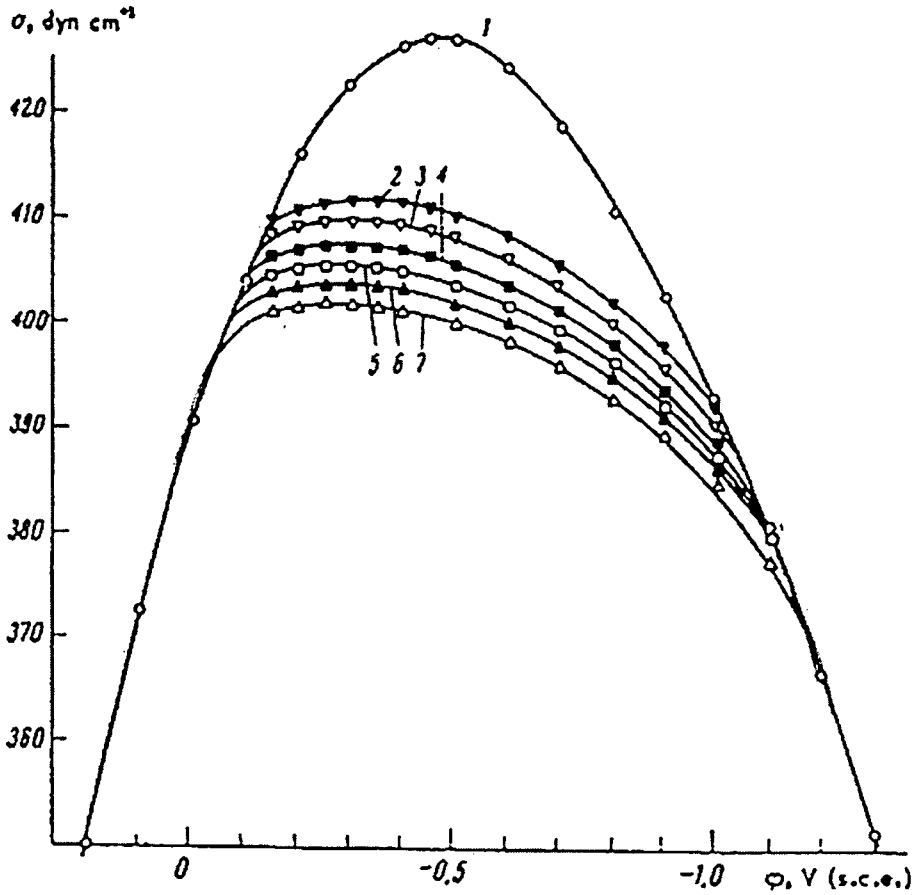

Figure 2-13 The diagram illustrating the electrocapillary curves for the adsorption of pentanol onto Hg electrode in 0.1M Na_2SO_4 containing various molar (M) concentrations of pentanol:(1); 0 (2) 0.01; (3) 0.02; (4) 0.025; (5) 0.03; (6) 0.04; and (7) 0.05. Taken from [38].

display a phenomenon in which on both arms of the curve, the interfacial tension is equal in the presence and absence of organic compound. This is evidence of the power of potential to displace the surfactant from the interface through substitution by water. The fact that the adsorbed organic molecules are assumed to form monolayers, the Gibbs excess is regarded as surface concentration and therefore the surface excess is given by

$$\left(\frac{\partial \gamma}{\partial \mu_L}\right)_{T,P.E_-} = -\Gamma_L \qquad 2\text{-}29$$

where L is the molecular adsorbate.

The interfacial tension is related to charge and capacitance shown previously. Since the measurements of the surface tension is tedious, the modern investigations have shifted attention to the measurements of capacitance by ac perturbation techniques. This technique is used in the current study. So by performing multiple integrations on either measured charged density or capacitance, the electrocapillary curve can be obtained

$$\gamma = \gamma^* - \int_{E^*}^{E} \sigma dE$$
$$\gamma = \gamma^* - \int_{E^*}^{E}\int_{E^*}^{E} C dE^2 \qquad 2\text{-}30$$

where E^* is the potential for which the surface tension, γ^* , which is the integration constant (usually known). It is worthwhile to note that these values are not easily determined. Moreover, the extension of this method to solid electrodes is equally difficult because of the dependence of capacitance on the frequency of measurements.

Organic surfactants generally generate a depression in the interfacial tension at the electrode-electrolyte interface in reference to Hg in the absence of surfactant. The degree of this interfacial tension lowering is the film pressure, π, expressed as

$$\pi(E_i) = \gamma_{\theta=0} - \gamma_\theta = \int_{E^*}^{E} \sigma_{m,\theta=0} dE - \int_{E^*}^{E} \sigma_{m,\theta} dE \qquad 2\text{-}31$$

Where θ is coverage of organic species.

This film pressure is equivalent to the difference between the electrocapillary curves measured on Hg in the presence and in the absence of the surfactant. The Gibbs excess is determined by differentiating the film pressure with respect to natural log of concentration. Thus

$$\Gamma = \left(\frac{\partial \pi}{RT \ln c} \right)_{T,P,E} \qquad 2\text{-}32$$

The capacitances of aliphatic compounds [39] exhibit a region of low capacitance symmetrical around the potential of zero charge (pzc). On each side of this region, pseudo-capacitance peaks occur, corresponding to dramatic changes in coverage at the electrode surface (Figure 2-14). When the surface is highly polarized, the capacitance in the presence and absence of surfactant merge, demonstrating that the surfactant has been displaced from the electrode surface [40,41]. The formation of these peaks is accompanied by a change in the dielectric constant hence current flow. These peaks are strongly dependent on the frequency of ac perturbation used for differential capacitance measurements. Therefore, the capacitance which is related to charge and which is considered a function of potential (E) and the surface excess (Γ), is given by

$$C = \left(\frac{\partial \sigma_M}{\partial E} \right)_\mu = \left(\frac{\partial \sigma_M}{\partial E} \right)_\Gamma + \left(\frac{\partial \sigma_M}{\partial \Gamma} \right)_E \left(\frac{\partial \Gamma}{\partial E} \right)_\mu = C_{true} + C_{pseudo} \qquad 2\text{-}33$$

The pseudo-capacitive peaks are sensitive to the kinetics of the adsorption-desorption process and therefore should exhibit frequency dependent. At very high frequency, the establishment of the adsorption-desorption is not accurate thus the term $\left(\frac{\partial \Gamma}{\partial E} \right)_\mu$ is zero and only capacitance C_{true} is measured leading to no peaks. The total capacitance measured is the contribution of C_{true} and

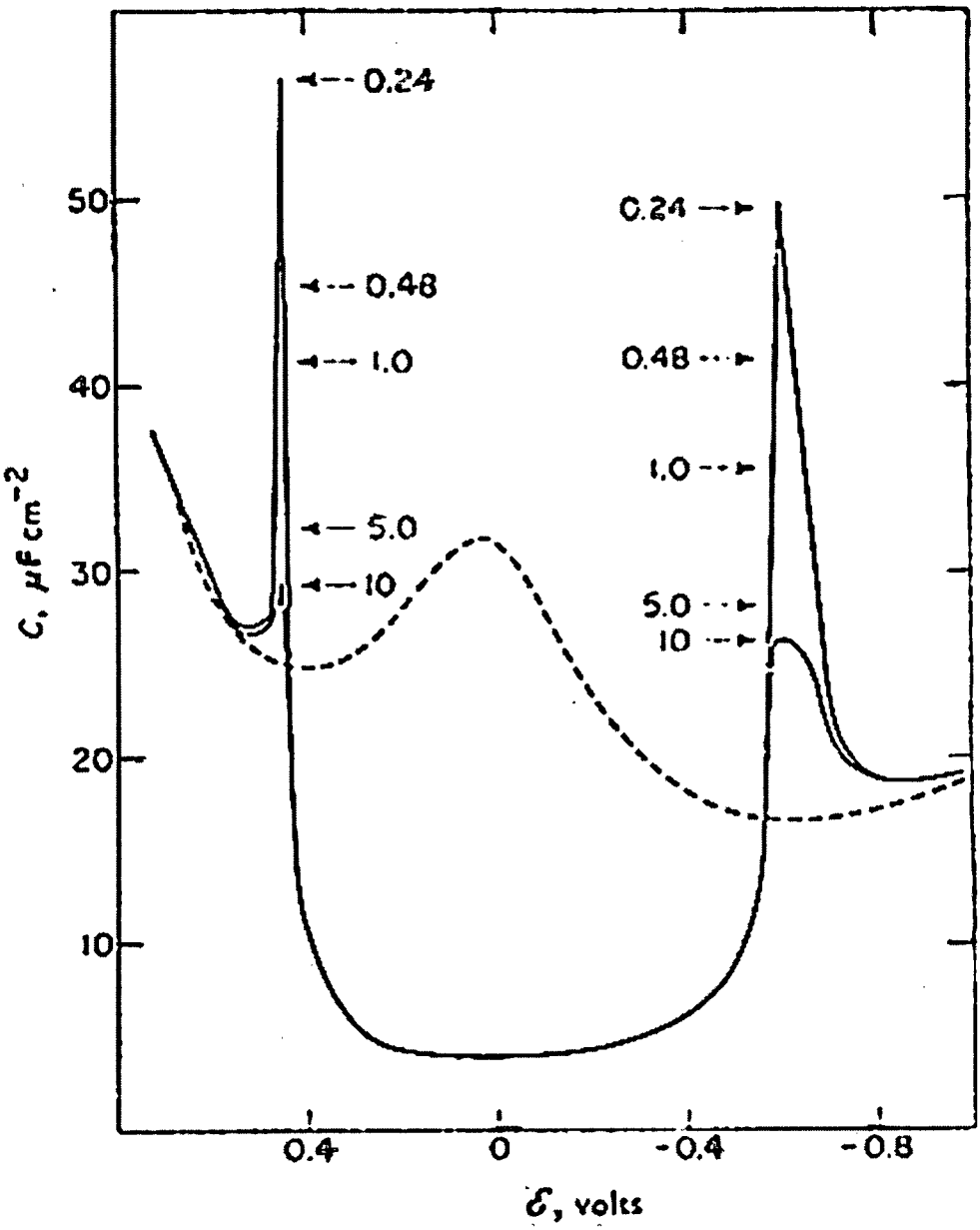

Figure 2-14 The diagram of differential capacitance of Hg electrode in contact with aqueous 1M KNO_3 at 25°C. indicated by dotted line. The full line indicates the capacity of the same electrode after the solution has been saturated with actyl alcohol. The arrows shows the height of the peak at other frequencies. Taken from [39].

C_{pseudo}. The pseudo-capacity is the product of electrosorption valency and the change in surface coverage with potential. It has been shown that the C_{pseudo} decreases from some equilibrium value at zero perturbation frequency to zero value at very high frequencies. These properties have been used to characterize the kinetics of adsorption/desorption processes at the electrode surface.

2.6 Biological Cell Membrane

2.6.1 Introduction

Biological membranes perform crucial functions in almost all cellular cells. In this section, a brief discussion of the biological membranes is presented since they are important in the current study. The discussion commences with the cell followed by some illustrations of the structural features of a biological membrane. A description of biological membrane composition and the discussion of membrane phospholipids will follow.

2.6.2 The cell

Life is characterized by an inconceivable heterogeneity of species of flora and fauna, which traverse infinitesimal bacteria to huge animals not forgetting microscopic algae to giant plants. Equally amazing is the underlying fact that these animals and plants have one thing in common; they are all made from cells, the smallest and autonomous units essentially believed to be "living"

Science has revealed immense information regarding structures of cellular membranes during the last century through the development of sophisticated instruments [42-44]. It is now known that inside the cells there are even tinier ingredients. Notwithstanding how far science has come, the fact remains that the intended goal of fully understanding the chemistry of life processes of the participating molecules is still far from being realized. Living cells consist of very complex collection of macromolecules each having millions of atoms. The most renowned of all these is of course the deoxyribonucleic acid DNA, in which the genetic code is stored. Next in hierarchy are proteins, which are the work stations of the cells. Nonetheless, the molecules that are investigated in the current study are neither proteins nor DNA but lipids, which on face value, are less captivating. However, they form the backbone of cellular membranes.

2.6.3 *Structure of biological membrane*

It took many years to uncover the structure of the cell membrane [45,46], until 1972 when the fluid mosaic model [47] was put forward. This is now recognized as the foundation for understanding the cell membrane. The lipids which form a bilayer and the protein molecules that are embedded in the lipid bilayer are indeed the cornerstones of this model. As the name suggests, the lipid bilayer is two layers of lipids sandwiched together (Figure 2-15). The plasma membrane, which is the outermost component enveloping the cell from its environment is made up of phospholipid bilayer and proteins molecules among other ingredients. It is perhaps the most important structure because it regulates all manner of interactions between the cell and its surroundings. One such important function is its screening role, in which it permits the diffusion of some substances but not others. Moreover, the membrane acts as a host for membrane proteins which transport ions across the membrane. This barrier functionality is critical for the physiological activity of cells [48].

The cell membrane, itself a phospholipid-protein bilayer, is highly non polar and a dielectric with a dielectric constant of about 9. Ions diffuse into and out of the cell via ion channels situated in the cell membrane. Since the lipid bilayer acts as a barrier to the diffusion of ions due to the selectivity of ion channels, an electric potential difference of about -60 to -70mV is typically established across the membrane.

2.6.4 *Biological membrane composition*

Biological membranes [49-52] regardless of origin, consist of lipids and proteins. Their ratios vary immensely and the heterogeneity in lipid composition is equally vast. The most commonly found molecules are glycerophospholipids, for instance phosphatidylcholine, phosphatidylethanolamine, and phosphatidylglycerol. Another membrane constituent is cholesterol which constitutes a large portion of the plasma membrane of mammalian cells. Plasma membranes have approximately one cholesterol per phospholipid molecule. The cholesterol molecule inserts itself in the membrane with the same orientation as the phospholipid molecule. They make the lipid bilayer less deformable and decrease its permeability. The proteins are located such that they can

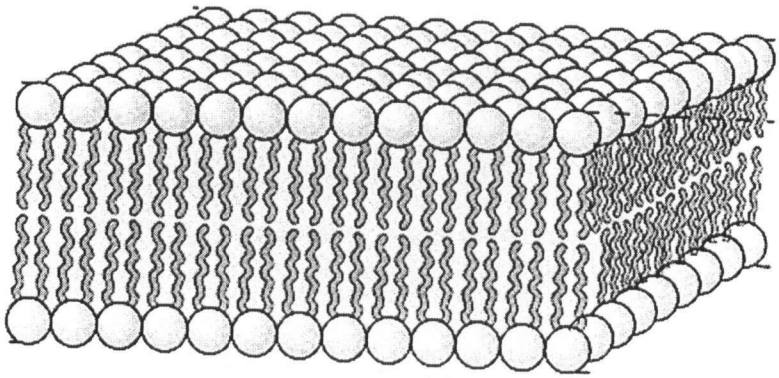

Figure 2-15 A schematic representation of a lipid bilayer formed from phospholipid molecules. Taken from [51].

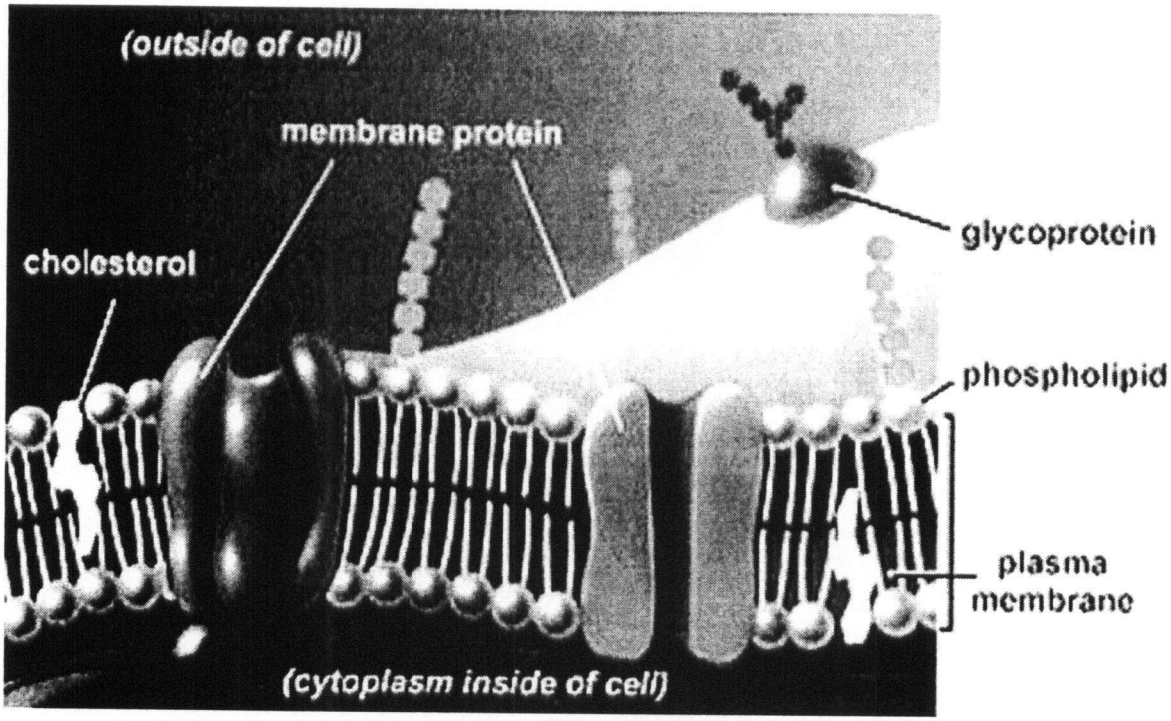

Figure 2-16 The diagram of a biological cell membrane showing the complexity in the composition of membrane structure. Taken from [53].

completely penetrate the membrane (trans membrane proteins) or are bound to one of the two lipid bilayer (peripheral membrane proteins) in which case they may be on the inside or outside of the cell. They may be protective, insulators, and sites of receptor binding. In addition, many membranes also contain carbohydrates bound to proteins or lipids. Figure 2-16 is a pictorial representation of this complex composition [53].

The rationale behind this complexity and diversity in composition is not yet well grasped. Therefore, it is only appreciated that a functional biomembrane is a complex infrastructure. Despite this complexity, the fundamental physio-chemical characteristics of membrane are dictated by the lipid molecules [54-57].

2.6.5 Membrane phospholipids

The lipids studied in this thesis are phospholipid, which are the primary component of all cellular membrane. Phospholipids are amphipathic [49]; that is they are both hydrophilic and hydrophobic. The head of a lipid molecule is negatively charged phosphate group and the two tails are highly hydrophobic hydrocarbon chain. Phospholipid tail will assemble together to form a hydrophobic atmosphere. This leaves the charged phosphate group facing out to the hydrophilic environment. Phospholipids can form three structures due to their ampiphatic nature, namely micelles, planner lipid bilayer and spherical lipid bilayer (vesicles).

The structure of phospholipids influences their packing and movement in the lateral plane of the membrane.The lipid bilayer gives the membrane its fluid characteristics. At low temperatures, the bilayer is in gel state and tightly packed. At higher temperatures, the bilayer melts and the interior is fluid allowing the lipid molecules to move around and rotate [58]. The phospholipid molecule used in this study is dioleoyl phosphatidylcholine DOPC. It consists of two unsaturated 18-carbon chains bonded to a phosphogylceride called phosphatidylcholine as shown in figure 2-17.

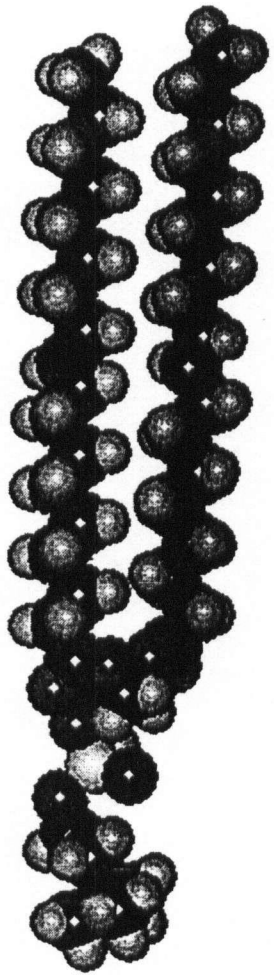

Figure 2-17 A Schematic diagram of Dioleoyl phosphatidylcholine (DOPC) molecule.

2.7 Electrochemical Impedance Spectroscopy

2.7.1 Introduction

An electric circuit consisting of resistors and capacitors and in which an alternating current (ac) is imposed offers' opposition, impedance, to the current flow. Therefore, impedance is a measure of the total opposition to the flow of current in an alternating current circuit. It consists of two components, the resistive and the reactant counterpart. Impedance spectroscopy (IS), involves the application of a sinusoidal signal (input signals) to a material system and monitoring the response (output signals) as a function of frequency of the applied signal. In electrochemistry, this technique has been employed to study electrochemical systems. Therefore, electrochemical impedance spectroscopy (EIS) consists of the polarization of electrode-electrolyte interfaces with a sinusoidal voltage and recording the current response as a function of frequency of the applied signal. This experimental methodology has lent itself as a powerful analytical tool for the investigation and characterization of electrochemical properties of electrode-electrolyte interfaces. It has also been applied to establish the interrelations and dependency of the electrode-electrolyte properties to the manipulated variables such as voltage and current.

In this section, a theoretical background for the practical application of EIS is examined with a focus on the interpretation of experimental systems based on electrochemical models. Fundamentals of electrochemical impedance spectroscopy are discussed. A review of ac circuits is also discussed and then used to illustrate the behavior of electrochemical cells. The equivalent circuits of electrochemical cells, which form the bedrock of the current research problem is also discussed.

2.7.2 Fundamentals of EIS

Electrochemical studies are now employing the frequency related probes rather than the traditional time-concentration phenomenon [59]. The frequency domain allows for the characterization of electrical double layers based on the distribution of their relaxation times. Various conditions in an electrochemical cell such as the presence of charged species, the structure of the electrolyte, and the texture and the nature of the electrode determine the cell electrical response. When a cell is electrically polarized, a number of electrochemical reactions and processes

take place throughout the cell. Such processes include the transport of electrons through the electrodes, electron transfer across the electrode-electrolyte interface (oxidation or reduction reactions) and the flow of ionic species.

In EIS measurements, a small electrical perturbation at fixed dc potential is applied to the electrode-electrolyte interface and the response, usually current, is then monitored as a function of frequency. The resulting sinusoidal current may have a different phase relationship and amplitude from the applied voltage signal. Therefore, in the frequency domain, the impedance is measured by applying a single frequency voltage to the interface and the shift in the phase and the change in amplitude of the current response are measured at that frequency. The investigation of nonlinear systems (most real systems) in a frequency domain is informative only for signals of small magnitude. If the amplitude of the applied signal is small, the overall response of electrode-electrolyte system is linear. However, if the perturbation signal is large, the response, especially from the interfacial region shows strong nonlinear behavior. When the amplitude of the applied signal is less than 25mV at 25°C, the linearity of the system response is achieved to an excellent approximation. In the current study, a 2mV perturbation is used.

The frequency of the applied voltage signal is chosen depending on the system being studied. However, advanced experimental equipments have been designed to measure and probe frequency responses between 0.1mHz and 1MHz. Moreover, these instruments provide the flexibility to control the frequency range to examine the regions of particular interest to the experimenter. Processes that influence the conductivity of an electrode-electrolyte system or those that affect the external inputs, e.g., voltage and current can be studied by EIS. The information extracted from EIS spectra originates from two sources: those emanating from the material itself, such as conductivity, dielectric constant, charge mobility, equilibrium concentrations of the charged species; and those from the electrode-material interface for example, adsorption reaction, capacitance of the interfacial region, and diffusion coefficient of neutral species. In order to understand the concepts of electrochemical impedance spectroscopy, a review of alternating current circuits is necessary.

2.7.3 *Review of ac circuits*

Sinusoidal voltage is given by the expression

$$e = E\sin\omega t \qquad 2\text{-}34$$

where, ω is the angular frequency and, E is the maximum voltage (amplitude). If this voltage is considered to be a rotating vector (phasor), its length (diameter) is equal to the amplitude of the voltage signal. The speed at which the phasor is rotating corresponds to the frequency, ω of the sine wave. Therefore, at any time, the observed voltage, e is the component of the phasor projection along a particular axis. The resulting sinusoidal current signal is separately considered as a rotating phasor at the same frequency (Figure 2-18). However, the two signals generally will not be in phase and their phasors will be separated by a phase angle, ϕ . Therefore, the current response is given by

$$i = I\sin(\omega t + \phi) \qquad 2\text{-}35$$

If a sinusoidal voltage (equation 2-34) is applied across a resistor, R Ohm's law always holds and the current passing through the resistor is given by the expression

$$i = \left(\frac{E}{R}\right)\sin\omega t \qquad 2\text{-}36$$

where $\phi = 0$, there is no phase difference between potential and current as shown in (Figure 2-19). However, applying the same sinusoidal voltage (equation 2-34) across a pure capacitor produces electrical charges on its plates, the amount of which is given by the product of the capacitance and the voltage, i.e., CE. The current flowing through the capacitor is obtained by differentiating the charge density with respect to time, hence

$$i = \omega CE\cos\omega t$$

$$i = \frac{E}{X_c}\sin\left(\omega t + \frac{\pi}{2}\right) \qquad 2\text{-}37$$

where X_c is the capacitive reactance, $1/\omega C$ (Ohms). The phase angle is $\frac{\pi}{2}$, i.e., the two signals are

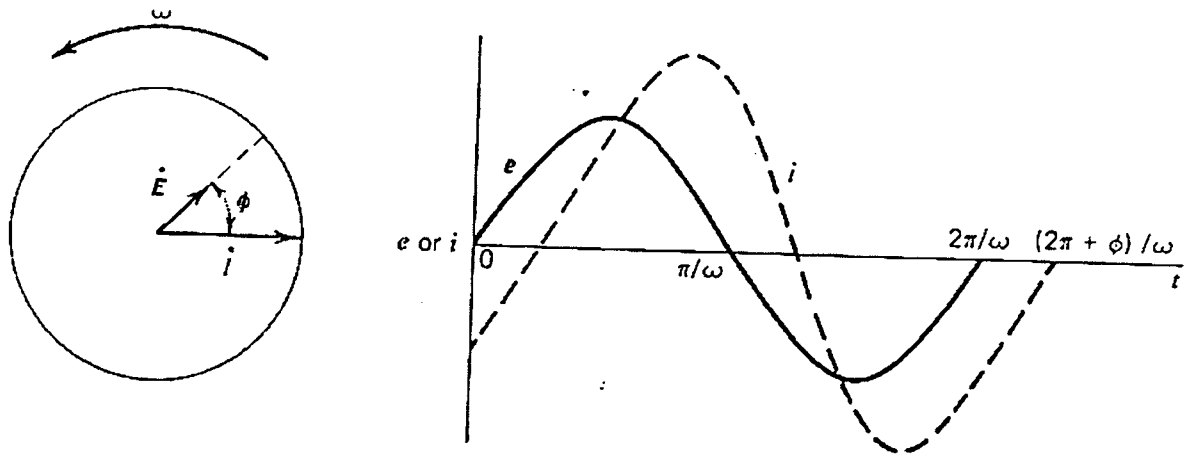

Figure 2-18 The Phasor diagram showing the relationship between alternating current and voltage signal at a frequency ω.The arrow indicate the direction of phasor rotation. Taken from[32]

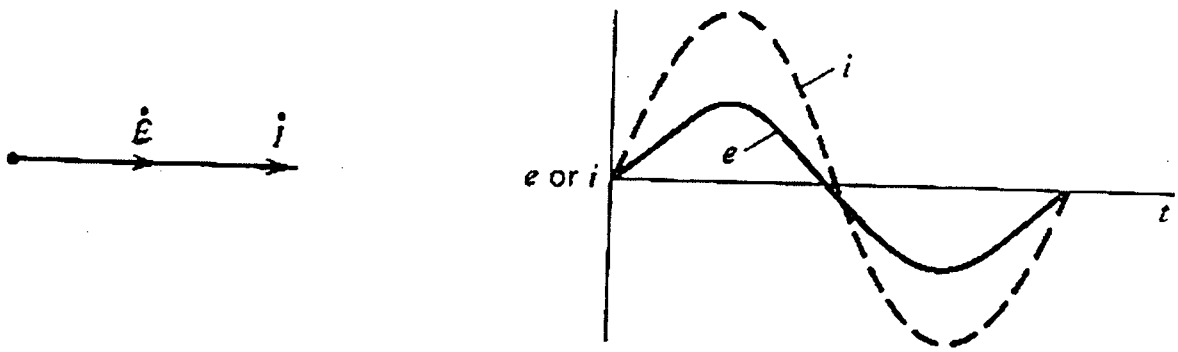

Figure 2-19 The diagram showing the relationship between current and voltage when the phase angle is zero i.e. when φ = 0. Taken from[32]

separated by 90° which means that the current leads the voltage as shown in Figure 2-18. The phasor projection is represented in a vector diagram and the magnitude and the direction of the planar vector in a right hand orthogonal system (Figure 2-20). The horizontal and vertical axes are represented by the vectors *a* and *b* respectively. The magnitude, Z is the sum of the components *a* and *b* along x and y axes respectively, i.e., the complex quantity, $Z = a + jb$. The imaginary number, *j* is given by

$$j = \sqrt{-1} \equiv \exp\left(\frac{j\pi}{2}\right) \qquad 2\text{-}38$$

Application of a sinusoidal voltage across an electric circuit consisting of a combination of resistors and capacitors either in series or in parallel adequately represent electrochemical cells. The response from the series combination of R and C is such that the potential drop across them is the same as the sum of the potential drops across the resistor and the capacitor. From Kirchhoff's law, the current through the capacitor and the resistor must be equal. The potential difference is proportional to R and X_c and thus, the voltage is linked to the current through a vector

$$Z = R - jX_c \qquad 2\text{-}39$$

called the impedance. The impedance, Z is a vector quantity, which is plotted in the plane with either rectangular or polar coordinates. The impedance is a more general concept than resistance because phase relationships are taken into consideration. In general, Z is frequency dependant and electrochemical impedance spectroscopy studies thus involve measurements of Z as a function of frequency over a wide range. The information regarding the electrochemical properties of the electrical-electrolyte system is deduced from the nature of impedance spectrum.

The magnitude of impedance for the series RC is

$$|Z| = \sqrt{\left(R^2 + X_c^{\,2}\right)} \qquad 2\text{-}40$$

and the phase angle is

$$\phi = \arctan\frac{X_c}{R} = \frac{1}{\omega RC} \qquad 2\text{-}41$$

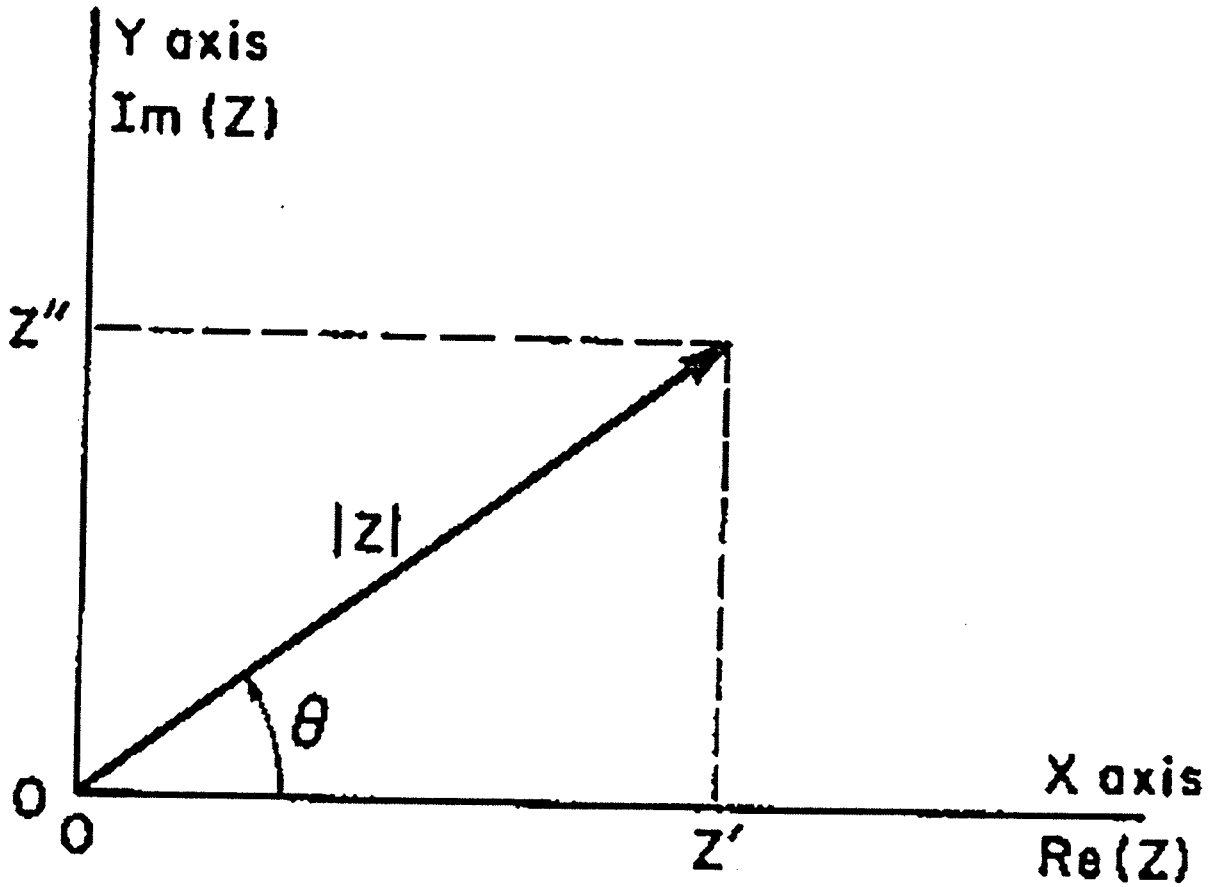

Figure 2-20 The impedance Z plotted as a planer vector using rectangular and polar coordinates. Taken from[59]

Often, the in-phase component ($\phi = 0$) of the impedance is referred to as the real part, Z' and the out-of-phase component of impedance, i.e., at $\phi = 90$ is the imaginary part, Z'' . Therefore, the impedance is given by the expression

$$Z = Z' + jZ''$$
$$\text{Or} \qquad \text{2-42}$$
$$Z = |Z|e^{j\phi}$$

The impedance is a complex quantity and is only real when $\phi = 0$, i.e., $Z = Z'$ and therefore, the impedance is independent of frequency and is purely resistive and is equivalent to the resistor, R hence

$$Z' = R\,(\text{Real Impedance})$$
$$Z'' = -jX_c = -j\frac{1}{\omega C}(\text{Imaginary Impedance}) \qquad \text{2-43}$$

The variation of the impedance with frequency may be represented in different ways: the Bode plot, featuring log $|Z|$ and phase angle, ϕ plotted against the log of frequency. The Nyquist plot (Cole-Cole plot), is a complex plot displaying Z'' vs. Z' for different values of frequency ω. In series RC circuits (Figure 2-21(a)), the real impedance (Z'), is conspicuously independent of frequency while the imaginary impedance (Z'') is dependent on the frequency. Therefore, the complex plot (Nyquist plot) is a vertical line as shown in (Figure 2-21(b)). For parallel RC (Figure 2-22(a)), the total current (resistive and capacitive) is given by the vector sum as shown in Figure 2-22(b). The circuit impedance is therefore given by

$$Z = \frac{R}{1 + j\omega RC} \qquad \text{2-44}$$

which can be separated into real and imaginary components to give

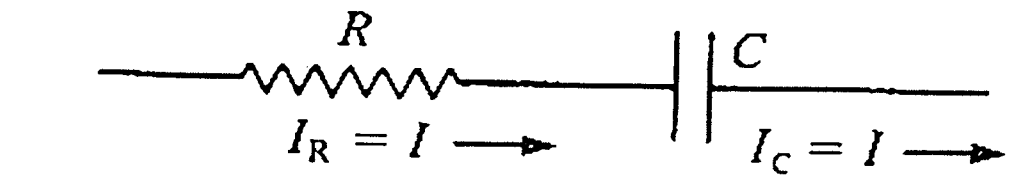

(a)

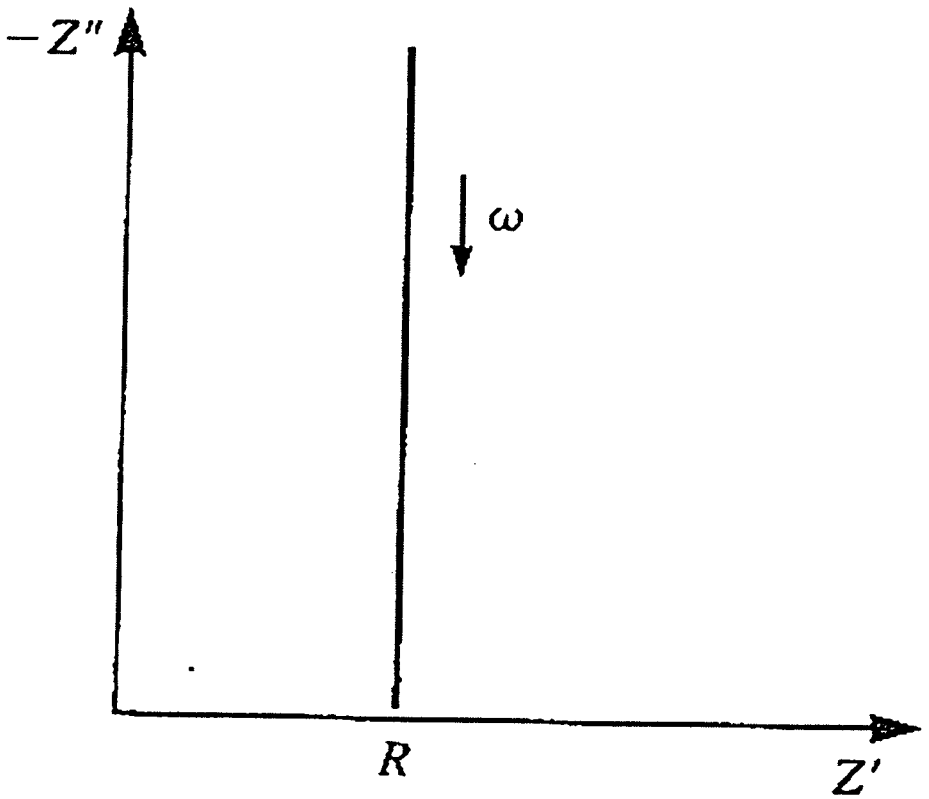

(b)

Figure 2-21 The diagram showing resistance and capacitance in series: (a) Is the electrical RC series circuit and (b) Is the complex plane plot . The arrow in (a) indicates the direction of the current while the one in(b) indicates the direction of increasing frequency ω. Taken from[31]

$$Z' = \frac{R}{1+(\omega RC)^2}$$
$$Z'' = \frac{-R^2C\omega}{1+(\omega RC)^2} \qquad 2\text{-}45$$

In this case, both real and imaginary parts of the impedance are functions of the frequency and a complex plot is a semicircle (Figure 2-22(c)). The radius of the semi circle is R/2 and a maximum value of Z'' must satisfy the condition ωRC = 1.

In general, a simple cell consists of a capacitor, C and a resistor, R either in parallel or in series. These elements lead to a time constant, τ given by

$$\tau = RC \qquad 2\text{-}46$$

This is the dielectric relaxation time of the basic material.

The reciprocal of impedance is admittance, Y.

$$Y = \frac{1}{Z}$$
Or
$$Y = \frac{1}{|Z|}e^{-j\phi} \qquad 2\text{-}47$$

This expression is ideal for the analysis of parallel circuits since admittance for circuit elements in parallel can be added directly. If the inphase components are represented by Z' and Y' respectively and the out-of-phase components represented by Z'' and Y'' then

$$Y = \frac{1}{Z} = \frac{1}{Z' + jZ''} = Y' + jY'' \qquad 2\text{-}48$$

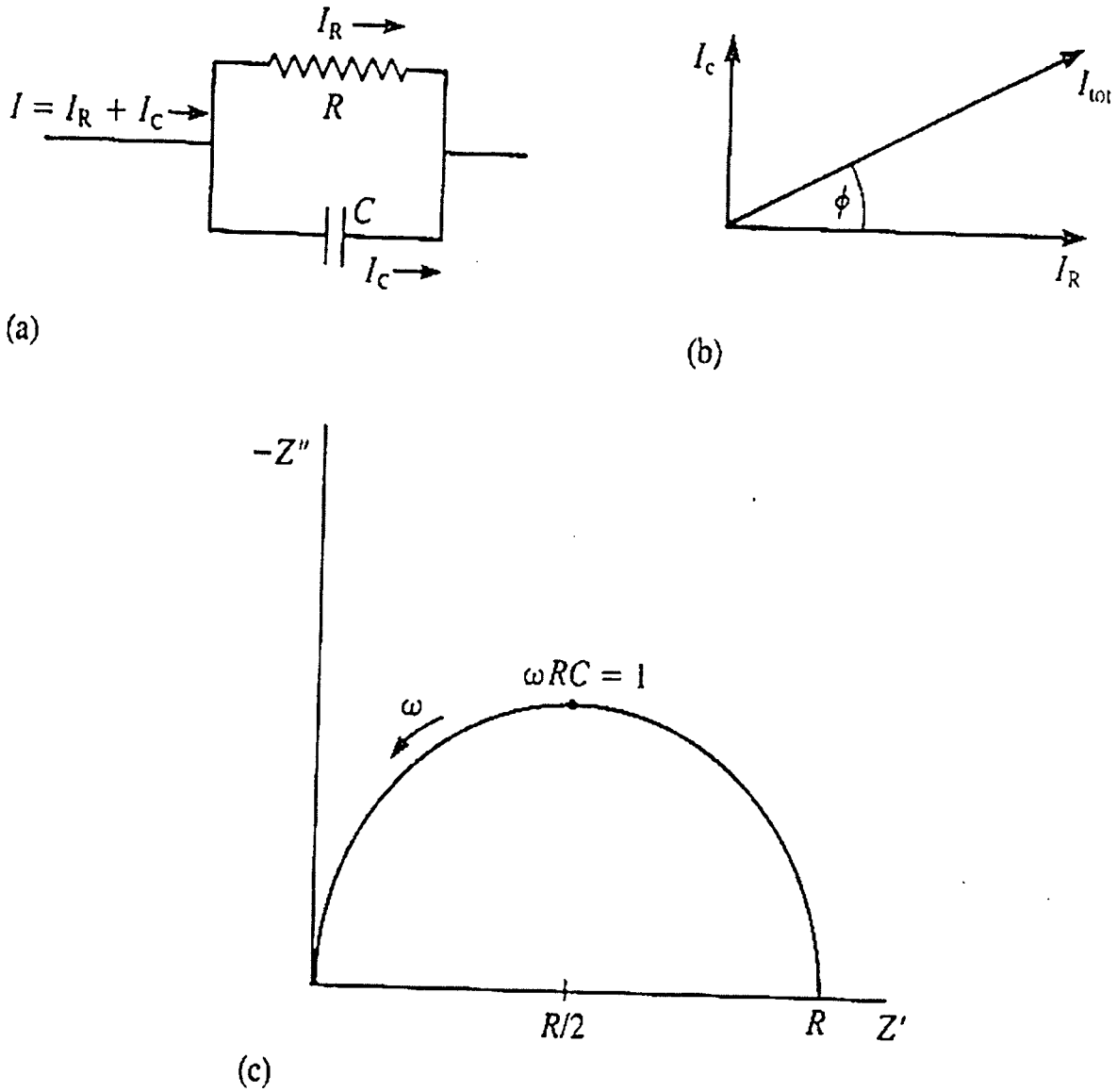

Figure 2-22 The diagram showing resistance and capacitance in parallel: (a) Is the electrical RC parallel circuit; (b) Is the vector sum of the resistive and capacitive currents and (c) The complex plane impedance plot. The arrow in (a) indicate the direction if the current flow while the arrow in (b) shows the direction of the increasing frequency ω.Taken from[31]

Therefore, the real admittance Y' and imaginary admittances Y'' are given by

$$Y' = \frac{Z'}{(Z')^2 + (Z'')^2}$$
$$Y'' = \frac{-Z''}{(Z')^2 + (Z'')^2} \qquad 2\text{-}49$$

Admittance data are commonly represented in a complex plot either as Y'' vs. Y' or frequency normalized admittance (Y''/ω vs. Y'/ω) when investigating non-faradaic processes. In the current study, the impedance results are represented as frequency normalized admittances. However, other methods of data presentation are also used.

The results from the electrochemical cell are usually compared with that of an equivalent electric circuit that contains a combination of resistors, capacitors and inductors. Another strategy is to choose a model for the reaction mechanism and kinetic parameters, derive the impedance expression, and compare with experimental values. In the current study, the experimental results are modeled by an electrical equivalent circuit.

2.7.4 Equivalent circuit of an electrochemical cell

An electrochemical cell is represented in terms of an equivalent circuit [59] that consists of a combination of resistors, capacitors and inductors. Each of these circuit elements contributes to the overall circuit impedance. Some parts of electrochemical cells also behave as a resistor, e.g., the electrolyte solution with resistance R_{sol} .The interfacial region formed between the electrode and the electrolyte solution (double layer region), fundamentally behaves as capacitors with the capacitance, C_{dl} . Therefore, the simplest electrochemical cell (ideally polarized electrodes) is made of a resistor, R_{sol} (solution resistance) in series with a capacitor, C_{dl} (double layer capacitance). The cell impedance is given by

$$Z = R_{sol} - \frac{1}{\omega C_{dl}} \qquad 2\text{-}50$$

At high frequencies, the cell impedance is controlled only by R_{sol} while at very low frequencies, the impedance is solely a product of the double layer capacitance. However, at intermediate frequencies, the impedance is affected by the contribution from solution resistance and the double layer capacitance. But in real cells, the impedance spectrum is much more complex especially with solid electrodes. Electrode roughness is a major contributor to this complexity. It introduces inhomogeneous reaction rates or a distribution (dispersion) of the values of some physical properties of the system. In addition, the varying thickness or composition of an electrode coating (adsorption reaction) may also be a significant factor. These conditions cause the double layer capacitance to show a phase angle of less than 90°. The phase angle is independent of the applied frequency, i.e., constant phase elements (CPE), Q. The cell impedance is then given by

$$Z = R_{sol} - \frac{j}{(\omega Q)^n} \qquad 2\text{-}51$$

When $n = 1$, Q resembles a capacitor hence ideal electrode process. However, for non-ideal electrode processes, n is in the range of $0 \leq n \leq 1$.

If faradaic reaction occurs at the electrode, a faradaic impedance Z_f, parallel to the double layer capacitance is introduced. Thus, the electrochemical cell is constructed with circuit components that include; a pure double layer capacitor of capacitance, C_{dl} the impedance of the faradaic process, Z_f and the uncompensated resistance, R_{sol}, which is the solution resistance between the working electrode and the counter electrode.

For a reaction in which the charge transfer is also influenced by diffusion process, to and from the electrode, the faradaic impedance Z_f (See Figure 2-23) is separated into an impedance, which measures the resistance, R_{ct} of charge transfer reaction and an impedance, Z_w that measures the difficulty of mass transport (diffusion process), i.e., Warburg impedance. This type of circuit arrangement, commonly known as Randle's circuit is shown in Figure 2-24. The Warburg phenomenon is easily depicted in Nyquist plot as a straight line with an angle of 45° in the low

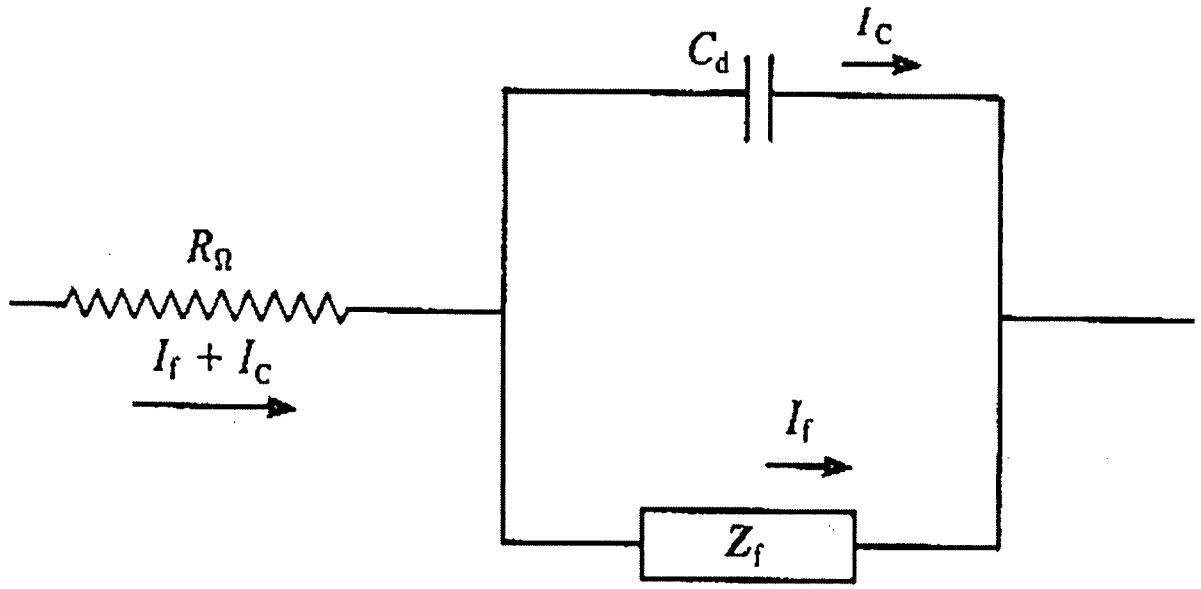

Figure 2-23 The diagram showing equivalent circuit of an electrochemical cell for a simple electrode process. R_Ω is the solution resistance, Z_f the impedance of the electrode process and C_d the double layer capacity. Taken from[32]

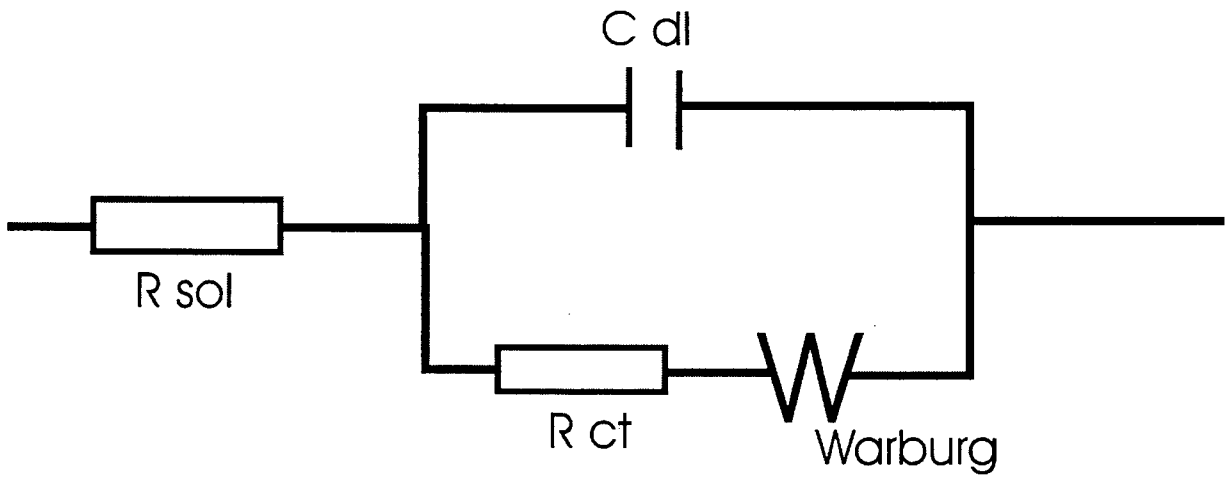

Figure 2-24 The diagram of Randles' equivalent circuit. R_{ct} is the charge transfer resistance, W is the Warburg impedance, C_{dl} is the double layer capacitance and R_{sol} is the solution resistance. Taken from [16]

frequency region. The Warburg impedance equation is derived from a portion of the Randle's circuit (see Figure 2-24), representing a faradaic process that involves a charge transfer reaction and a linear (homogeneous) diffusion process. For example, a reduction reaction represented by a general equation

$$O + ne^- \rightarrow \text{Red} \qquad 2\text{-}52$$

The Warburg impedance, Z_W for the above reaction is given by [60]

$$Z_W = \sigma/\omega^{1/2} - j\,\sigma/\omega^{1/2} \qquad 2\text{-}53$$

where σ is the Warburg constant and is given by the equation

$$\sigma = \frac{RT}{F^2 A\sqrt{2}}\left(\frac{1}{D_O^{1/2}C_O^*} + \frac{1}{D_R^{1/2}C_R^*}\right) \qquad 2\text{-}54$$

where D and C^* represent diffusion coefficients and bulk concentrations respectively, the subscripts' O and R represent the oxidized and the reduced forms of the species and A is the electrode area. The magnitude of the Warburg impedance, $|Z_W|$ is given by

$$|Z_W| = \sqrt{2}\,\sigma/\omega^{1/2} \qquad 2\text{-}55$$

Hence the Warburg impedance is inversely proportional to the square root of the frequency or directly proportional to the square root of time. At low frequencies where the Warburg phenomenon dominates, both the real and the imaginary parts of the impedance are equal. There exists a relationship between the constant phase element (CPE) and the Warburg impedance, e.g., both have a constant phase angle with respect to the applied frequency. And, from the comparison of equation 2-51 and 2-55, the Warburg impedance can be modeled as a CPE [61] with n = 0.5 and $Q = (2\sigma^2)^{-1}$

The faradaic impedance, Z_f can be written in terms of the Warburg impedance which includes the charge transfer reaction component

$$Z'_f = R_{ct} + \sigma\omega^{-1/2}$$
$$Z''_f = -\sigma\omega^{-1/2} \qquad 2\text{-}56$$

The plot of Z'_f and $-Z''_f$ verses $\omega^{-1/2}$ gives a straight lines as expected (Figure 2-25) with the slope σ, intercept R_{ct} and 0 for in-phase and out-of-phase components respectively. The intercept, R_{ct} suggests that at very high frequencies the contribution of diffusion on the measured current is negligible. Hence, the measured current depends only on the kinetics of the process.

The real and the imaginary components of the impedance for the equivalent circuit shown in Figure 2-24 are therefore given by

$$Z' = R_{sol} + \frac{R_{ct} + \sigma\omega^{-1/2}}{\left(\sigma\omega^{1/2}C_{dl} + 1\right)^2 + \omega^2 C_{dl}^{\,2}\left(R_{ct} + \sigma\omega^{-1/2}\right)^2}$$
$$-Z'' = \frac{\omega C_{dl}\left(R_{ct} + \sigma\omega^{-1/2}\right)^2 + \sigma^2 C_{dl} + \sigma\omega^{-1/2}}{\left(\sigma\omega^{1/2}C_{dl} + 1\right)^2 + \omega^2 C_{dl}^{\,2}\left(R_{ct} + \sigma\omega^{-1/2}\right)^2} \qquad 2\text{-}57$$

Figure 2-26 shows the complex plot using equation 2-57. By considering the two frequency limits of equation 2-57, it follows that as $\omega \rightarrow 0$

$$Z' = R_{sol} + R_{ct} + \sigma\omega^{-1/2}$$
$$Z'' = -\sigma\omega^{-1/2} - 2\sigma^2 C_{dl} \qquad 2\text{-}58$$

The low frequency region exhibits a straight line behavior of a unit slope, which if extrapolated to the real axis gives an intercept of ($R_{sol} + R_{ct} - 2\sigma^2 C_{dl}$). The straight line is indicative of a reaction, which is controlled by diffusion, described by Warburg impedance. However, at a high frequency limit, i.e., $\omega \rightarrow \infty$

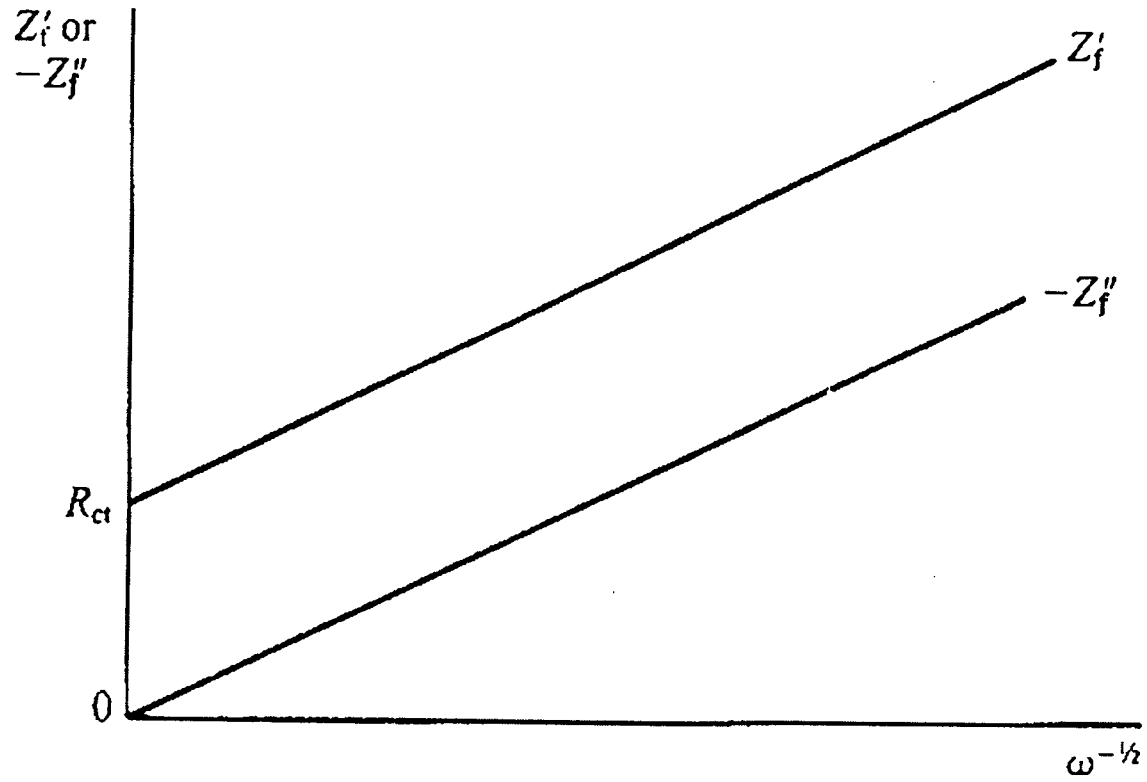

Figure 2-25 The diagram showing the dependance of Z'_f and Z''_f on the inverse square root of the frequency ω (Randles plot). The slope of the two plots is σ. Taken from[31]

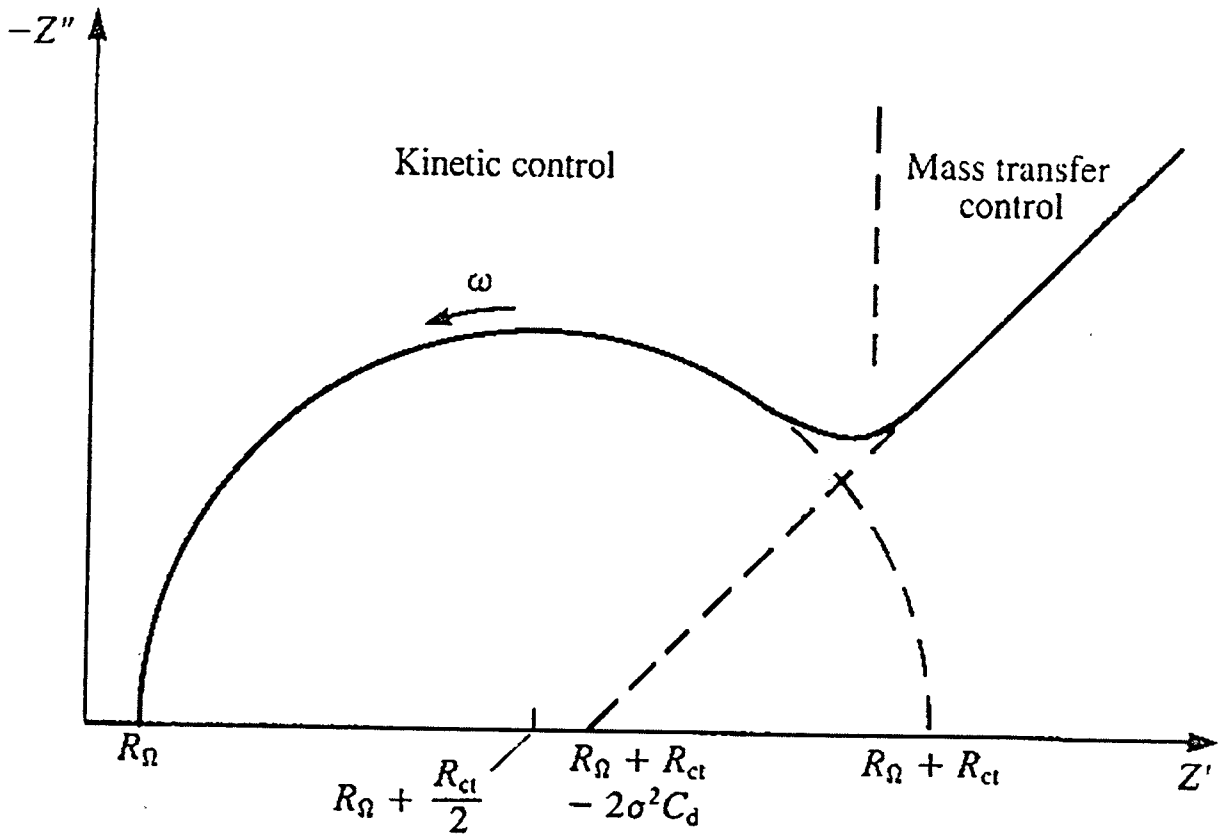

Figure 2-26 The diagram showing an impedance plot in a complex plane for a simple electrochemical system. The arrow indicates the direction the increasing frequency ω. Taken from[31]

$$Z' = R_{sol} + \frac{R_{ct}}{1+\omega^2 C_{dl}^{\ 2} R_{ct}^{\ 2}}$$
$$Z'' = -\frac{\omega C_{dl} R_{ct}^{\ 2}}{1+\omega^2 C_{dl}^{\ 2} R_{ct}^{\ 2}} \qquad 2\text{-}59$$

and the semicircular portion of the graph suggests that the reaction process is purely controlled by kinetics. Therefore it may be true to believe that at high frequencies, the electrochemical system is analogous to a parallel RC circuit. Equation 2-59 can be simplified to give

$$\left(Z' - R_{sol} - \frac{R_{ct}}{2}\right)^2 + \left(Z''\right)^2 = \left(\frac{R_{ct}}{2}\right)^2 \qquad 2\text{-}60$$

which is an expression describing equation of a circle of radius, $\frac{R_{ct}}{2}$ and an intercept, R_{sol} on the Z' axis ($\omega \rightarrow \infty$) and $R_{sol} + R_{ct}$ ($\omega \rightarrow 0$). The value of ($Z'' = -\frac{1}{\omega C_{dl}}$) at very high frequencies is very small but increases as the frequency diminishes. At very low frequencies, C_{dl} gives a higher conductance but the current passing through R_{ct} increases Z' and diminishing Z''.

3 Literature Review

3.1 Introduction

Adsorption of insoluble organic molecules onto solid electrodes has been for many years, a topic of great interest for scientific research. The formation of organic thin films, i.e., deposition of a thin monolayer of organic molecules onto a substrate (electrode) has been achieved through the Langmuir-Blodgett technique, a method of transferring a monolayer of surfactant previously spread at a gas-solution interface to the substrate surface [62,63]. The substrate is coated with the surfactant by immersing it through the monolayer at the gas-solution interface. A modification of this technique (Langmuir-Schaefer) has been developed, and the transfer of the monolayer from the gas-solution interface to the substrate is accomplished by touching the monolayer with the electrode surface [64]. In addition, deposition of surfactants from solutions or suspensions via chemical reactions at the electrode surface is also documented in literature [65,66]. These methodologies of thin film production result in self-assembled monolayers (SAMs) of well-organized structures, with limited morphological defects and modest stability. The SAMs have been used and applied widely as biomembrane model systems.

The application of organic thin films in various scientific and technological sectors has been emphasized in a review [67] in which the authors identified fibre optic and biological sensing as one of the major areas where organic thin films have found direct and significant applications. They also pointed out that the utilization of these films has been frustrated by the inability to produce films free from defects and contamination, with mechanical, thermal and chemical stability without losing their admired properties. In addition, they suggested the employment of new characterization techniques, e.g., scanning tunnelling microscopes (STM) to further understand the morphology of organic thin films. Since then, tremendous work has been done to characterize these films, using various techniques in an attempt to address the said shortcomings and to find other areas of application.

The current study encompasses many disciplines, which includes the adsorption of organic molecules. The monolayers studied in the current study were produced by Langmuir-Schaefer technique, i.e., horizontal touching technique. Therefore, it is prudent to review some selected studies in this field and other areas relevant to this thesis. Emphasis is laid on the adsorption of

phospholipids on mercury since the work is closely related to the work in this thesis. The adsorption and characterization of insoluble surfactants onto electrode-electrolyte interfaces are discussed below followed by the description of the adsorption and characterization of phospholipid compounds onto mercury-electrolyte interfaces. The interaction of heavy metal ions (divalent metal ions) with phospholipids monolayers and bilayers spread at electrode-electrolyte interfaces is also discussed. The impedance spectroscopy technique (frequency response analysis), a powerful tool for characterizing monolayers and bilayers spread at electrode-electrolyte interfaces, is also reviewed as well.

3.2 Adsorption of Insoluble Surfactants onto Electrode-electrolyte Interfaces

Self-assembled monolayers (SAMs) of alkyl thiols and their derivatives adsorbed onto a metal substrate, produces chemisorbed layers that are characterized by ease of preparation, well defined and oriented structures and strong stability. It is worth noting that the understanding of the factors that affect the structure and stability of these layers are vital to their application in electrochemistry and other technologies. Gold and silver substrates have been used for the formation of thiol monolayers, and the Langmuir-Blodgett, Langmuir-Schaefer and other technques of monolayer formation have been applied to produce thiol monolayers on these substrates [65]. The substrate and the thiol molecules are rigidly linked together through a strong covalent bond resulting in a stable and robust structure. The chemisorption of alkylthiols onto gold substrates is due to the formation of covalent bonds between Au(I) and alkyl thiolate (RS^-), while for mercury electrodes, the sulfur atoms are bound firmly to the surface of a mercury drop. Because of a strong covalent bond between thiol and the substrate, SAMs are characterized by conformational rigidity, which makes it difficult to incorporate other molecules into the adsorbed monolayer. However, the production of high purity SAMs require careful attention with regard to deposition condition in order to obtain well-organized monolayers. Recently, electrochemical deposition of thiols has been identified as a reliable alternative to forming thiol self-assembled monolayers under more controlled conditions [68-70].

Self-assembled monolayers of thiols on metal electrodes are a promising new class of materials with wide range of applications [71-75]. SAMs have been investigated on polycrystalline gold and single crystal electrodes using cyclic voltammetry [71,76-78], chronoamperometry [79] and open circuit potential measurements[80,81]. In addition, FTIR, ellipsometry and STM including a number of surface science techniques [82-84] have also been used to characterize these layers. Electrochemical characterization of SAMs concentrated on measuring the pinhole defect sizes and density. Porter et al. [78,85,86] have demonstrated that SAMs of alkyl thiol can be desorbed electrochemically from gold and other surfaces through a reductive desorption. They studied the chemistry associated with these processes together with their kinetics and thermodynamics, the role of gold surface morphology, alkyl chain and pH on the reductive removal and oxidative redeposition of thiol monolayers have been investigated and interpreted in terms of the monolayer rigidity, solubility of the thiol molecules and molecular interaction between neighbouring adsorbate molecules. Recently, Slowinski et al. [87-89] investigated the long-range electron trough alkyl thiol SAMs supported on hanging drop mercury.

The study of adsorption of water insoluble surfactants spread onto gas-solution interfaces was pioneered by Bizzotto and Lipkowski [3,90] on Au and Hg electrodes. Various surfactants have been studied by this group. The interactions between the surfactant and the electrode are nonspecific, i.e., there are no chemical reactions, thus their adsorption on these surfaces has been described as physisorption. Electrochemical techniques, e.g., capacity measurements and charge density measurements were employed to characterize these layers in a Langmuir trough, which served as electrochemical cell. They also applied elastic scattered light and electroreflectance spectroscopy on their systems. Their studies revealed that the transfer of surfactant from gas-solution to metal-solution strongly depends on the applied electrode potential. Other studies [91,92] have detailed electrochemical and spectroelectrochemical investigation of insoluble organic molecules onto electrified interfaces. In this studies, the monolayer was formed at potential of zero charge (pzc) and the adsorbed monolayer displayed a low capacitance region at this potential. When the applied electrode potential was scanned to more negative values, the surfactants were displaced from the electrode surface (desorbed) and replaced by water. More recently, Shepherd et al. [93] studied the absorption and desorption of octadecanol monolayer on Au (111) using epi-fluorescent imaging.

Their investigation demonstrated the existence of desorbed species near the electrode surface. Since fluorescent near a metal is quenched (relaxation of excited molecules without photon emission) only molecules away from the surface could be observed, which is why there was no fluorescence at adsorption potentials. As the potential was scanned to more negative desorption values, an increase in fluorescence and the numerical number of desorbed particles was observed. The desorbed aggregates did not diffuse away from the electrode and their presence or existence close to the electrode was confirmed by scanning the potential positively to adsorption values, which was accompanied by a corresponding decrease in fluorescence and the number of desorbed particles. This phenomenon indicated that the desorbed species resided close to the electrode surface from where they were re-adsorbed once the potential was made less negative.

3.3 Adsorption of Phospholipids onto Mercury-electrolyte Interfaces

The study of adsorption of surfactants onto electrified interfaces commenced with their investigation on hanging mercury drop electrodes (HMDE). Frunkin and Grodetskaya [94,95] pioneered the research work on this field. They studied the adsorption of different kinds of carboxylic acids and hexadecanol on Hg electrodes. Later, Miller et al. [8] advanced Fumkin and Grodetskaya's work and proposed the technique of studying lipid monolayers on Hg electrode and Langmuir troughs. They calculated the surface concentration of lipids adsorbed onto mercury in contact with an electrolyte solution using radioactive labelled oleyl alcohol. Also shown in this study was the fact that at very negative potential, the monolayer could be displaced from the electrode surface and replaced by water. Further, they demonstrated that electrochemical techniques could be employed to characterize potential induced changes in the adsorbed monolayer, e.g., they observed adsorption and desorption pseudocapacitace peaks in the Cyclic Voltammetry and differential capacitance for their system, which was a hanging Hg drop coated with a lipid monolayer.

The study of monolayers spread onto hanging mercury drop electrodes (HMDE) has been given special attention by Nelson et al. [17-23] and Guidelli and Moncelli [24,25] who have extensively studied phospholipid monolayers on this electrode. They developed a technique for spreading lipid monolayers onto gas-solution interfaces. The lipid was first dissolved in a volatile solvent (spreading solvent) and injected on the electrolyte surface, allowing it to evaporate, thus

leaving a monolayer spread on a gas-solution interface. The transfer of the monolayer from the gas-solution interface to the Hg-solution interface was accomplished by pushing the Hg drop through the monolayer, and, in the process, the Hg drop was coated with the lipid molecules. The deposited phospholipid monolayer had characteristics of well-ordered structures and free from defects. Characterization of these layers was performed utilizing electrochemical techniques particularly differential capacity measurement.

In their biomimicking research, Nelson et al. [17-19,20] have particularly targeted the adsorption of dioleoyl phosphatidylcholine (DOPC) onto hanging Hg drop electrodes. Their work has yielded remarkable findings and has propelled adsorption/desorption to an interesting area of research. They investigated the organization of the monolayer morphology on Hg and showed that at -0.4V (Ag/AgCl), which is the pzc of Hg, the monolayer displayed a minimum capacitance of 1.85$\mu F/cm^2$. This low capacitance is evidence of a perfectly ordered monolayer free from defects. When the potential was scanned negatively, pseudocapacity peaks were observed and were considered to represent drastic changes (phase transition) in the monolayer morphology due to the formation and growth of defects. Further, they tested the degree of permeability of the lipid monolayer by investigating the transport of metal ions through the lipid monolayer [4,96,97]. They found that the layer became susceptible to ion penetration at potential of pseudocapacitance peaks, which again confirmed that the peaks represented some kind of porosity in the monolayer. Bizzotto et al. [4] employed charge density step experiments to quantitatively characterize one of these phase transitions. In their further studies, Nelson et al. [2,98] incorporated biological compounds, e.g., gramicidin into the phospholipid monolayer as Rueda [26].

Guidelli et al. [30] studied the DOPC-coated mercury in 0.1M aqueous solutions' of KCl, LiCl and tetramethyl ammomnium chloride (TMACl). Their investigation illustrated the effect of type of supporting electrolyte on the desorption of DOPC from the surface of a mercury drop. While the lipid desorbed at -1.85V in KCl electrolyte solution, there was no desorption at -2.1V when LiCl was the supporting electrolyte. However, when TMACl solution was used, the desorption was observed much earlier, i.e., at -1.75V. They explained that the observed differences were due to the fact that the interaction of the cations with the lipid increases with the increase in their hydration Gibbs energy. Recently, Stoodley et al. [99] used the monolayer of DOPC adsorbed onto Hg

electrode to study the interaction between the lipid monolayer and an antibiotic drug, Amphotericin B (AmB), by characterizing the changes in the lipid order due to interaction with the drug. They also estimated the mean size and number density of AmB formed in the monolayer by fitting the reduction current transient to random array of microelectrode model. Very recently still, Guidelli et al. [100] investigated films supported on a Hg drop to understand processes of biological importance. They reported that the transport of hydrated Tl^+ ions through the channel formed by polypeptide gramicidin incorporated in a DOPC monolayer is controlled by diffusion and dehydration step, while the influx of dehydrated Tl^+ ion emanating from Tl amalgam electro-oxidation is driven by Tl atoms within the amalgam.

Liposomes (vesicles) adsorption onto electrified interfaces has been studied by Stauffer et al. [29]. They investigated the adsorption of different forms of DOPC onto Hg electrode, DOPC monolayer at a gas-solution interface, DOPC vesicles adsorbed from liposomal solution and co-adsorbed layer, which composed of an adsorbed monolayer in the presence of liposomes in solution. Furthermore, they demonstrated that the adsorption of liposomes was distinctively different from the layer adsorbed from the gas-solution interface, while the co-adsorbed layer retained most of the liposome layer characteristics. Using impedance spectroscopy to measure capacitance at different frequencies, they showed that at low frequencies, the desorption of DOPC was observed at very negative potentials for all the systems studied but as the frequencies increased, only the gas-solution system maintained this behaviour. The liposome system exhibited a frequency dispersion in its measured capacitance. Another recent study [101] investigation of adsorption of liposomes from aqueous electrolyte solution onto a Hg electrode suggested that suspended liposomes diffused to the electrode surface where they busted and spread. The resulting capacitive current due to busting and spreading of these liposomes permitted the counting of the number of liposomes involved in the process and the number of molecules in each liposome as well.

3.4 Interaction of Cations with Phospholipds Layers

Cations especially divalent cations strongly influence membrane properties, e.g., permeability, adhesiveness and rigidity to critical stimuli and chemical agents. Different groups have investigated the interaction of divalent ions in the subphase solution with phospholipid monolayers

and bilayers [102-108]. Membrane fusion, which is a characteristic of many biological processes depends strongly on calcium ion concentration in the medium. Calcium ions interact with the individual membrane constituents, e.g., lipids, proteins and carbohydrates and have been known to interact and bind with negatively charged phospholipid head groups, resulting in the stabilization of the lipid assembly. This phenomenon is well documented in literature[109-112].

Reviakine et al. [113] used atomic force microscopy (AFM) to investigate the morphology of supported phospholipid bilayers (SPBs) containing mixtures of phospholipids in gel (dipalmitoyl phosphatidylcholine, DPPC) and fluid (dioleoyl phosphatidylserine (DOPS) or -choline (DOPC)) states at room temperature. The presence or absence of Ca^{2+} in the subphase was found to have a dramatic effect on the organization of the gel phase when the fluid phase was composed of pure DOPC. Ross et al. [114] investigated the calcium-induced formation of phosphatidylserine-enriched lipid in Langmuir-Blodgett (LB) monolayers composed of a mixture of two saturated lipids 1,2-dipalmitoyl-*sn*-glycero-3-phosphocholine(DPPC) and 1,2-dipalmitoyl-*sn*-glycero-3-phosphoserine (DPPS). They utilized fluorescence microscopy together with pressure-area isotherms, time-of-flight secondary ion mass spectrometry (TOF-SIMS) imaging, scanning electron microscopy (SEM), and lateral force microscopy to examine and analyze lipid domains based on their chemical and physical properties. TOF-SIMS and SEM images of DPPC/DPPS LB monolayers transferred onto gold surfaces revealed that small amounts of calcium ions in the aqueous phase are enough to induce the formation of circular DPPS-enriched domains. Knebel et al. [115] studied the structural dynamics of surfactant by epifluorescence light microscopy at the air-water. Small unilamellar vesicles of dipalmitoylphosphatidylcholine, dipalmitoylphosphatidylglycerol, and a small amount of a fluorescent dipalmitoylphosphatidylcholine-analog were injected into the buffer solution. The lipids aggregated to large clusters in the presence of Ca^{2+} and adsorbed from these units to the interface. They showed that Ca^{2+} interacted and bound with the lipid to form large aggregated structures.

3.5 Electrochemical Impedance Spectroscopy

Impedance spectroscopy is a powerful analytical tool with the capability of providing vast information about electrode-electrolyte interfaces. However, impedance measurements at very high frequencies always have the problem of phase shifts introduced by the reference electrode, which has

the potential of wrongful interpretation to be due to high-frequency time constants. Mansfeld et al. [116] demonstrated that the use of an auxiliary wire reference electrode (Pt or Au) placed near the tip of reference electrodes (SCE) capillary in solution, connected via a capacitor to the reference electrode in parallel, greatly reduce the high-frequency artifacts (see appendix for details).

Wandlowiski and Levie [117] developed a model to explain the interfacial admittance at a sharp narrow peak (needle peak). The admittance was found to be dominant at low frequencies. They suggested that this dominance is due to the growth of patches of condensed film in a narrow potential window where they coexist with areas not covered. They argued that at high adsorbate concentration, the additional admittance can be represented with a series RC circuit in parallel with the usual admittance.

Lingholm-Sethson et al. [118] studied DOPC monolayer-covered Hg electrode using impedance spectroscopy and analysed data from the experiment with different electrolytes, using multivariate analysis. They were able to show that different metal ions interact differently with the DOPC monolayer on Hg electrode. In addition, their results showed that interaction of lipid monolayer with drugs can be studied in this manner. Rueda et al. [119] also applied EIS to study gramicidin-modified DOPC-coated mercury in the absence and in the presence of electroactive species (Tl^+ ion) in solution using different approaches in terms of potential and frequency scans and the kind of monolayer (single adsorbed or successively formed DOPC monolayer), in an attempt to establish the most suitable experimental conditions. Their findings showed that in the presence of electroactive species with the capability of disrupting the organization of the lipid film, the ideal procedure should involve experiments performed at successive frequency or potential scans on successively formed DOPC monolayers. Hason et al. [120] employed electrochemical impedance spectroscopy to study electrochemical behaviour of echinomycin and its interaction with single-stranded (ss) and double-stranded (ds) DNA at the hanging mercury drop electrode (HMDE). They combined adsorptive transfer technique and EIS to discriminate between ss and sd DNA.

4 Experimental Instrumentation & Methodology

A general description and illustration of the experimental instrumentation and methodology used in this thesis are described in this Chapter. The description focuses on the materials used during the experiment, the methodology employed to carry out the experiment, the systems studied and the procedure followed during the experiments. It begins with the electrochemical investigations followed by the description of electrochemical impedance spectroscopy technique.

4.1 Electrochemical Investigations

The electrochemical methods used in this study involved differential capacity measurements. AC voltametry was employed to measure the differential capacitance at 70 Hz. In this section, the electrochemical experimental instrumentation and methodology is discussed. The systems studied and the procedures used for the electrochemical investigations using the said technique are described as well.

4.1.1 Electrochemical instrumentation

Electrochemical measurements utilized a FHI-ELAB potentiostat, an Autolab (Eco Chemie, the Netherlands) and a 5210 EG&G lock-in amplifier. The data were collected via a plug-in data acquisition board from National Instrument (PCI-6052E). Software written in Labview was used to record electrochemical measurements. Typical differential capacity measurements were performed with a 2 mV rms ac potential perturbation (70 Hz) superimposed on a linear voltage ramp at 5 mV/s. AC voltammetry was used to measure the capacity of the Hg interface, the capacitance calculated by assuming a series RC circuit.

4.1.2 Experimental methodology

The electrochemical cell was a four-electrode cell. The working electrode (WE) was a hanging mercury drop electrode (HMDE) Metrohm model EA 290. This electrode was filled with triply distilled mercury (JT Baker, Anachemical). The electrode capillaries were salanized using 4% dimethyl-dichlorosilane in dichloroethane before filling it with Hg. Silanization of the capillary was

done by aspirating concentrated nitric acid though the capillary to remove residual mercury before rinsing thoroughly with water and methanol, drying in an oven for 2 hours at 200°C . A 4% dimethyl-dichlorosilane in dichloroethane prepared immediately prior to use was then used to fill the capillary and baked in the oven at 207°C for 4 hours. The silanization of the inside of the capillary made it hydrophobic ensuring reproducible and stable drop characteristics. The tip of the capillary was treated with sodium hydroxide solution when filled with Hg to return the hydrophilicity of the glass and to eliminate silane contamination

The WE is a Kemula type syringe electrode consisting of a piston pushing mercury from the reservoir down into the capillary producing a small drop with an area of 0.00888 cm^2. The graduation at the top allows for making identical drops thus guaranteeing reproducibility. The Hg filled capillary was cleaned by dipping in H_2SO_4 and rinsed with methanol and water before introducing it into the cell. The reference electrode (RE) was a saturated calomel electrode (SCE) connected to the electrochemical cell working solution through a salt bridge. The counter electrode (CE) was a platinum coil placed at a fixed distance from the working electrode. The electrochemical cell, CE and all other glass-ware were cleaned in a warm acid (H_2SO_4 + HNO_3) mixture, washed with high purity Millipore water (18.2 Ω). The fourth electrode was a platinum wire placed close to the reference electrode in solution and connected to the reference electrode via a 1 nF capacitor (see appendix for more explanation). The experimental set up is shown in Figure 4-1.

The 0.1M electrolyte solutions used in this thesis were prepared using salts from Fluka in high purity Millipore water. KCl was calcined at 500°C for 48 hours to remove organic impurities before use. LiCl and TMACl were used without further purification. The electrochemical cell was then filled with about 50ml of the electrolyte solution and deaerated with argon before filling the salt bridge and beginning the experiments. A blanket of argon was maintained on the surface of the electrolyte solution to prevent the re-oxidation of the electrolyte solution. The formation of DOPC (Lipid products (UK)) monolayer at a gas-solution interface and onto a mercury drop was achieved by injecting about 9-10 µl of 2 mg/ml DOPC in pentane onto the electrolyte interface and the solvent allowed to evaporate (Figure 4-2). The Hg drop was extruded in the inert argon atmosphere and then deposited through the monolayer surface. Reproducible layers were formed after a number of these deposition steps. $CaCl_2$ and TMACl solutions were injected through the monolayer and stirred.

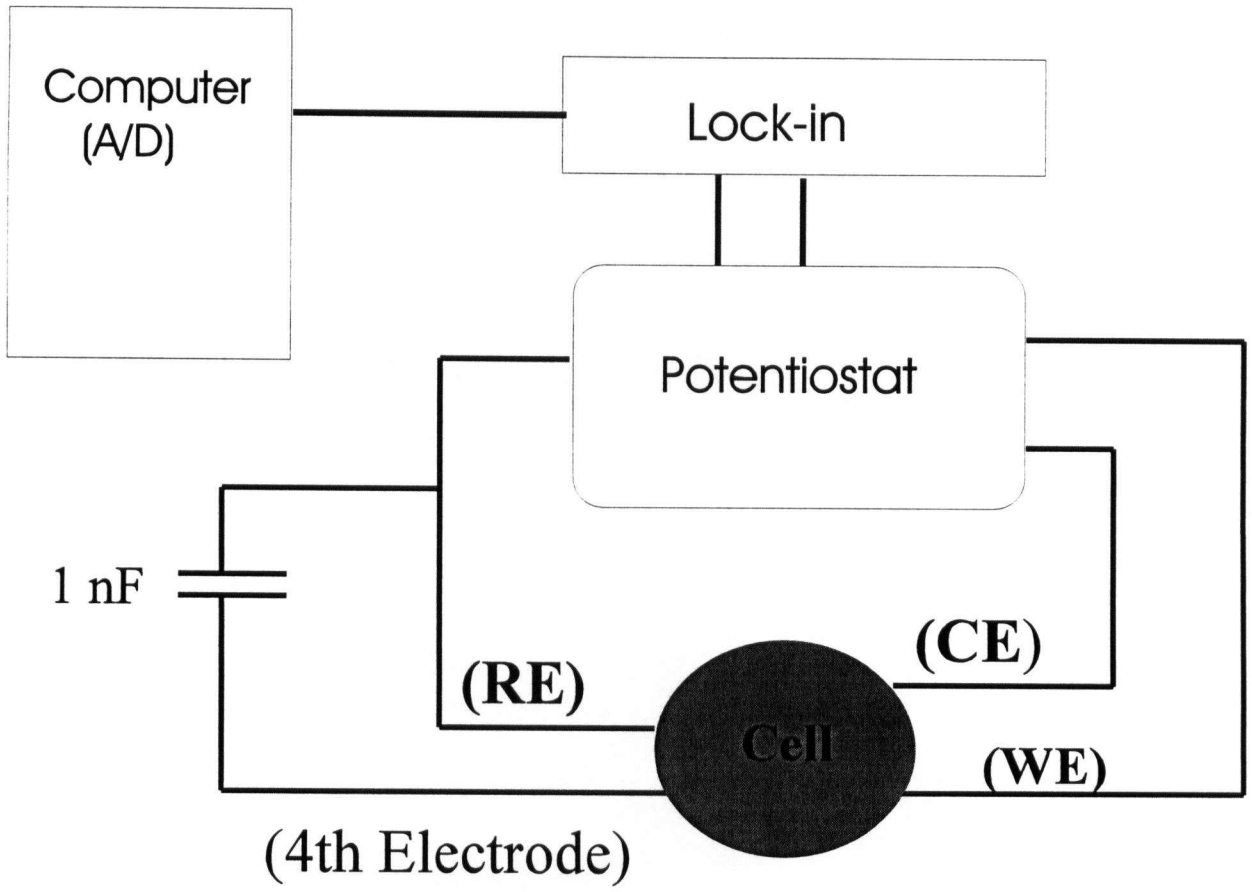

Figure 4-1 A schematic diagram for the electrochemical and impedance spectroscopy instrumentation.

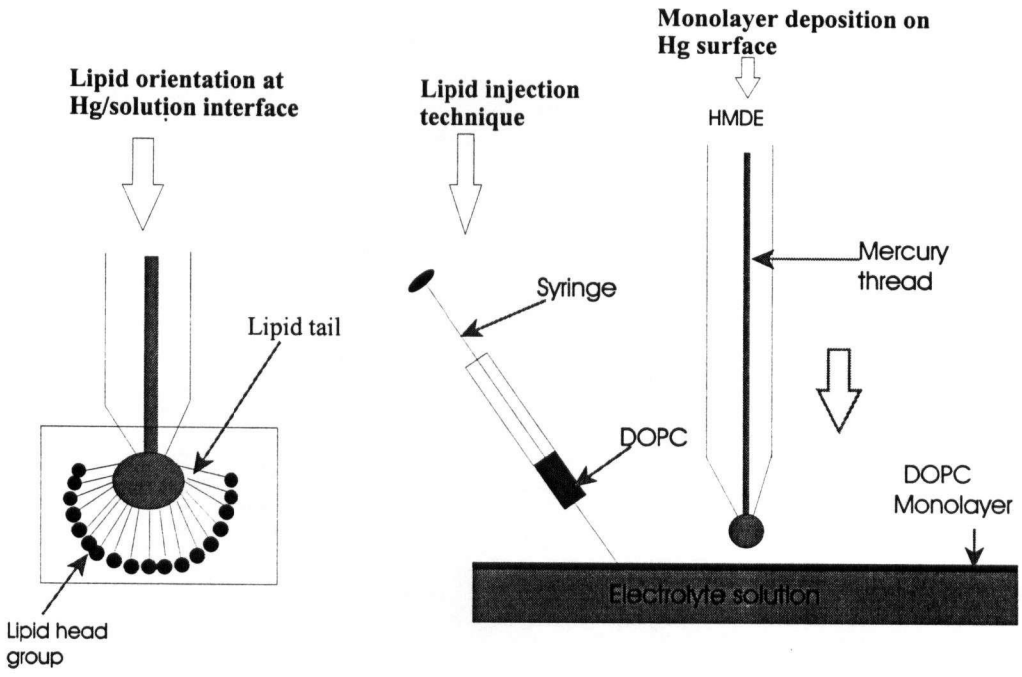

Figure 4-2 A schematic diagram for the technique used for the forming the monolayer on the solution surface and transferring the monolayer onto the electrode surface.

4.1.3 Systems studied

The interaction of cations with DOPC monolayer adsorbed onto Hg-solution interface was studied on five systems. They were DOPC monolayer adsorbed onto Hg-0.1M KCl interface in which the influence of potassium cations on the lipid monolayer was the primary concern, the DOPC monolayer supported onto Hg-0.1M LiCl interface was to investigate the interaction of lithium cations with the surfactant and the DOPC monolayer adsorbed onto Hg-0.1M TMACl interface, and the purpose was to study the effect of tetramethly ammonium cations on the monolayer. Other systems were DOPC monolayer supported onto Hg-0.1M KCl interface in which different amounts of Ca^{2+} had been added into the working solution subphase. This was the most studied system, aimed at investigating the interaction of Ca^{2+} with the lipid monolayer, and the last was the DOPC monolayer adsorbed onto Hg-0.1M KCl interface with 0.1M Ca^{2+} and 0.1 M TMA^{+} present in the working solution subphase, which targeted the investigation of the simultaneous interactions of the two cations with the monolayer.

4.1.4 Electrochemical procedures

The electrochemical technique adopted for this project was the differential capacity measurement. For all experiments, the initial potential was set at -0.4 V (SCE) which was close enough to the potential of zero charge for Hg. During the capacity measurements, the potential was scanned at 10 mV/s from -0.3 V to -1.85 V (SCE) on a bare Hg drop in contact with the respective electrolyte solutions (0.1 M KCl, LiCl and TMACl). The capacitance of a Hg / 0.1M KCl, LiCl and TMACl interface was first recorded and then used to verify the stability of the Hg drop, the reproducibility of the drop size and to ensure that the system was free from contamination. The monolayer was formed on the electrode surface at the minimum potential of -0.4V (SCE) which gave a capacitance of 1.85$\mu F/cm^2$. The characteristics of the DOPC modified interface were then examined by exploring the capacitance over a limited potential range (-0.3 to -1.2V (SCE)). Depending on the information being sought, the potential window was then increased to a more negative potential (desorption potential), during which the capacitance of the DOPC modified interface was measured between the potential ranges -0.3 V to -1.85 V (SCE) for KCl, -0.3 V to -2.1 V (SCE) for LiCl and -0.3 V to - 2.0 V (SCE) for TMACl. Usually, this experiment was carried out

to investigate the adsorption-desorption processes. In both potential windows, the potential was scanned more slowly at 5 mV/ s and at -0.8V (SEC) which is slightly more positive potential than the pseudo-capacity peak potential, the sensitivity of the lock-in was amplified (×33) times in order to have a closer look at the potential induced phase changes represented by the pseudo-capacity peaks.

The modification of the DOPC monolayer adsorbed onto Hg-0.1M KCl with various concentrations of calcium chloride and tetramethyl ammonium chloride was accomplished through their careful introduction to the working solution subphase.The monolayer was first modified by injecting 0.1 mM Ca^{2+} into the supporting electrolyte and stirred gently and carefully to allow for the formation of homogeneous mixture while avoiding the disruption of the monolayer. Normally, the mixing was done for 1 minute before characterizing the modified monolayer. This procedure was repeated for various concentrations of calcium chloride. The concentration of calcium chloride in the cell was varied from its initial concentration of 0.1 mM to 10.0 mM by a factor of 10. This was done to determine appropriate concentration of calcium chloride that could effectively stabilize the monolayer without disrupting the peaks. Then the monolayer was modified using a combination of calcium chloride and TMACl by introducing 0.1M calcium chloride first followed by 0.1M TMACl. The DOPC monolayer spread onto Hg electrode has been well characterized previously [4]. The results obtained with calcium chloride and tetramethyl ammonium chloride was compared with this well characterized system.

4.2 Electrochemical Impedance Spectroscopy

4.2.1 Instrumentation

The impedance spectroscopy measurements utilized an Autolab (Eco Chemie, the Netherlands) which is a multi-functional instrument loaded with a frequency analyzer module, Frequency Response Analysis (FRA2). It was used as a single sine Fourier transformation instrument. The amplitude of the ac perturbation was 2 mV and the frequency was varied from 10^6 Hz to 30Hz for high frequency analysis using single sine waveform and 30Hz to 0.1Hz for lower frequency experiments using multisine waveforms. The high frequency range was made accessible through the use of a 4^{th} electrode, which was a Pt wire was inserted into the working solution and

connected to the RE through a 1 nF capacitor. The ac perturbation was applied for five cycles before commencing the measurements in order to attain the steady state conditions. An integration time of 5 sec., which is the time taken between the application of the signal and when the signal is actually measured, was used. The instrument provided the real and imaginary impedance of the cell, Z' and Z'' or the corresponding admittance components Y' and Y''.

4.2.2 Methodology

A general purpose electrochemical system (GPES) project software, written in Autolab was used to perform the FRA measurements. The project gives the freedom to perform a variety of experiments within one set up and involves the execution of different tasks sequentially. A Cyclic Voltametry (CV) procedure combined with a Labview program was used to measure the capacitance of the monolayers. The procedure scanned the potential while the data was collected and recorded using Labview. This ensured that the monolayer was perfect and defect free. After the scan, the potential was held at minimum potential -0.4V (SCE). A sweep and scan (sas) procedure was then used to sweep the potential from minimum potential to the FRA potential and to hold the potential at the FRA potential. FRA project was then called to perform FRA measurements. After the measurements, the potential was held at the FRA potential. Another sweep and scan procedure was then employed to sweep the potential from the FRA potential back to the minimum potential, -0.4V (SCE). Another CV procedure similar to the first, was used to measure the capacitance to check if the morphology of the monolayer was not significantly disrupted.

5 Results and Discussions

The main aim of the current study was development of an electrochemical impedance spectroscopy methodology for further characterization of potential induced behavior, for a phospholipid (DOPC) monolayer supported on a hanging mercury drop electrode (HMDE) in contact with an aqueous electrolyte solution. The motivation behind this project was to design a methodology that could be used to study potential induced changes in monolayer behavior (adsorption-desorption process and kinetics of phase transitions) observed using standard electrochemical techniques, but which require quantitative interpretation. This was indeed a very challenging task and in order to achieve this goal, the developed technique had to be tested in order to justify its validity.

The adsorption of DOPC onto Hg in 0.1M aqueous solutions of KCl, LiCl and TMACl respectively at different negative potential limits, was characterized utilizing a standard electrochemical technique, i.e., AC voltametry, measuring the differential capacitance of the modified interfaces. Various concentrations of Ca^{2+} were introduced to the solution subphase of the KCl system and characterized by capacitance. The influence of both applied electrode potential and cations on the monolayer organization was studied. Also demonstrated was the dependence of the kinetics of phase transitions on the nature of the lipid monolayer influenced by cationic species present in the supporting electrolyte.

The impedance spectroscopy methodology was then tested on the system consisting of DOPC monolayer adsorbed onto Hg-0.1M KCl interface, with various concentrations of Ca^{2+} in the solution subphase. The focus was on the pseudo-capacitance peaks, the adsorption and desorption potential regions. The aim was to show that the technique developed could be applied to investigate the influence of Ca^{2+} on adsorbed DOPC monolayer. This study emphasizes that the results obtained from the impedance spectroscopy are preliminary findings and are discussed only on the basis of qualifying the validity of the methodology developed. The detailed interpretation of these results is in progress.

5.1 Electrochemical Characterization of DOPC Monolayer on Hg Electrode.

The current study focuses on the characterization of pseudo-capacitance peaks, the effect of cations on the lipid layer and the nature of the desorbed species. The results obtained with different electrolyte solutions are compared emphasizing any differences or similarities. In this study, all the capacitance measurements using AC voltametry were perfomed at 70 Hz. All the potentials have an accuracy of ± 2 mV.

5.1.1 Differential capacitance measurements (-0.30 V to -1.20 V (SCE))

Capacitance measurements of the modified Hg interface over a limited potential window, i.e., -0.40 V to -1.20 V (SCE), was performed as the initial characterization of the adsorbed layers. The capacitance for Hg in contact with the respective electrolyte solutions was recorded first and the characteristics of the modified surface were examined by exploring the capacitance over the limited potential range (Figure 5-1).

The DOPC monolayer assembled on the Hg electrode surface, with 0.1M KCl supporting electrolyte (Figure 5-1(a)), displayed a low capacitance region (1.85 $\mu F/cm^2$) at around -0.40V (SCE), which remained constant between the potentials around -0.30V and -0.80V (SCE). The vertical arrow at -0.80V (SCE) represents an increase in sensitivity (×33) permitting a more detailed investigation of the low capacitance region. When the potential was scanned to more negative values, two sharp pseudo-capacitance peaks (peak 1 and peak 2) were observed at -0.967V and -1.045V (SCE) respectively. Beyond the potential of peak 2, the capacitance curve for the monolayer remained relatively constant but lower than that of bare Hg within this potential limit. These results were consistent with the previous work [4]. The peaks represent a complex structural reorientation of the lipid monolayer [4,19,20], where it has been suggested that peak 1 corresponds to phase change due to formation of defects in the monolayer organization, while peak 2 corresponds to a nucleation and growth process [29]. The peaks and capacitance of the minimum capacitance region were identical during the return scan (positive going scans). The adsorption of DOPC monolayer in 0.1M LiCl (Figure 5-1(b)) was similar to that of 0.1M KCl within this potential window. The adsorption of DOPC monolayer in 0.1M TMACl (Figure 5-1(c)), showed that the minimum capacitance was the same as in the previous two cases (0.1M KCl and 0.1M LiCl) and was identical

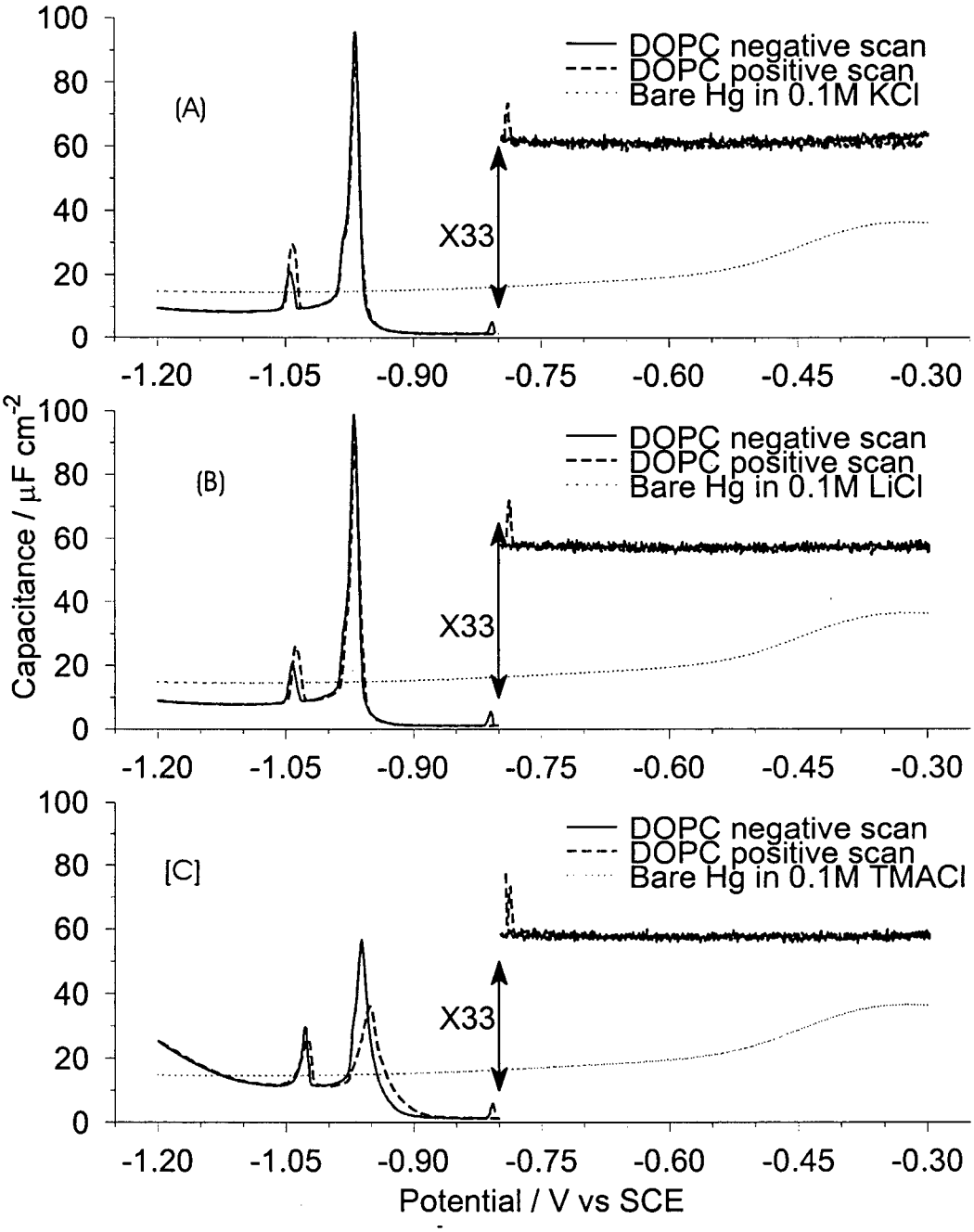

Figure 5-1 Capacitance curves for DOPC monolayer adsorbed onto Hg electrode in contact with different aqueous electrolytes at restricted potential window. (A) 0.1M KCl, (B) 0.1M LiCl and (C) 0.1M TMACl.

during both the negative and positive going scans. However, there were distinct differences with regard to the structural features of the peaks. Peak 1 occurred at slightly more positive potential (-0.961 V (SCE)) and was short and broad. Peak 2 was also observed at a more positive potential (-1.028 V (SCE)). During the positive going scan, peak 2 was superimposed, while on the return scan peak 1 was observed at -0.951 V (SCE).

The low capacitance (1.85 μFcm^{-2}) displayed in the minimum capacity region for all the systems studied, indicated that the lipid organization at the electrode-electrolyte interface was characterized by well-organized structures, free from defects. The fact that the capacitance curves were identical in all cases, during both negative and positive going scans, suggested that the monolayer remained undisrupted after the potential scan, which further revealed that the potential induced phase changes are reversible processes. The defects created during the negative going scan were annealed during the positive scan. The height of the peaks is related to the kinetics of these processes and therefore, for KCl and LiCl, the kinetics of the phase transition are fast, which could be assumed to mean little or no interaction between the cations with the lipid negative head groups. Interestingly, the monolayer in TMACl had similar minimum capacitance as in KCl and LiCl. However, peak 1 was short, broad and non superimposed suggesting sluggish kinetics of phase transition, possibly due to strong interaction between the TMA^+ cations with the lipid head groups. It is most probably true because TMA^+ being a hydrophobic cation, may penetrate into the disrupted layer and interact with the lipid tails as well as the lipid head groups. But, when the potential is made less negative and the disrupted layer heals, TMA^+ may be squeezed out and this could explain the recovery of the minimum capacitance.

The similarities in the monolayer behavior for the KCl and LiCl systems, offered very little information about the level of interaction of the alkali metal ions with the lipid monolayer. It was therefore prudent to investigate these systems further over a wider potential window in order to elucidate the degree of interaction of the lipid layer with the alkali metal ions. The extension of the negative potential limit was also meant to investigate the desorption of the lipid molecules from the Hg surface and the influence of the cations on the nature of the desorbed species.

5.1.2 *Differential capacitance measurements (-0.30V to -2.10V (SCE))*

The extension of the potential limit to a more negative domain caused significant changes in the adsorbed monolayer organization. The capacitance measurement was performed over a large potential range, i.e., -0.30 to -1.85 V for KCl, -0.30 to -2.10 V for LiCl and -0.30 V to -2.0 for TMACl. The choice of the negative potential limit was dictated by the ease with which such potential could be accessed without jeopardizing the experimental information being sought. For example, the more negative potential beyond -1.85 V in KCl, introduced the problem of potassium amalgam formation, which obscures the observation of lipid desorption from the electrode.

The capacitance for DOPC adsorbed from the gas-solution interface onto Hg in contact with 0.1M KCl (Figure 5-2(a)), displays a broad pseudo-capacitance peak (peak 3) at -1.34 V (SCE) during the negative going scan in addition to the two previously described peaks. Peak 3 corresponds to pre-desorption of the adsorbed layer from the Hg surface. The capacitance curve for the lipid remains higher than that of uncovered Hg immediately after peak 3, forming a kind of a plateau from -1.35 V to -1.55 V (SCE) before plunging below the bare Hg curve. At very negative potentials (-1.85 V (SCE)), the capacitance for the DOPC-covered Hg surface was equivalent to that measured for the uncovered Hg. This is interpreted as the desorption of the DOPC from the Hg surface. However, Guidelli and his coworkers [30] suggested that desorption could not be certain due to K^+ reduction to amalgam. The potential induced desorption has also been observed for unsaturated organic molecules adsorbed onto Hg [121] and for octadecanol and other lipid-like molecules adsorbed onto gold electrodes [2].

In contrast to the limited potential range, when the potential was scanned beyond peak 3 to desorption potential (-1.85 V (SCE)), a large difference in the resulting capacitance was observed. For the positive going potential scan, peak 3 was shifted positively, -1.2 0V (SCE), and the minimum capacitance after desorption-readsorption process was higher, indicating the presence of defects in the readsorbed layer organization.

The capacitance curve measured for DOPC adsorbed onto Hg drop in 0.1M LiCl supporting electrolyte (Figure 5-2 (b)), produced similar behavior as in KCl electrolyte except at very negative

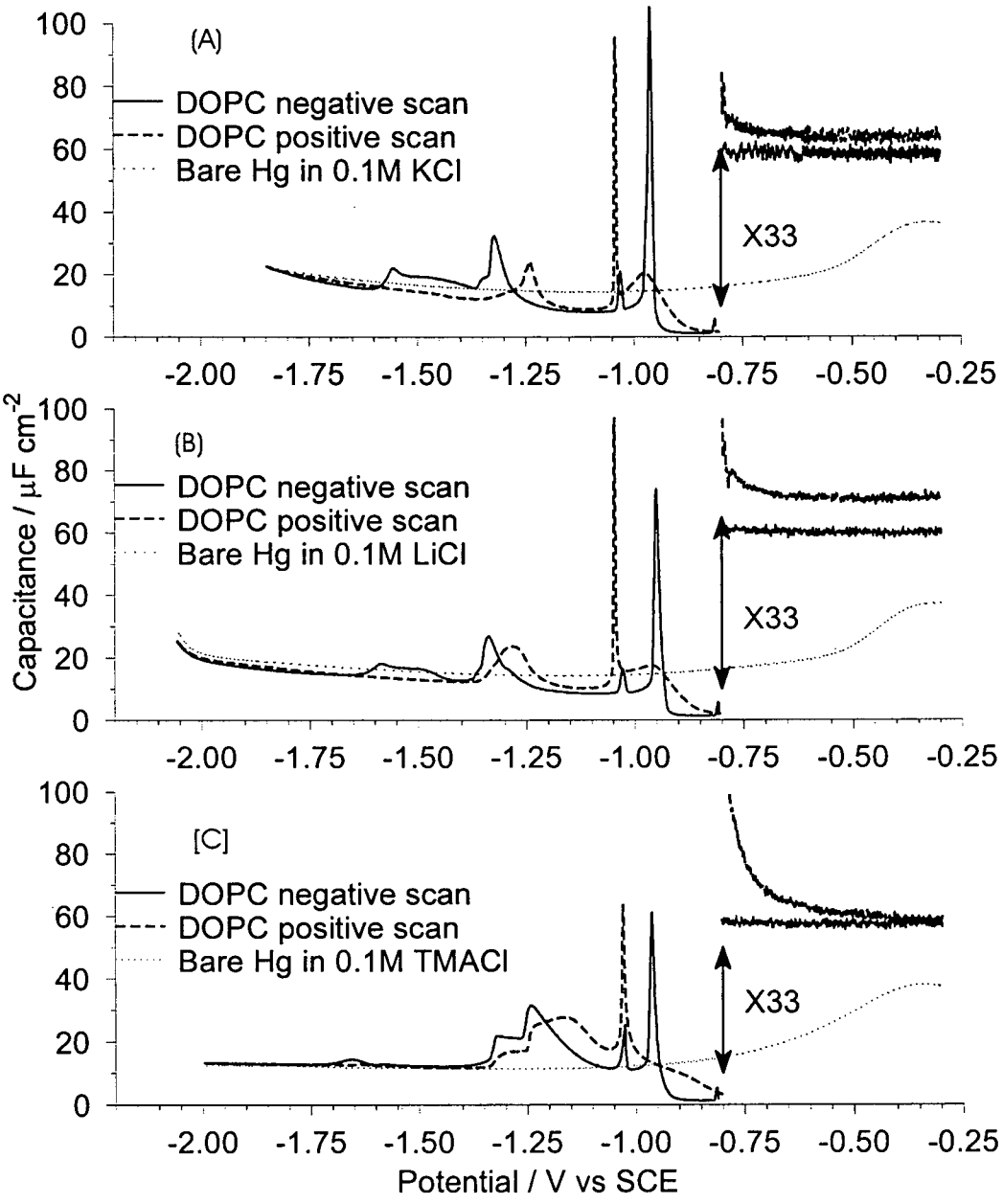

Figure 5-2 The capacitance curves for DOPC monolayer adsorbed onto Hg electrode in contact with different aqueous electrolytes at extended potential window. (A) 0.1M KCl, (B) 0.1M LiCl and (C) 0.1M TMACl.

potentials. The capacitance curve measured for bare Hg showed the discharge of lithium ions to the Hg surface at extremely negative potentials, -2.10V (SCE), forming lithium amalgam. The capacitance curve measured for the DOPC-covered Hg, produced a broad peak (peak 3) at -1.33 V (SCE) in addition to the two peaks described previously. Immediately after peak 3, the capacitance curve drops below the bare Hg curve before the formation of a plateau from -1.42 V to -1.56 V (SCE). As the potential was made more negative, the capacitance curve measured for the lipid ran parallel to that of bare Hg between the potentials, -1.60 V to -2.10 V (SCE), before the onset of lithium ion discharge. However, it remained lower than the bare Hg curve indicating that desorption failed to take place. Reversing the potential scan to positive going values, peak 3 was shifted positively, -1.28 V (SCE), peaks 1 and 2 were quite different and the minimum capacitance was higher. It is believed that the non-superimposition of these peaks was due to the formation of defects in the lipid layer after being exposed to very negative polarization, which is clear from the higher minimum capacitance measured at -0.40 V (SCE).

For TMACl supporting electrolyte, the capacity measurements showed very interesting behavior both at adsorption and desorption potential values (Figure 5-2(c)). During the potential scan to the negative direction, a very broad peak (speak 3) was observed at -1.24 V (SCE) alongside the other two peaks seen previously. Beyond peak 3, the capacitance curve measured for the lipid remain slightly above that measured for bare Hg until the potential of -1.65 V (SCE) where a very small plateau was observed from -1.61 V to -1.70 V (SCE) before a complete desorption from -1.75 V to -2.0 V (SCE). When the potential scan was reversed, peak 3 was shifted positive to -1.16 V (SCE). Even though peak 2 did not shift during the positive going scan, it was taller. However, peak 1 completely disappeared during the positive potential scan while the minimum capacitance was very high but progressively decreased to match the initial capacitance values. The disappearance of peak 1 and the extremely high minimum capacitance during the positive scan may suggest a strong interaction of TMA^+ cations with the lipid layer disrupting the lipid organization. The interaction may be ionic or hydrophobic in nature. Nonetheless, it is amazing how this severely disrupted layer heals and recovers its original organization at adsorption potentials. This may be due to the squeezing out of TMA^+ from the hydrophobic region (lipid tails) near the Hg.

The potential-induced desorption of lipid film, is believed to proceed with the formation of

micelles, which reside in the neighborhood of the electrode surface from where they can be reabsorbed [3,122]. Some studies [123-125] have also shown that the interaction of cations with phosphatidylcholine vesicles increases with the increase in their hydration Gibbs energy. Therefore, different behavior displayed by various alkali metal ions and by TMA^+ in the desorption of DOPC from the Hg electrode seems to support this claim. It is postulated that due to high hydration Gibbs energy of Li^+, the surface charge of desorbed DOPC micelles in the presence of lithium ions remains high thus, inhibiting their displacement from the electrode surface. This may explain why the capacitance curve for this system was consistently lower than that of bare Hg even at extreme negative potentials. In contrast, the low hydration energy of TMA^+ reduced the degree of interaction, which attempts to explain the desorption of the lipid at more positive potential in its presence than in the presence of alkali metal ions. In addition, the super-equivalent adsorption of TMA^+ cations especially onto a negatively charged Hg electrode [126], is believed to introduce adsorption competition between the TMA^+ and the lipid molecules onto Hg surface. Therefore, at negative potentials, the adsorption of TMA^+ ions out-compete the physisorption of the lipid molecules hence displaces the lipid from the Hg electrode surface.

The changes observed with different supporting electrolytes, and with the different potential limits, are too severe, i.e., with such big deviations, other processes of significant importance could easily be obscured. Smaller changes were therefore required in order to investigate the effect of cations on the lipid layer in fine details. Therefore, the system consisting of adsorbed DOPC with 0.1M KCl working electrolyte, was chosen for further studies with addition of calcium ions in the subphase. Calcium ions are known to play an important role in lipid monolayer organization. In this study, differing concentrations of calcium chloride in the supporting electrolyte subphase and its effect on the adsorbed lipid monolayer was investigated, by both electrochemical and impedance spectroscopy techniques.

5.1.3 The Effect of Ca^{2+} ions on the adsorbed DOPC monolayer

Figure 5-3 shows the capacitance scans for bare Hg-0.1M KCl interface and the DOPC modified interface, with additions of $CaCl_2$ to the concentrations of 0.0 mM, 0.1mM, 1.0mM and 10mM respectively in the solution subphase. In the absence of Ca^{2+}, the capacitance for the DOPC-

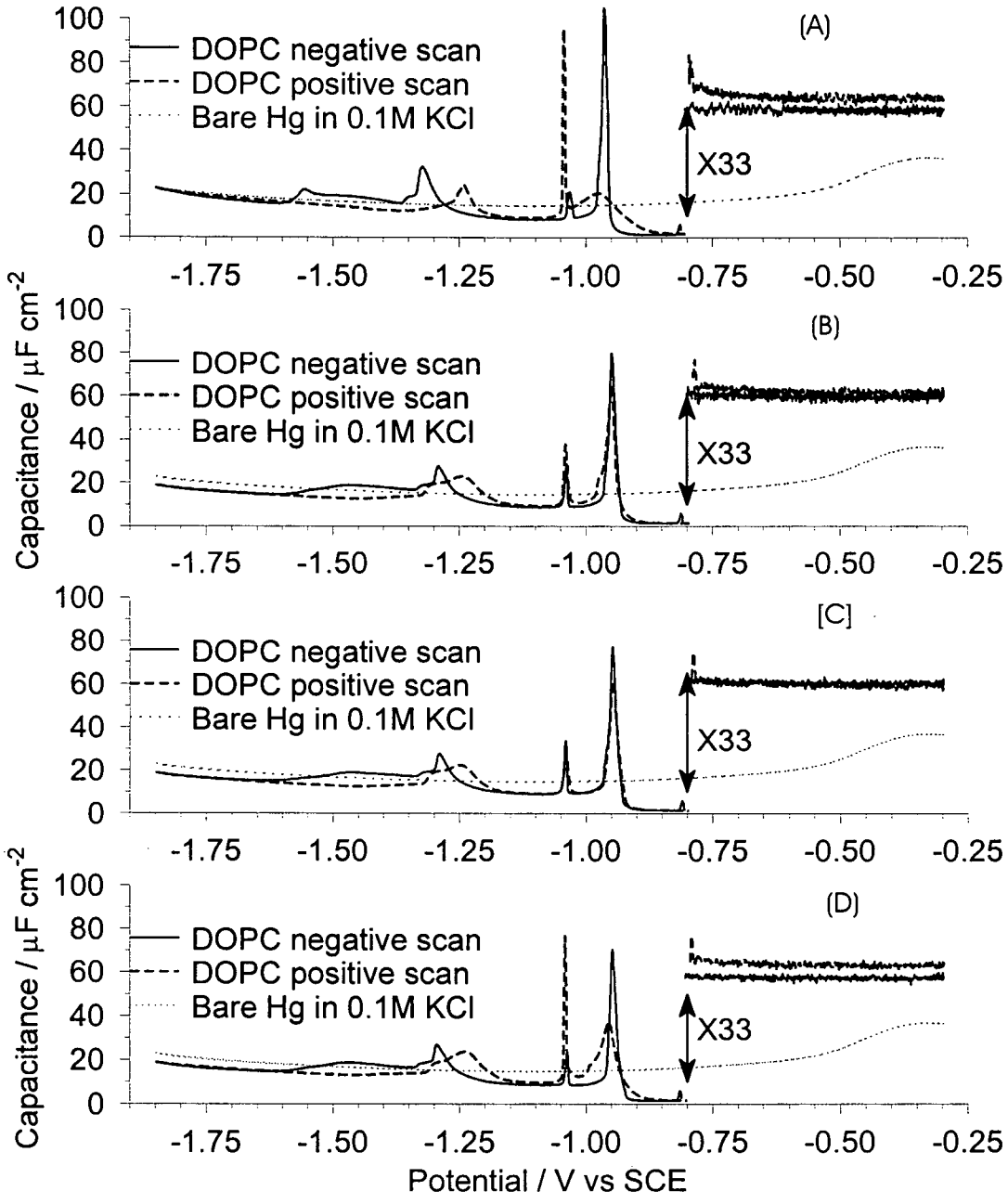

Figure 5-3 The capacitance curves showing the effect of Ca^{2+} on adsorbed DOPC monolayer . (A) 0.0 mM Ca^{2+}, (B) 0.1 mM Ca^{2+}, (C) 1.0 mM Ca^{2+} and (D) 10.0 mM Ca^{2+}.

covered Hg drop (Figure 5-3 (a)), has already been discussed. Briefly, when the potential was scanned negatively from the adsorption potential, -0.40 V (SCE), the lipid underwent potential induced phase transition manifested as peaks in the capacitance plot. Further negative potentials, the lipid molecules are displaced from the Hg surface accompanied by severe disruption of the layer. Reversing the potential scan, the peaks failed to retrace and the minimum capacitance was higher. The capacitance curve is used as reference (control experiment) and the results obtained from the effect of calcium ions experiments are compared with it.

The influence of Ca^{2+} is shown in Figure 5-3. It can be seen from Figure 5-3(b) that the presence of the Ca^{2+} ion in the subphase modified the monolayer organization. The difference in the minimum capacitance measured during the negative and positive scans was reduced. The height of peak 1 decreased but was nearly retraced during positive going scan. Peak 2 on the other hand was slightly reduced in height on the positive going potential scan and was retraced. Peak 3 also experienced potential induced modifications to a broad, and negatively shifted peak on the return scan. The plateau like-structure at -1.35 V (SCE) changed slightly. More negative potentials displayed a situation where the capacitance curve for the lipid remained permanently below and parallel to that of the bare Hg curve, which could be interpreted to mean non displacement of the lipid from the Hg surface.

Figure 5-3 (c) represents the influence of 1.0mM Ca^{2+} ions on the lipid monolayer. The minimum capacitance was identical at the start of the scan and after returning from -1.85 V (SCE), which indicates that the lipid layer regained its initial molecular organization after the potential scan. Peak 1, even though continued to decrease in height, it was also shifted further more positive during the positive going scan, where it aligned itself with its negative scan counterpart. Another consistent change was observed in peak 2, which did not only continue to exhibit a low peak intensity but also continued to be shifted slightly positively on the return scan. However, the two peaks remained superimposed. Also, peak 3 was shifted further negative as the potential was scanned back but was still broad in shape. The features of the plateau did not change much, while at very negative potentials, the capacitance curve measured for the lipid continued to be lower than, and parallel to that of bare Hg curve.

Figure 5-3 (d) shows the effect of 10.0mM Ca^{2+} ions. It can be seen from the capacitance curve that the concentration of Ca^{2+} ions is more than the threshold concentration necessary to bring about the stability of the adsorbed monolayer. It is believed that the monolayer experienced a strong interaction with the Ca^{2+} ions leading to the disruption of monolayer organization, i.e., the instability of the lipid layer toward the negative potential excursion is reintroduced. This is clearly illustrated by the difference in the minimum capacitance measured during the negative and positive going scans. In addition, the disorganization of the layer is clearly evidenced by the differences observed in peak 1 and 2 during the positive going potential scan.

With the peaks (except for peak 3) retracing each other during the negative and positive going potential scan, and the minimum capacitance being identical Figure 5-3(c), the monolayer is believed to have attained mechanical and chemical stability at 1.0 mM Ca^{2+}. The corresponding Ca^{2+} ions' concentration may be considered as the optimum value required to achieve this characteristic.

5.1.4 Effect of combined Ca^{2+} and TMA^{+} ions on DOPC monolayer

Figure 5-4 shows the interesting effect of both 1.0mM Ca^{2+} and 1.0mM TMA^{+} cations due to their simultaneous interaction with the lipid monolayer supported on a Hg-0.1M KCl interface. Clearly, it can be noted that each cation (Ca^{2+} or TMA^{+}) interacts independently with the monolayer. The capacitance curve demonstrates the stability of the layer, which is due to its interaction with the Ca^{2+} cations. The peaks and the minimum capacitance respectively, are identical when the potential scan was cycled negatively and positively. Another capacity feature appearing prominently in the curve, is the likelihood of a complete desorption of the lipid from the Hg surface. This is indicated by the capacitance curve for the lipid and of uncovered Hg merging together at very negative potentials. The displacement of the lipid from the electrode was accomplished via the process of competitive adsorption between the calcium-stabilized lipid molecules and the TMA^{+} cations.

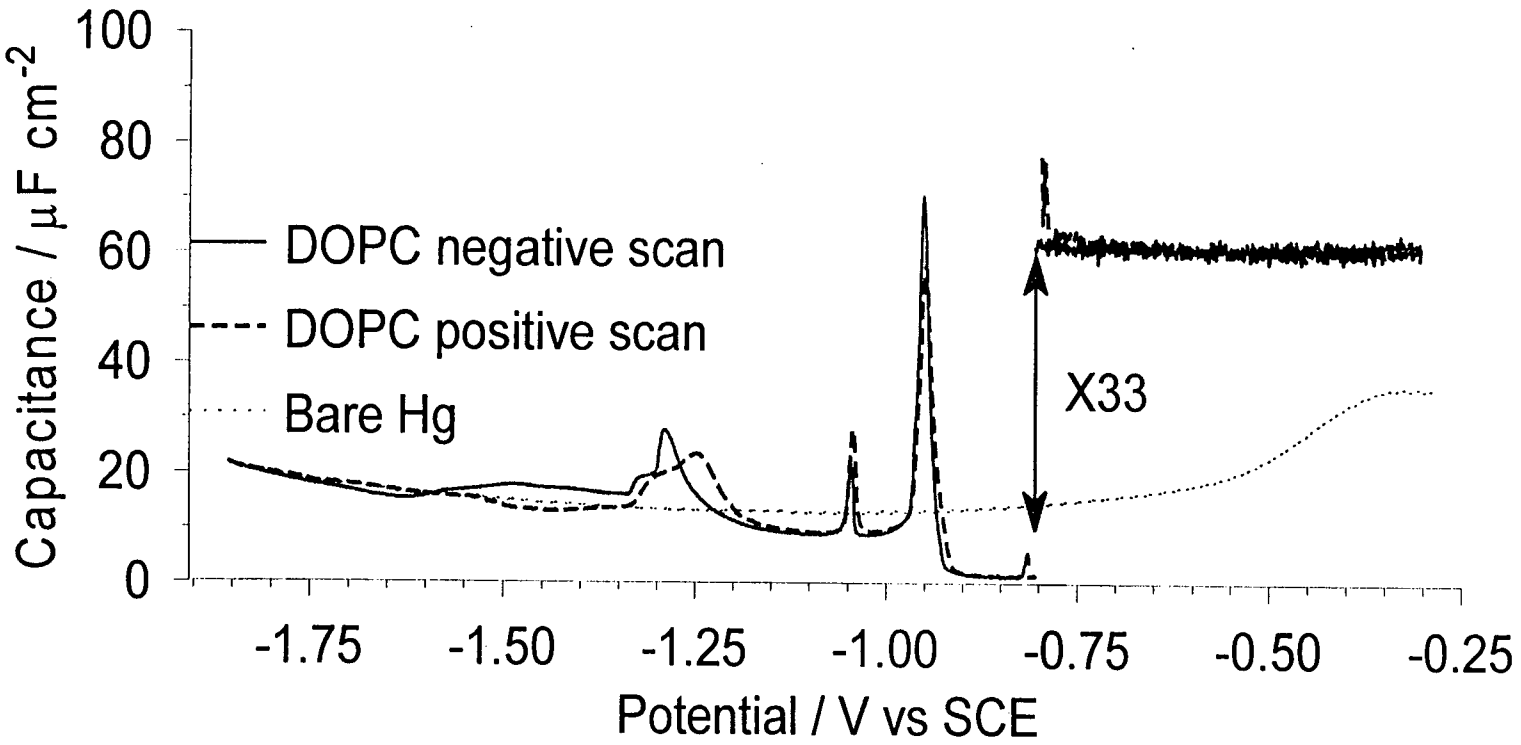

Figure 5-4 The capacitance curve showing the influence both 0.1M Ca^{2+} and 0.1M TMA^{+} on DOPC adsorbed onto Hg electrode.

5.1.5 Conclusions

The electrochemical investigation of the adsorbed DOPC monolayer has revealed that both negative potential and the presence of cations affect the monolayer organization. Large negative polarizations displaced the adsorbed lipid molecules from the charged interface replacing them with water. In addition, exposing the lipid monolayer to very negative potentials also disrupted its morphology. The presence of Li^+ stabilized the monolayer towards negative potential excursion but this stability collapses as soon as the potential is made more positive. Tetramethyl ammonium cations (TMA^+), effectively competed with lipid molecules for adsorption onto negatively charged Hg surface and coupled with its small hydration Gibbs energy, it displaced the surfactant from the electrode surface at more positive potential than the alkali metal ions. It was found to desorb even the Ca^{2+} stabilized monolayer.

Addition of various amounts of Ca^{2+} to the supporting electrolyte systematically changed the capacitance curves. The height of the pseudo-capacitance peaks decreased with the increase in Ca^{2+} ions concentration due to stability of the monolayer thus slowing the kinetics of phase transition. The largest effect of Ca^{2+} was observed at the extreme potential limits. At the negative potentials, the capacitance was below and parallel to that of bare Hg, and the capacitance decreased with the increase in Ca^{2+} concentration from 0.1mM to 10mM suggesting an incomplete desorption of the lipid from the electrode surface. The most remarkable observation was the stability towards negative potential excursion afforded to the layer by addition of 1.0 mM Ca^{2+} ions. High concentrations of Ca^{2+} tended to disrupt the layer because of strong interactions with the monolayer. These results are consistent with the known fact that Ca^{2+} binds to the PC head groups of the lipid thus stabilizing the monolayer towards negative potential excursion. From the experiment with combined Ca^{2+} and TMA^+ cations on DOPC monolayer adsorbed onto Hg-0.1M KCl, an attempt was made to demonstrate the possibility of stabilizing the monolayer towards negative potential excursion, desorb it from the electrode surface and readsorb it without altering its morphology.

5.2 Impedance Spectroscopy Characterization of DOPC Monolayer on Hg

5.2.1 Introduction

In the preceding section, it was shown how the applied potential and the presence of various cations, together affect the lipid monolayer organization, the kinetics of the phase transitions and the nature of the desorbed species. These findings prompted a more detailed investigation of the lipid monolayer employing electrochemical impedance spectroscopy (EIS).Therefore, an EIS methodology was developed and tested on DOPC adsorbed onto Hg-KCl interface. The procedure used to perform the EIS study was described in Chapter 4. Briefly, peaks 1 and 2 were characterized by scanning the potential from adsorption potential to the potential corresponding to the peak (the peak potential) and recording the impedance over a wide frequency range. Peak 3 was investigated by first scanning the potential from the adsorption value to a potential just positive of the top of the peak and then measuring the impedance spectrum at different potentials running across the peak. The impedance spectra were also used to study the minimum capacitance region and the desorption potential region. For all the systems, the impedance was measured for the Hg-KCl interface in the absence and in the presence of DOPC. The differential capacity was recorded before and after the impedance measurements to ensure a good layer and to check if the layer was disrupted during the impedance measurement respectively.

5.2.2 Data presentation and analysis

The impedance data is plotted in various ways in order to show clearly the behavior of each component, i.e., the real and imaginary component of the impedance with respect to frequency at different potentials of the experiment. The inverse of impedance, admittance (Y) is plotted after dividing by frequency, yielding a frequency normalized admittance, which is plotted against the log of frequency. This representation shows clearly the distribution of data over the whole frequency range. The maximum displayed in the real admittance plot corresponds to the time constant of the cell. The capacitance calculated assuming series RC circuit is also plotted verses the log of frequency and is used to check against the results obtained with AC voltametry. Finally, the data is plotted in a Nyquist plot where each semicircle represents a series RC time constant.

5.2.3 *Impedance at peak 1(-0.96 V(SCE))*

Peak 1 was characterized by first scanning the potential from adsorption value (-0.4 V) to the potential corresponding to the peak maximum in uncovered Hg-KCl interface and impedance measured over a wide range of frequencies. This was used as a reference. Then the DOPC covered Hg-KCl interface was characterized using a similar procedure. The potential was scanned from adsorption value to the top of the peak and impedance measured. Shown in Figure 5-5 are impedance data plotted as described previously. The series capacitance is shown in figure 5-5(a). The value measured at 70 Hz is 120 $\mu F/cm^2$. This is consistent with the DOPC monolayer capacitance (100 $\mu F/cm^2$) measured by AC voltametry at 70 Hz using a series RC circuit as the model for the interface (see Figure 5-3). Addition of Ca^{2+} to the electrolyte subphase was observed to change the character of the peak and this effect was analyzed using the same scanning procedure. The presence of Ca^{2+} resulted in a decrease in capacitance peak height, evident also in these impedance measurements. The frequency dependence of the peak shows a flat region at low frequency and eventual roll off at high frequencies.

Figure 5-5(b) shows the Nyquist plot. All the DOPC systems show a single semicircle, characteristic of one series RC time constant for the process. This behavior can also be seen in real vs. log of frequency plot (Figure 5-5(d)), in which only one maximum is displayed by the system. Addition of Ca^{2+} consistently decreased the size of the semicircle, consistent with the decrease in capacitance peak height. This effect, which was also observed in the previous reactions, can be explained similarly as being due to the interaction of Ca^{2+} with the lipid head groups, leading to the modification of lipid layer in response to potential perturbation. The decrease in capacitance height and the size of the semicircle indicate slow kinetics for the phase transformation.

5.2.4 *Impedance at peak 2 (-1.04 V (SCE)*

A similar procedure as in peak 1 was followed where the potential was scanned from -0.4 V to the potential corresponding to peak 2 and the impedance measured, first for the uncovered Hg and then for the DOPC covered Hg. The peak series capacitance shown in Figure 5-5(a) is quite different when compared to peak 1, showing that this peak may represent significantly different type of phase transformation. However, the capacitance value measured at 70 Hz was consistent with the value

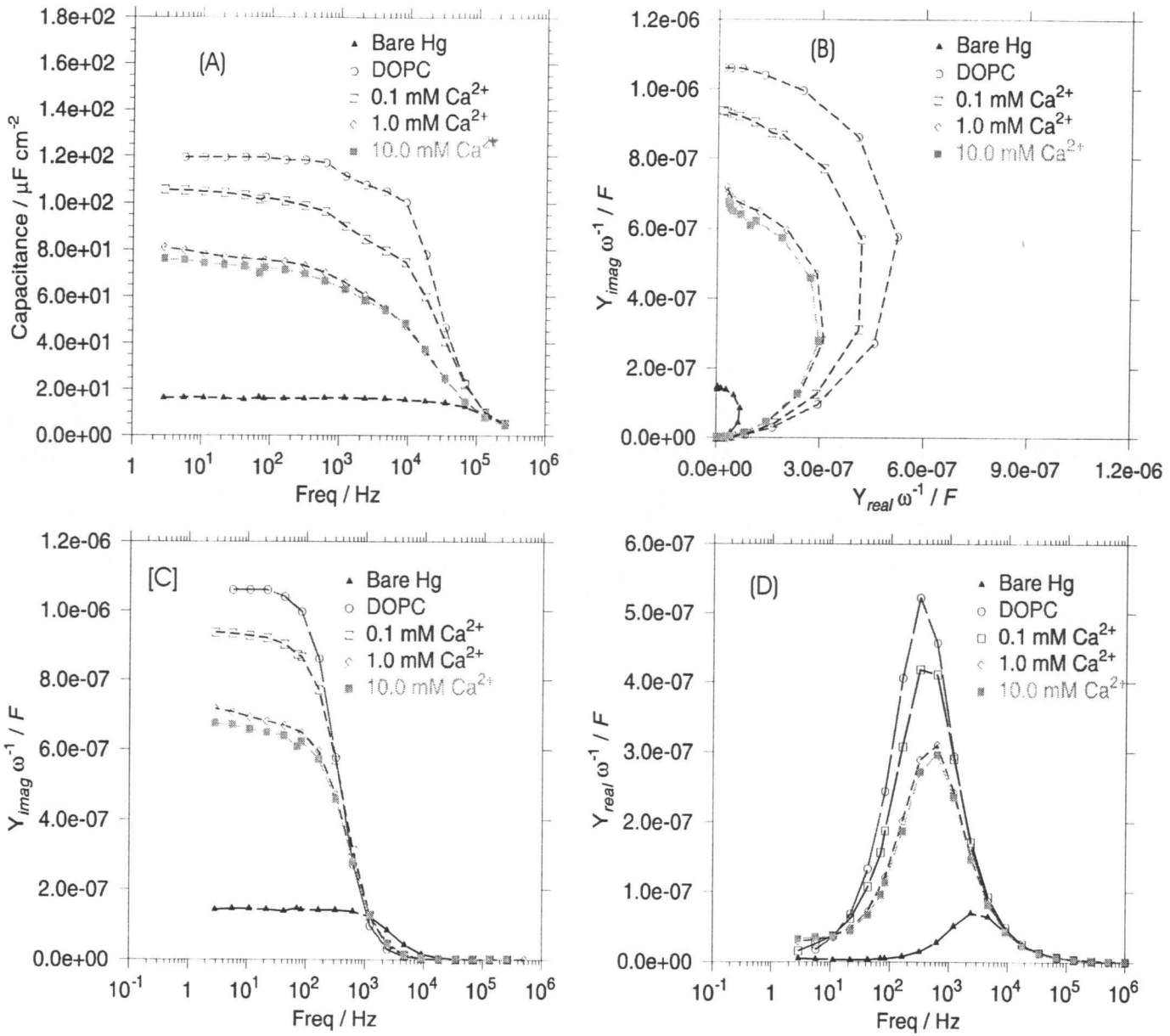

Figure 5-5 Different plots for impedance spectra of peak 1. (A) Capacitance plot, (B) Nyquist plot, (C) Imaginary impedance plot, and (D) Real impedance plot.

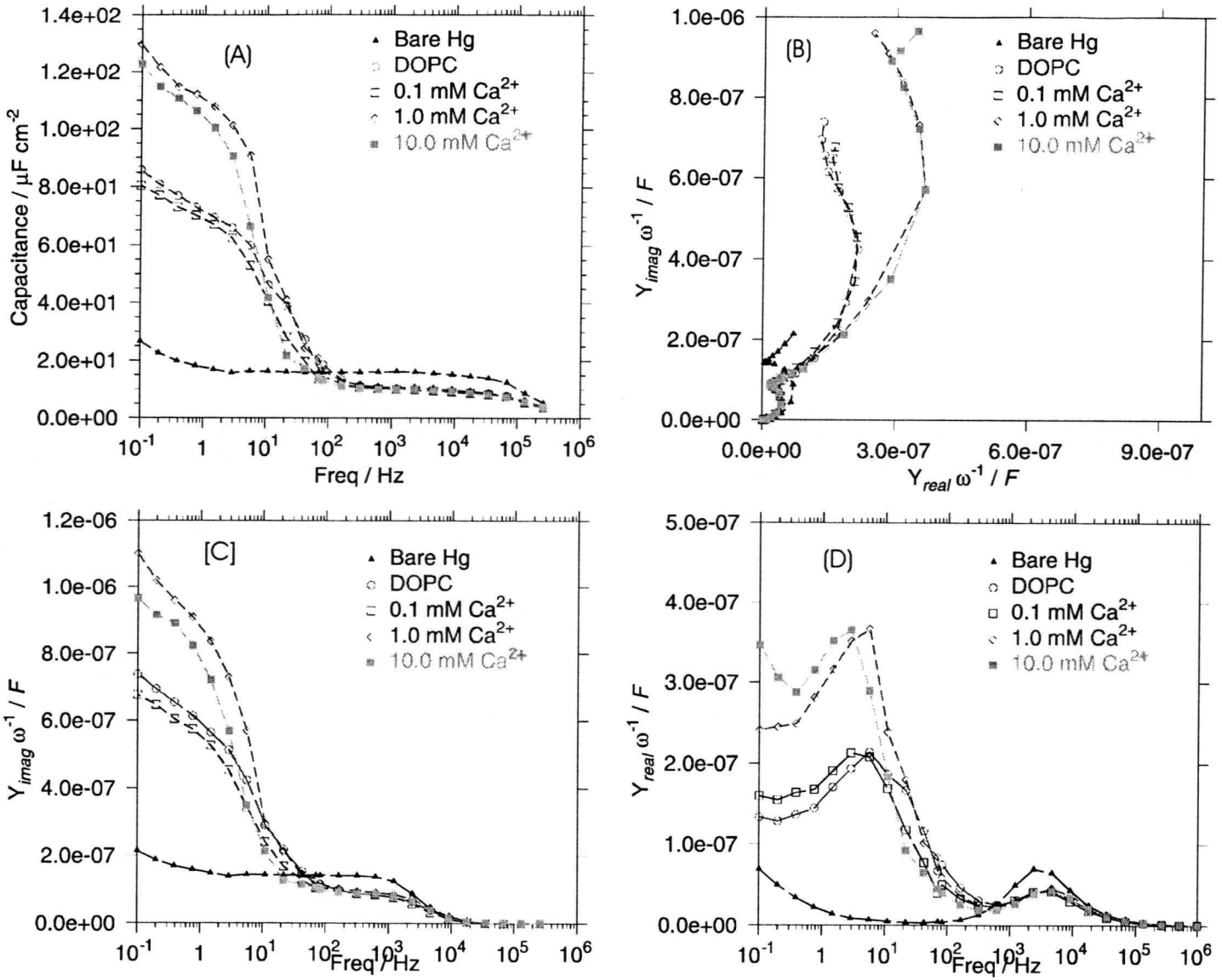

Figure 5-6 Different plots for impedance spectra of peak 2. (A) Capacitance plot, (B) Nyquist plot, (C) Imaginary plot and (D) Real impedance plot.

measured by AC voltametry shown in Figure 5-3. The Nyquist plot (Figure 5-6(b)), shows evidence of two semicircles, which is a characteristic of two series time constants. This is also clearly demonstrated in the real impedance plot (Figure 5-6(d)), displaying two maxima with time constants around 5 and 1500 Hz respectively.

The influence of Ca^{2+} was similar to peak 1, in that its presence changed the capacitance peak height and the size of the semicircle. However, it seemed to influence only the low frequency process. Increasing Ca^{2+} concentration led to an increase in the size of the semicircle, signifying an increase in the time constant for this process. This is also consistent with the influence of Ca^{2+} on this peak observed using AC voltametry (see Figure 5-3). This is a clear indication, as observed in peak 1 situation, that the interaction of Ca^{2+} with the lipid seems to reduce the rate of phase transformations.

5.2.5 Impedance at peak 3 (-1.34 V (SCE))

The impedance spectra of peak 3 was measured in a slightly different way when compared to peak 1 and 2. The potential was scanned from -0.4 V to a value just positive of the peak maximum. The impedance was measured at various potentials running across the peak. The potential corresponding to the highest measured capacitance was chosen to represent the top of the peak. The impedance data are plotted in two figures, Figure 5-7 and Figure 5-8. The first figure (Figure 5-7) is for DOPC covered Hg measured from 1 MHz to 0.1 Hz, while in Figure 5-8, the low frequency of measurement was limited to 1 Hz and shows the influence of Ca^{2+} on the monolayer at peak potential. This peak displayed three semicircles, most clearly evident in Figure 5-7(b). This is a characteristic of three series RC time constants. The real admittance plot (Figure 5-7 (d)), clearly show evidence of three maxima, and indicates that the changes taking place at the electrode at this potential are characterized by three time constants.

The effect of Ca^{2+} is shown in Figure 5-8. Addition of Ca^{2+} altered the sizes of the semicircle in different fashions. Increasing Ca^{2+} concentration showed a corresponding increase in the size of the semicircle at the low frequencies (Figure 5-8(b)), similar to peak 2. However, a reverse effect of Ca^{2+} was observed on the small semicircle formed at intermediate frequencies, i.e., increasing Ca^{2+} systematically reduced the size of the semicircle. Even though the high frequencies' semicircle was

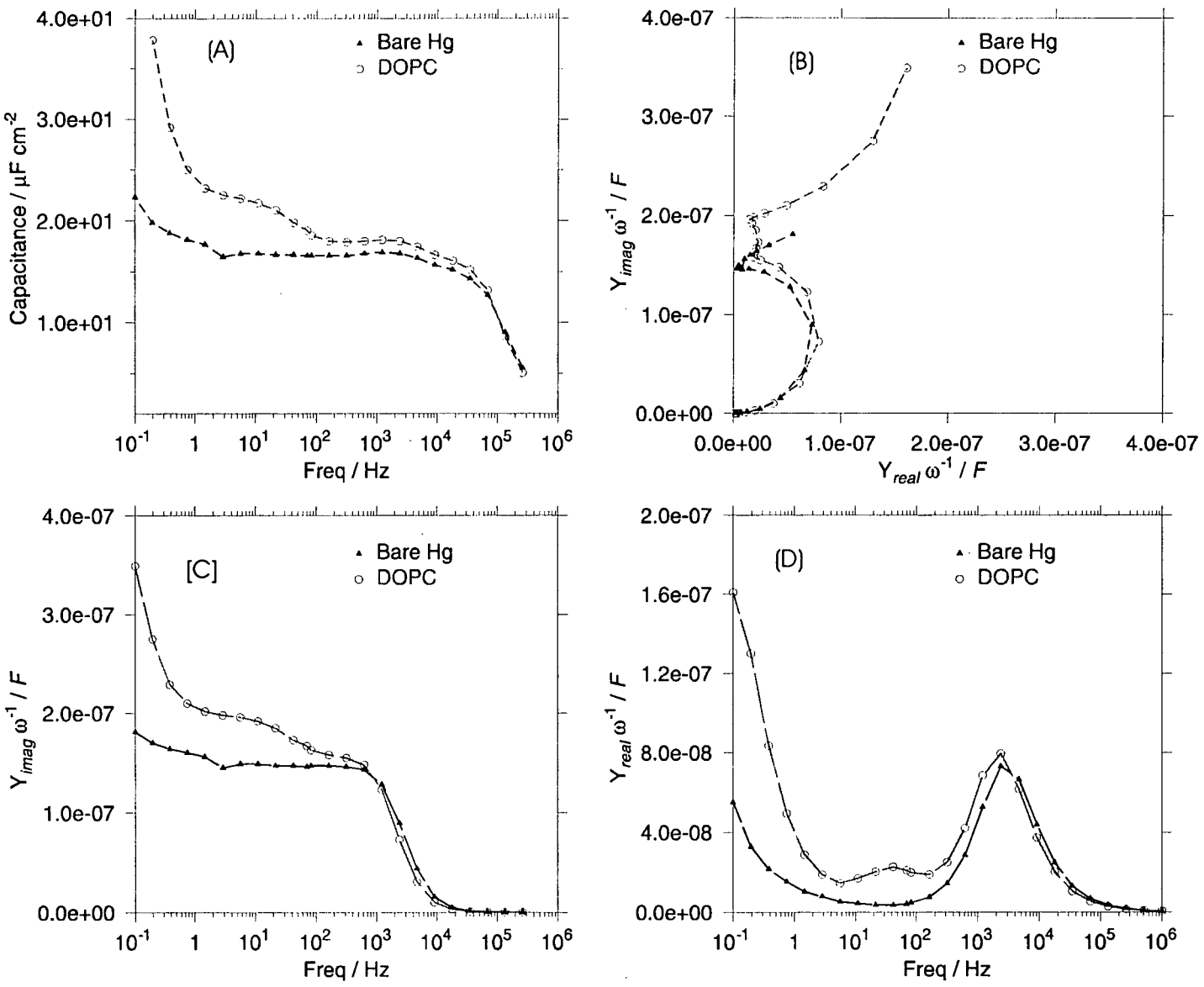

Figure 5-7 Different plots for impedance spectra of peak 3 with very low frequency of measurements of 0.1 Hz (A) Capacitance plot (B) Nyquist plot, (C) Imaginary impedance plot and (D) Real impedance plot

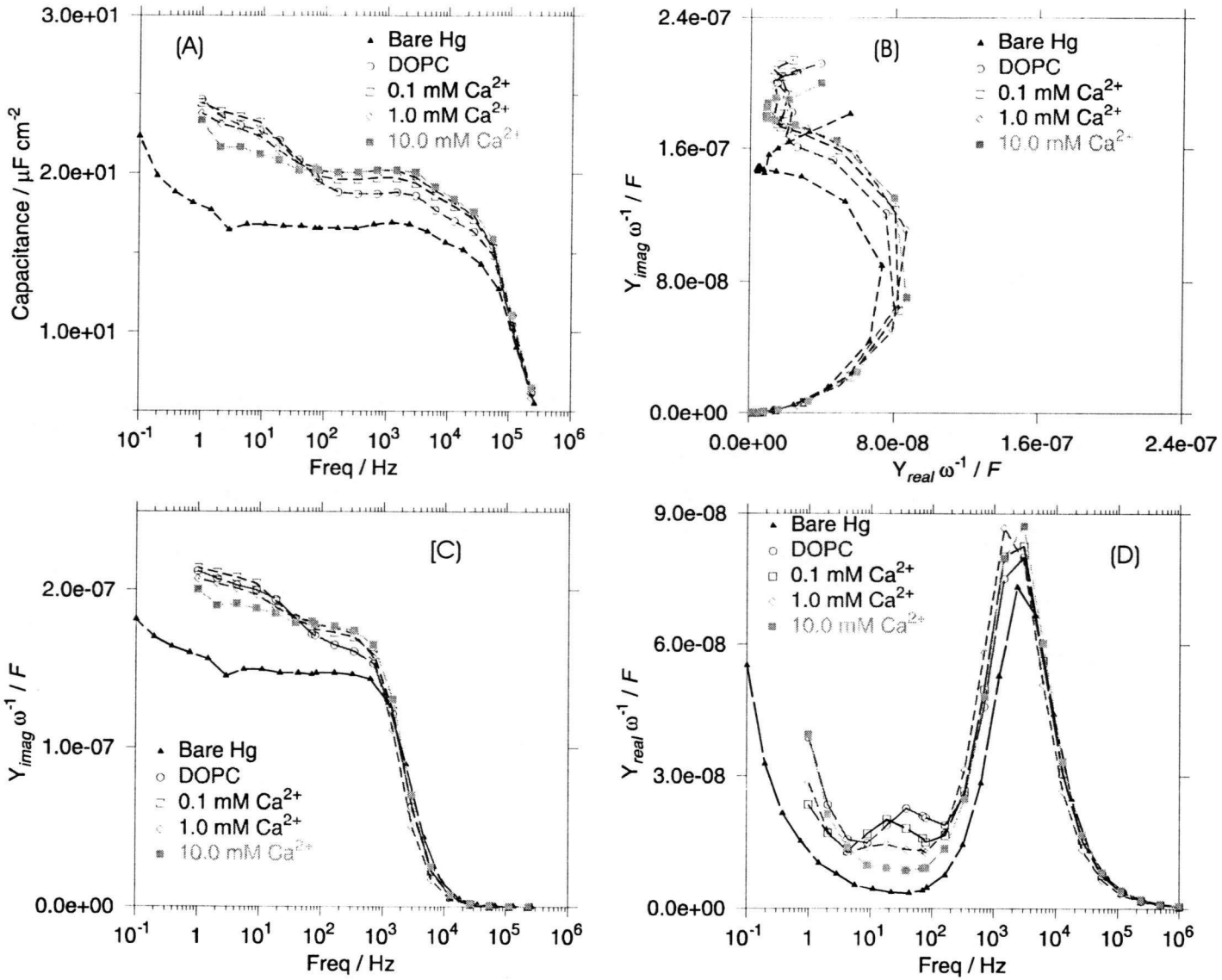

Figure 5-8 Different plots for impedance spectra of peak 3, with low frequency of measurement of Hz. (A) Capacitance plot, (B) Nyquist plot (C) Imaginary impedance plot and (D) Real impedance plot.

not fully measured, the increase in Ca^{2+} seems to increase the size of the semicircle. These observations are similar to peak 1 and 2 cases as well as what was seen previously using AC voltametry. Therefore, these changes observed in the sizes of the semicircles due to the presence of Ca^{2+} are consistent with the decrease in the peak capacitance heights. This indicates that Ca^{2+} influenced the phase transformation process at this potential over all the frequency range.

5.2.6 The impedance at desorption (-1.85 V(SCE))

The desorption potential was studied at the same time with the adsorption potential region. The impedance was measured at -0.4 V (adsorption potential) and on the same layer, the potential was scanned from adsorption value to desorption value (-1.85 V) and the impedance measured. Figure 5-9 (a) shows the series capacitance measured at the desorption potential (-1.85 V). The value measured at 70 Hz is consistent with the value measured using AC voltametric method. The capacitances of DOPC and bare Hg are identical over a wide range of frequencies, up to 1 kHz. This is an indication that at low frequencies both interfaces appear to be the same, i.e., water covered. This is interpreted as desorption and is similar to the capacitance AC voltametry data (Figure 5-3). Addition of Ca^{2+} systematically decreased the capacitance, which is also in good agreement with the previous data (see figure 5-3). The Nyquist plot is shown in Figure 5-9(b). Two regions are conspicuous: the semicircle at high frequencies and a diffusion controlled reaction evident by a Warburg impedance at low frequencies, which is due to K^+ reduction. Addition of Ca^{2+} consistently decreased the size of the semicircle, consistent with the decrease in capacitance at this potential, observed using AC voltametry. In addition, the presence of Ca^{2+} changed the slope of line due to the Warburg impedance. These changes are believed to be due to Ca^{2+} binding with the lipid head groups thus influencing the lipid response to potential perturbation.

A model was proposed in terms of a simple Randles equivalent circuit shown in Figure 5-10(a). The impedance spectra were analyzed by fitting the data to the proposed model (Figure 5-10(b)). The fit parameter results are shown in Table 1. The values in brackets are percent error associated with the fits. The standard deviations associated with the measurements are also listed in parentheses calculated from triplicate runs. Again we emphasize that these are preliminary results and are only reported to justify the methodology developed. The detailed interpretation of the results

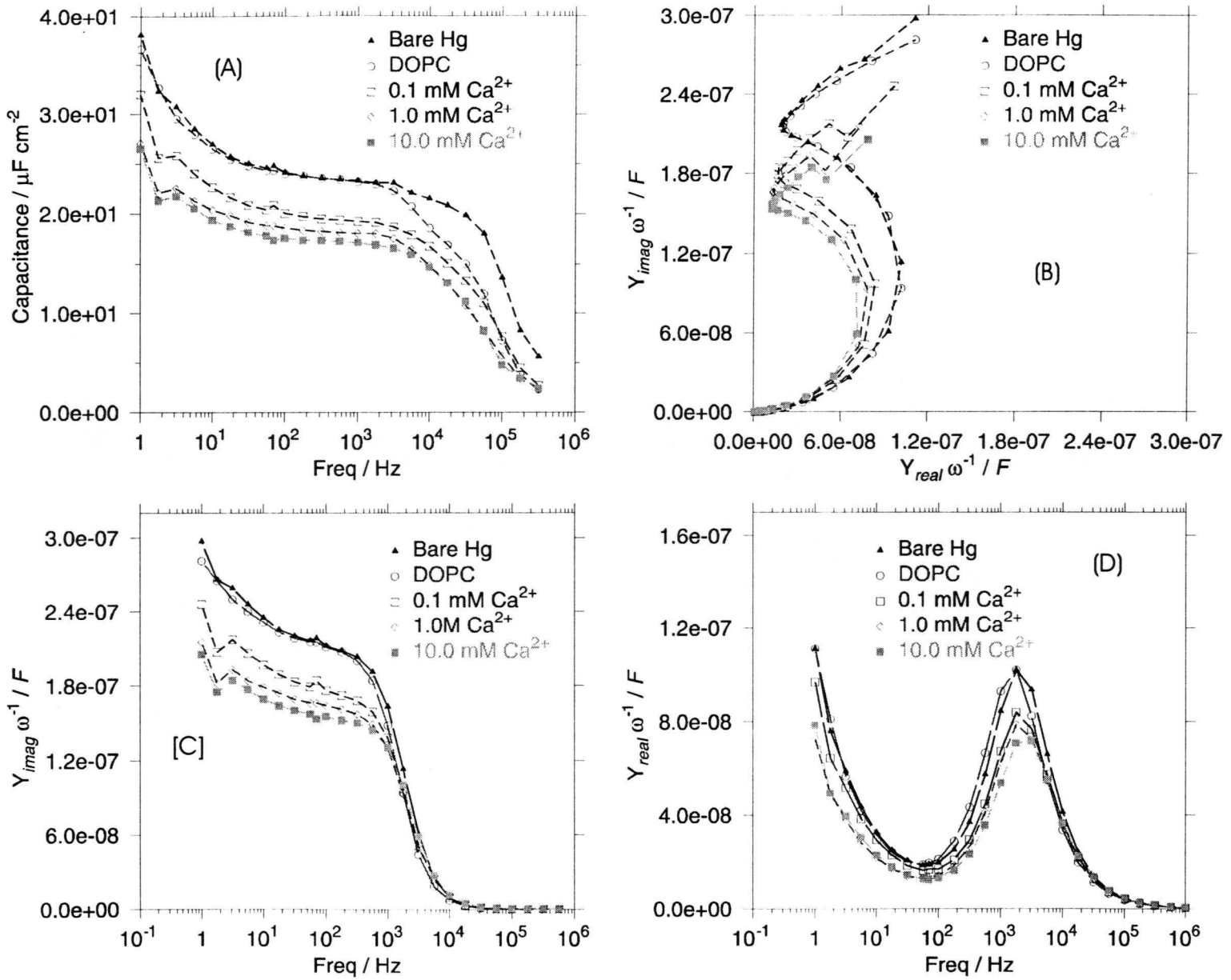

Figure 5-9 Different plots for impedance spectra at the desorption. (A) Capacitance plot, (B) Nyquist plot (C) Imaginary impedance plot and (D) Real impedance plot.

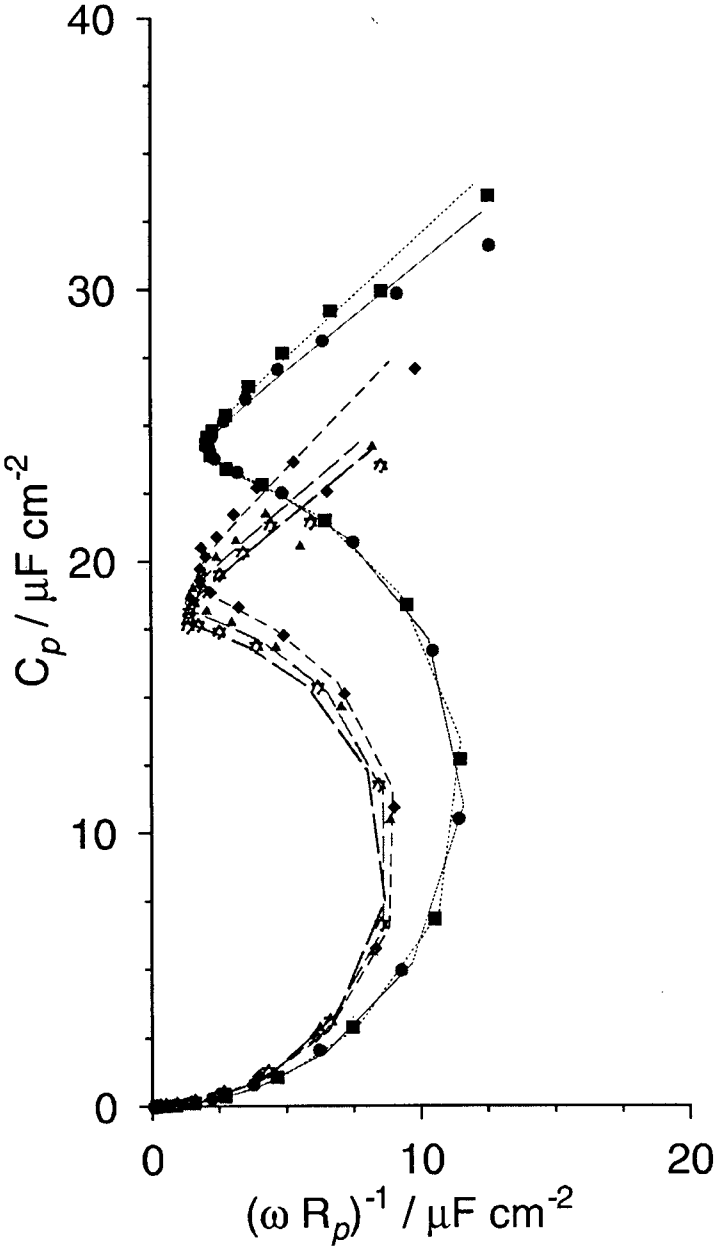

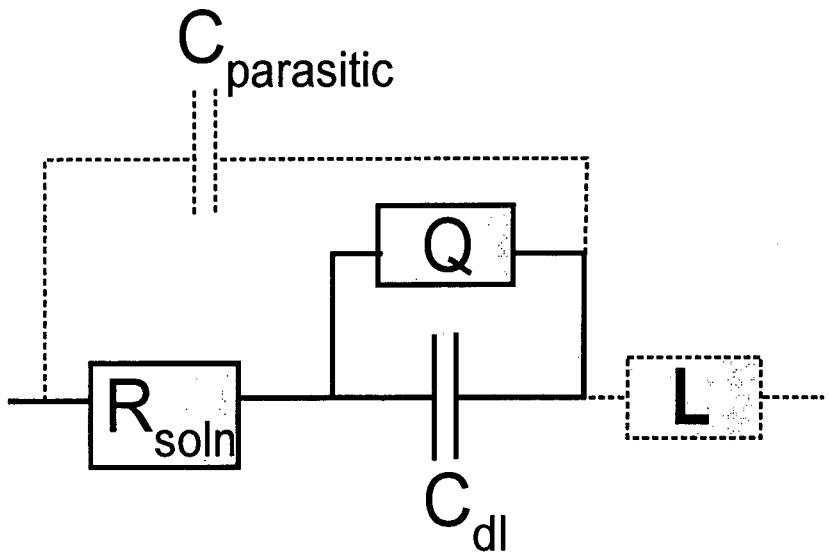

Figure 5-10 (A) The electrical equivalent circuit for the proposed model. Where R_{sol} is solution resistance, Q is constant phase element, C is parasitic capacitance, C_{dl} is double layer capacitance and L is inductance.

Figure 5-10 (B) The fitting plots using the proposed model.

- ■ Bare Hg
- ● DOPC
- ♦ 0.1 mM Ca^{2+}
- ▸ 1.0 mM Ca^{2+}
- ★ 10.0 mM Ca^{2+}

	0.1 M KCl	DOPC (G/S)	0.1 mM Ca^{2+}	1.0 mM Ca^{2+}	10.0 mM Ca^{2+}
Edes (1-.85 V /SCE)					
Rsol (Ω)	372 (6)	442 (20)	410 (6)	404 (14)	388 (12)
C (nF)	207 (6)	205 (1)	166 (4)	160 (2)	154 (4)
QY	8.4 (8.4)	0.55 (0.56)	53 (63)	1.2 (0.6)	0.63 (0.18)
Qn	0.443 (0.03)	0.415 (0.02)	0.48 (0.02)	0.439 (0.01)	0.432 (0.01)
χ^2	0.0158	0.0214	0.0439	0.0580	0.0314
Eads (-0.4 V /SCE)					
Rsol	374 (5)	442 (13)	390 (11)	375 ((7)	354 (4)
C (nF)	320 (9)	16.4 (1.1)	15.4 (0.2)	14.8 (0.6)	14.7 (1.7)
χ^2	0.0486	0.0056	0.0208	0.00036	0.0105

Table 1 The fit parameters for the DOPC systems using the proposed model.

is still ongoing. The Hg-KCl interface at both potentials gave expected capacitance values, 320 nF (36.0μF/cm^2) at -0.4 V (SCE) and 207 nF (23.3 μF/cm^2) at -1.85 V (SCE). In the presence of DOPC, the capacitance at -0.4 V (SCE) was lowered to 16.4 nF (1.85μF/cm^2), which is in a good agreement with the literature [29]. At the desorption, the capacitance remained unchanged, i.e., 205 nF (23.0 μF/cm^2), indicating the desorption of the lipid from the electrode surface, which is consistent with the AC voltametric data (Figure 5-3).

A surprising increase in the solution resistance (70 Ω) was noted due to the adsorbed DOPC monolayer as compared to uncovered Hg electrode. However, in the presence of DOPC no difference was observed between the adsorption and desorption potentials except when Ca^{2+} was introduced. This was also surprising since only the dc potential was changed. These measurements indicate that the interface is not a simple RC circuit and work is ongoing to explain these results.

Addition of Ca^{2+} changed both the capacitance and the solution resistance. At the adsorption potential, the capacitance changed slightly from 16.4 nF (1.85 μF/cm^2) to 14.7 nF (1.66 μF/cm^2) in the presence of 0.0 mM and10.0 mM Ca^{2+} respectively. The corresponding desorption potential also experienced a decrease in capacitance from 205 nF (23.0 μF/cm2) with no Ca^{2+} in solution to 154 nF (17.3 μF/cm2) in the presence of 10 mM Ca^{2+}. This is consistent with the AC voltametric measurements discussed previously (Figure 5-3). Addition of Ca^{2+} also changed the solution resistance at both potentials. At adsorption potential, the solution resistance dropped from 442 Ω to 354 Ω when the concentration of Ca^{2+} was increased from 0.0 mM to 10.0 mM. At the desorption potential, there was a decrease in solution resistance from 449 Ω to 365 Ω. A decrease in solution resistance was expected due to increase in ions concentration in solution, but the difference in resistance between the adsorption and desorption potentials can only be explained through an interference of the desorbed lipid monolayer on conductance. Further work is planned to address this issue.

5.2.7 Conclusions

The impedance measured at adsorption potentials (-0.4 V) confirmed that at this potential, the monolayer is well-organized and free from defects. Addition of Ca^{2+} was found to have little effect on the lipid morphology at this potential except at very low frequencies and with high concentrations of Ca^{2+}. Potential induced phase transformation at peak 1 was characterized by one time constant, representing only one phase change. Peak 2 on the other hand was characterized by two time constants, which suggests two distinct potential induced phase transformations. Peak 3 represented a potential induced phase transformation characterized by three time constants, which is indicative of three distinct phase changes. The impedance at the desorption potential region has also confirmed the desorption of the lipid, which seems to remain close to the electrode surface. Therefore, a methodology was developed that allowed for the electrochemical impedance spectroscopy to be performed on the peaks at potential of peak maximum and at other potentials of interest. The methodology clearly demonstrates the ability to measure the impedance at these potentials (especially at peak maximum of narrow needle-like peak 1) without disrupting the monolayer organization.

6 Conclusions

Electrochemical impedance spectroscopy has provided a powerful methodology and technique to characterize the adsorption-desorption of DOPC supported on a Hg-electrolyte interface. The DOPC was found to adsorb on the electrode surface at -0.4 V (SCE), forming a well-organized defect free monolayer. When the potential was made more negative, the adsorbed monolayer underwent some potential induced phase changes before being desorbed from the electrode surface at very negative potentials depending on the supporting electrolyte. The phase changes were manifested as peaks in the capacitance measurements. Three peaks were observed within the accessible potential window of the experiments.

Both potential and cations either forming the supporting electrolyte or added to the working solution subphase were found to have significant influence on the organization of the adsorbed DOPC monolayer, the kinetics of phase transitions and the nature of the desorbed aggregates. When the negative potential limit was restricted to -1.2 V (SCE), the lipid layer was found to be stable towards negative potential excursion for all the electrolytes. The stability was demonstrated by the reproducibility of the peaks and the minimum capacitance. However, the peak height was greatly reduced in TMACl electrolyte. Increasing the potential limit to more negative values changed the monolayer organization in all the electrolyte systems. When the lipid was exposed to very negative polarizations, they were displaced from the electrode surface at -1.85 V (SCE) in KCl and at -1.75 V (SCE) in TMACl. However, there was no desorption observed for LiCl electrolyte. Li^+ stabilizes the lipid layer due to its large Gibbs energy of hydration. On the other hand, the lipid was desorbed from the Hg surface in TMACl at less negative potential due to its (TMA^+) small Gibbs energy of hydration and also due to competitive adsorption at the Hg surface. For all the electrolyte systems, the exposure of the lipid to large negative polarizations was also accompanied by the destruction of the layer organization. The peaks were not traced for the negative and the positive going potential scans and the minimum capacitance increased after re-adsorption, i.e., the monolayer was unstable towards negative potential excursion. Addition of Ca^{2+} to the solution subphase of the KCl system, systematically changed the peak heights. The Ca^{2+} interacted and bound with the lipid head groups stabilizing the lipid layer toward negative potential excursion and slowing the kinetics of the phase transitions, decreasing the height of the peaks.

Impedance spectroscopy analysis was performed at the adsorption potential, at the peak potentials and at the desorption potential. The impedance spectrum at these potentials showed monolayer characteristics similar to the results obtained with AC voltametric method. Potential induced phase transformation at peak 1 was characterized by one time constant, representing only one phase change. Peak 2 on the other hand was characterized by two time constants, which suggested two distinct potential induced phase transformations. Peak 3 represented a potential induced phase transformation characterized by three time constants, which was indicative of three distinct phase changes. At very negative potentials, the lipid was completely displaced from the electrode but remained close to the electrode surface. A small amount of K^+ reduction at the Hg surface was also observed at this potential and was indicated in the impedance spectra by Warburg impedance at low frequency. Addition of Ca^{2+} changed the monolayer organization and the kinetics of phase changes.

Therefore, an electrochemical impedance spectroscopy methodology was developed that allowed for the impedance spectroscopy to be performed on the peaks at the potential of peak maximum and at other potentials of interest, to investigate the potential induced changes in the monolayer. The methodology clearly demonstrated the ability to perform impedance measurements (especially on the marrow needle-like peak 1) without disrupting the monolayer. These experiments have not been attempted previously and it appears that this methodology provides a means of employing electrochemical impedance spectroscopy to characterize the potential induced phase transformations for adsorbed lipid monolayers on a Hg electrodes.

7 Suggestions for Future Study

Several routes were available to further investigate the adsorption of DOPC on Hg electrode. Due to limited time, only some of the many options were explored and I feel obliged to suggest some of the methodologies and techniques that would provide useful information. The rate constants for the phase transitions could be studied by performing impedance measurements at potentials around the peaks. By slowly climbing over the peak, it would be possible to watch the rate at which the defects form and grow. This is particularly important for peak 1 and 2. It would also be informative to perform the impedance analysis at the desorption potential with both the Ca^{2+} and TMA^{+} in the solution subphase. This would help understand whether the calcium-stabilized DOPC is desorbed or remain adsorbed on the electrode surface at very negative potentials. Since TMA^{+} displaces the lipid in the presence of Ca^{2+}, it should be expected that the impedance spectra would be identical to the Hg-KCl interface. Electroreflectance spectroscopy and/or elastic scattered light experiments would provide some information as to whether the lipid is desorbed from the electrode especially in the Ca^{2+} case. If the lipid layer is not desorbed in the presence of Ca^{2+}, then the reflected light intensity would be different from the intensity generated by Hg-KCl interface.

Bibliography

1. N. Batina, Z. Kozarac, and B. Cosovic, *J. Electroanal. Chem.,* 188(1985)153.
2. D. Bizzotto, V. Zamlynny, I. Burgress, C. A. Jeffrey, H. Q. Li, J. Rubinstein, R. A. Merril, J. Lipkowski, Z. Galus, A. Nelson and B. Pettinger, Amphiphilic and Ionic Surfactants at electrified interfaces, In A. Wieckowski (Ed.), *Interfacial Electrochemistry: Theory, Experiment, and Applications,* Marcel Dekker, New York, 1999, p. 405.
3. D. Bizzotto and J. Lipkowski, *J. Electroanal. Chem.,* 409(1996)33.
4. D. Bizzotto and A. Nelson, *Langmuir.,* 14(1998)6269.
5. D. Bizzotto and B. Pettinger, *Langmuir.,* 15(1999)8309.
6. K. J. Mysels,and L. H. Princen, *J. Phys. Chem.,* 59(1955)325.
7. J. N. Phillips and K. J. Mysels, *J. Phys. Chem.,* 63(1959)1699.
8. I. R. Miller, *Bioelectrochem. Bioenerg.,* 4(1981)161.
9. D. L. Allara and R. G. Nuzzzo, *Langmuir.,* 1(1985)45.
10. E. Sackmann, *Science,* 271(1996)43.
11. M. Stelze, W. Weissmuller and E. Sackmann, *J. Phys. Chem.,* 97(1993)2974.
12. H. M. McConnel, T. H. Watts, R. M. Weis and A. A. Brian, *Biochim. Biophys. Acta,* 864(1986)932.
13. M. Olivotto, A. Arcangeli, M. Carla and E. Wanke, *Bioessays*, 18(1996)495.
14. A. Nelson, *Langmuir.,* 12(1996)2058.
15. A. Nelson, *Langmuir.,* 13(1997)5644.
16. S. de Marie, *Leukemia,* 12(1996)93.
17. A. Nelson and A. Benton, *J. Electroanal. Chem.,* 202(1986)253.
18. A. Nelson and N. Auffret, *J. Electroanal. Chem.,* 244(1988)99.
19. A. Nelson and F. A. M. Leermakers, *J. Electroanal. Chem.,* 278(1990)73.
20. F. A. M. Leermakers and A. Nelson, *J. Electroanal. Chem.,* 278(1990)53.
21. A. Nelson, N. Auffret, and J. Readman, *Anal. Chim. Acta,* 207(1988)47.
22. A. Nelson, N. Auffret, and J. Borlakoglu, *Biochim. Biophys. Acta,* 1021(1990)205.

23. A. Nelson and D. Bizzotto, *Langmuir.*, 15(1999)7031.

24. M. R. Moncelli, L. Becucci, R. Herrero and R. Guidelli, *J. Phys. Chem.*, 99(1995)9940.

25. M. R. Moncelli, L. Becucci, *J. Electroanal. Chem.*, 385(1995)183.

26. M. Rueda, I. Navarro, G. Ramirez, F. Prieto, C. Prado and A. Nelson, *Langmuir.*, 15(1999)3672.

27. I. Brzozowska, and Z. A. Figaszewski, *Biophys. Chem.*, 95(2002)173.

28. A. Nelson and N. Auffret, *J. Electroanal. Chem.*, 248(1998)167.

29. V. Stauffer, R. Stoodley, J. O. Agak and D. Bizzotto, *J. Electroanal. Chem.*, 516(2001)73.

30. F. T. Buoninsegni, L. Becucci, M. R. Moncelli and R. Guidelli, *J. Electroanal. Chem.*, 500(2001)395.

31. C. M. A. Brett and A. M. O. Brett, *Electrochemistry: principles, methods and applications,* Oxford University Press, New York, 1993.

32. A. J. Bard and L. R. Laulker, *Electrochemical methods: Fundamentals and applicatios,* John Wiley and Sons, New York, 1980.

33. J. Koryta, J. Dvorak and L kavan, *Principles of Elecrochemistry*, John Wiley and Sons, Chichester, 1993.

34. A. C. Fisher, *Electrode Dynamics*, Oxford University Press, New York, 1996.

35. J. Goodisman, *Electrochemistry: Theoretical Foundations,* John Wiley and Sons, New York, 1987.

36. R. Parsons, *Chem. Rev.*, 90(1990)1813.

37. J. Lecoeur, J. Andro and R. Parsons, *Surf. Sci.*, 114(1982)320.

38. D. M. Mohilner, In A. J. Bard (Ed.), *Electroanalytical Chemistry*, Vol.1, Marcel, New York, 1966, p.241.

39. D. C. Grahame, *Chem. Rev.*, 41(1947)441

40. B. B. Damaskin, O. A. Petrii and V. V. Batrakov, *Adsorption of Organic Compounds on Electrodes,* Plenum Press, New York, 1971.

41. A. Frumkin, O. A. Petrii and B. Damaskin, In J. O'M. Bockris, B. E. Conway and E. Yeager (Ed.), *Comprehensive Treatise of Electrochemistry*, Vol.1, Plenum, New York,

1980.

42. K.E. van Holde, W.C. Johnson and P. S. Ho, *Physical Biochemistry,* Prentice Hall, New Jersey, 1998.
43. J. C. Venter, M. D. Adams, E. W. Myers, P. W. Li, R. J. Mural, G. G. Sutton, H. O. Smith, M. Yandell, *et al., Science,* 291(2001)1153.
44. I. H. G. S. Consortium, *Nature*, 409(2001)860.
45. E. Overton, *Vjsch. Naturf. Ges. Zurich*, 40(1895)159.
46. E.Gorter and F. Grendel, *J. Exp. Med.* 41(1925)439.
47. S. J. Singer and G. L. Nicolson, *Science,* 175(1972)720.
48. R. B. Gennis, *Biomembranes: Molecular structure and functions, Springer Advanced Text in Chemistry, Springer,* New York, 1989.
49. B. Alberts, A. Johnson, J. Lewis, M. Raff, K. Roberts and P. Walter, *Molecular Biology of the cell,* Grandland Science, New York, 2002.
50. D. W Fawcett and Bloom, *A TextBook of Histology,* Chapman & Hall, New York, 1994.
51. S. L. Wolfe, *Molecular and cell,* Wadsworth, Baltimore 1993.
52. G. Guidotti, *Annu. Rev. Biochem.*, 41(1972)731.
53. V. Stauffer, *Adsorption of DOPC onto Mercury from a Monolayer and from a Liposomal Suspension*, Bachelor of Science Thesis, University of British Columbia Vancouver (2000), 67 p.
54. B. D. Kruijff, *Nature,* 329(1987)587.
55. S. Spiegel and S. Fishman, *Proc. Natl. Acad. Sci. USA,* 84(1987)141.
56. D. A. Doyle, J. M. Cabral, R. A. Pfuetnzer, A. Kuo, J. M. Gulbis, S. L. Cohen, B. T. Chait and R. MacKinnon, *Science,* 280(1998)69.
57. B. Roux and R. MacKinnon, Science, 285(1999)100.
58. W. J. Sun, R. M. Suter, M. A. Knewtson, C. R. Worthington, S. Tristram-Nagle, R. Zhang, and J. F. Nagle, *Phys. Rev.* 49(1994)4665.
59. I. D. Raistrick, J. R. Macdonald and D. R. Franceschetti, In J. R. Macdonald, *Impedance Spectroscopy: Emphasizing Solid Materials and Systems,* John Wiley and Sons, New York, 1997, p. 27.

60. A. M Bond, R. G. Compton, D.A. Fiedler, G. Inzelt, H. Kahlert, S. Komorsky-lavric, H. Lohse, M. Lovric, F. Marken, A. Neudeck, U. Retter, Z. Stojek and F. Scholz (Ed.), *Electrochemical Methods: Guide to experiments and applications*, Springer, Berlin, 2002.
61. M. Sluyters-Rehbach, J. H. Sluyters and A.J Bard (Ed.), *Sine Wave Methods in the Study of Electrode Process*, Vol.4, Dekker, New York, 1970.
62. G. L. Gaines Jr., *Insoluble Monolayer at Liquid-Gas interfaces*, Interscience, New York, 1966.
63. G. Roberts, *Langmuir-Blodgett Films*, plenum, New York, 1990.
64. S. D. Argade, M. A. Genshaw, H. D. Hurwitz, K. Muller, B. J, Piersma, A. K. N. Reddy and E. Gileadi (Ed.), *Electrosorption,* Plenum, New York, 1967.
65. A. Ulman, *Charactrization of Organic Thin Tilms, Manning*, Greenwich, 1995.
66. C. J. Zhong and M. D. Porter, *Anal. Chem.*, 67(1995)709A.
67. J. D. Swalen, D. L. Allara, J. D.Andrade, E. A. Chandrss, S. Garoff, J. Israelachvili, T. J. McCarthy, R. Murray, R. F. Pease, J. F. Rabolt, K. J. Wynne, and H. Yu, *Langmuir*, 3(1987)932.
68. D. E. Weisshaar, B. D. Lamp and M. D. Porter, *J. Am. Chem. Soc.*, 114(1992)5860.
69. R. J. Willicut and R. L. McCarley, *Langmuir.*, 11(1995)296.
70. C. N. Sayre and D. M. Collard, *Langmur.*, 11(1995)302.
71. D. F. Yang, C. P. Wilde and M. Morin, *Langmuir.,* 13(1997)243.
72. S. E. Creager and K. G. Olsen, *Anal. Chim. Acta*, 307(1995)277.
73. K. L. Prime and G. M. Whitesides, *J. Am. Chem. Soc.*, 115(1993)10714.
74. N. L. Abbott and G. M. Whitesides, *Langmuir.*, 10(1994)1493.
75. C. B. Gorman, H. A. Biebuyck and G. M. Whitesides, *Langmuir.,* 11(1995)2242.
76. D. F. Yang, C. P. Wilde and M. Morin, *Langmuir.,* 12(1996)6570.
77. C. J. Zhong and M. D. Porter, *J. Electroanal. Chem.*, 425(1997)147.
78. C. A. Widrig, C. Chung, M. D. Porter, *J. Electroanal. Chem.*, 310(1991)335.
79. D. F. Yang and M. Morin, *J. Electroanal. Chem.*, 441(1998)173.
80. C. J. Zhong, N. T. Woods, G. B. Dawson, M. D. Porter, *Electrochem. Commun.,* 1(1999)17.

81. P. Krysinski, R. V. Chamberlain II and M. Maida, *Langmuir.*, 10(1994)4286.

82. A. Ulman, *An Introduction to Ultrathin Organic Films: From Langmuir-Blodgett to Self-assembly*, Academic Press, Boston, 1991.

83. J. K. Schoer, F. P. Zamborini and R. M. Crooks, *J. Phys. Chem.*, 100(1996)11086.

84. D. L. Allara, and J. Swalen, *J. Phys. Chem.*, 86(1982)2700.

85. M. M. Walczak, D. D. Popenoe, R. S. Deinhammer, B. D. Lamp, C. Chung and M. D. Porter, *Langmuir*, 7(1991)2687.

86. C. J. Zhong and M. D. Porter, *J. Am. Chem. Soc.*, 116(1994)11616.

87. K. Slowinski, R. V. Chamberlain, C. J. Miller, M. Majda, *J. Am. Chem. Soc.*, 119(1997)11910.

88. K. Slowinski, K. U, Slowinska, M. Majda, *J. Phys. Chem. B,* 103(1999)8544.

89. K. Slowinski, H. K. Y, Fong, M. Majda, *J. Am. Chem. Soc.*, 121(1999)7257.

90. D. Bizzotto and J. Lipkowski, *Progress in Surface Science*, 50(1995)237.

91. D. Bizzotto, and J. Lipkowski, *Progr. Colloid Polym. Sci.*, 103(1997)201.

92. T. Sagara, V. Zamlynny, D. Bizzotto, A. McAlees, R. McCrindle and J. Lipkowski, *Israel J. Chem.*, 37(1997)197.

93. J. Shepherd, Y. Yang and D. Bizzotto, *J. Electroanal. Chem.*, 524-525(2002)54.

94. A. V. Gorodetskaya and A Frumkin, *Akad. Nauk SSSR,* 18(1938)649.

95. A. V. Gorodetskaya, Zh. Fiz. Khim., 14(1940)371.

96. A. Nelson, H. P. van leeuwen, *J. Electroanal. Chem.*, 273(1989)183.

97. A. Nelson, H. P. van leeuwen, *J. Electroanal. Chem.*, 273(1989)201.

98. A. Nelson, *J. Electroanal. Chem.*, 303(1991)221.

99. R. Stoodley, J. Shepherd, K. M. Wasan and D. Bizzotto, *Biochim. Biophys. Acta.*, 1564(2002)289.

100. R. Guidelli, L. Becucci, A. Dolfi, M. R. Moncelli, F. T. Buoninsegni, *Solid State Ionics*, 150(2002)13.

101. D. Hellberg, F. Scholz, F. Schauer and W. Weitschies, *Electochem. Commun.*, 4(2002)305.

102. D. M. Haverstick and M. Glaser, *J. Cell Biology*, 106(1988)1885.

103. S. Mittler-Neher and W. Knoll, *Biochim. Biphys. Acta,* 1152(1993)295.

104. J. Gradadolnik and D Hadzi, *Chem. Phys. Lipids,* 65(1993)121.

105. J. Wilschut, J. Scholma, S. J. Eastman, M. J. Hope and P. R. Cullis, *Biochem.,* 31(1992)2629.

106. F. Castelli and R. Raciti, *Thermochimica. Acta,* 186(1991)205.

107. J. R. Silvius, *Biochem.,* 29(1990)2930.

108. C. P. S. Tilcock, R. P. Cullis and S. M Gruner, *Biochem.,* (1988)1415.

109. G. Puu and I. Gustafson, *Biochim. Biophys. Acta*, 1327(1997)149.

110. J. M. Holopainen, J. Y. A. Lehtonen and P. K. J. kinnunen, *Biophys. J.*, 76(1999)2111.

111. I. Reviakine and A. Brisson, *Langmuir.,* 16(2000)1806.

112. S. Chen and K. Huang, *Anal. Chem.,* 72(2000)2949.

113. I. Reviakine A. Simon and A. Brisson, *Langmuir.,* 16(2000)1473.

114. M. Ross, C. Steinem, H. J. Galla and A. Janshoff, *Langmuir.,* 17(2001)2437.

115. D. Knebel, M. Sieber, R. Reichelt, H. J. Galla and M. Amrein, *Biophys. J.,* 83(2002)547.

116. F. Mansfeld, S. Lin, Y. C. Chen and H. shih, *J. Electrochem. Soc.,* 135(1988)907.

117. T. Wandlowski and R. de Levie, *J. Electroanal. Chem.,* 352(1993)279.

118. B. Lindholm-Sethson, P. Geladi and A. Nelson, *Anal. Chim. Acta*, 446(2001)121.

119. M. Rueda, I. Navarro, C. Prado and C. Silva, *J. Electrochem. Soc.,* 148(2001)139.

120. S. Hason, J. Dvorak, F. Jelen and V. Vetterl, *Talata,* 56(2002)905.

121. N. Ivosevic, J. Tomaic and V. Zutic, *Langmuir.,* 10(1994)2415.

122. F. T. Buoninsegni, R. Herrero, M. R. Moncelli, *J. Electroanal. Chem.,* 452(1998)33.

123. H. Akutsu and J. Seelig, *Biochem.,* 20(1981)7366.

124. J. Seelig. P. M. Macdonald and P. G. Scherer, *Biochem.,* 26(1987).

125. R. J. Clarke, *Biochim. Biophys. Acta*, 1327(1997)269.

126. F. M Kimmerle and H. Menard, *J. Electroanal. Chem.,* 54(1974)101.

127. P. Millet and P. Dantzer, Electrochem. Commun., 1(1999)163.

Appendix A

The Fourth Electrode

The high frequency region was accessed with the help of a fourth electrode. A normal reference electrode is relatively slow and thus has problems in dealing with high frequencies. The consequence of that is that at higher frequencies, the influence of the reference electrode is clearly manifested in the measured impedance results (usually an inductance, but also additional capacitance). This problem is solved by the use of a fourth electrode. Placing the Pt wire in the solution next to the reference electrode and connecting it to the reference electrode *via* a capacitor makes sure that the high frequency signals go through the Pt *via* a capacitor (capacitor is conductive at high frequencies), and the low frequency signals (especially the DC signal, i.e. the DC potential that you would like to keep stable) go through the normal reference electrode(those signals cannot go through the capacitor).

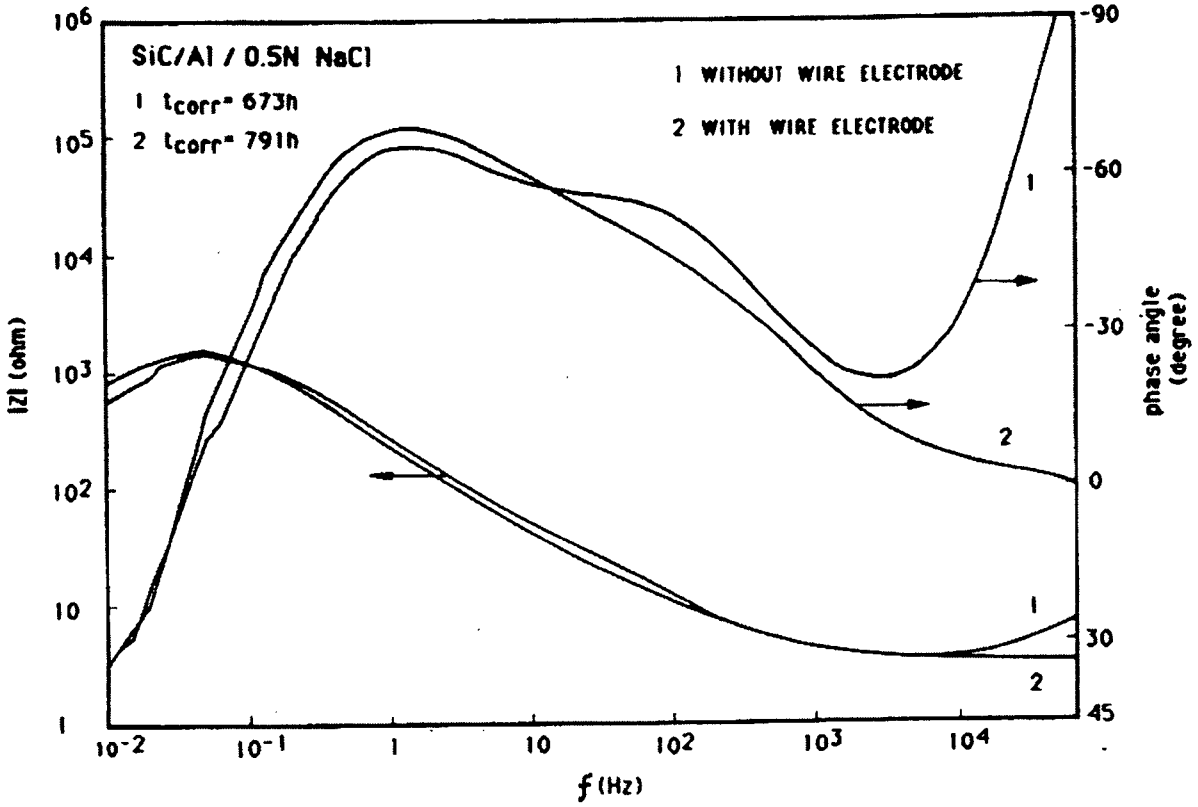

The diagram showing the influence of 4th electrode on impedance at high frequencies. 1 is with the 4th electrode and 2 is without the 4th electrode. The arrows show corresponding y-axis for the plots. Taken from [116].